UNIVERSITY OF CALIFORNIA, SAN DIEGO

Oceanographic and ecological consequences of iron localization in

phytoplankton photosystems

A dissertation submitted in partial satisfaction of the requirements for the degree

Doctor of Philosophy

in

Oceanography

by

Brian Matthew Hopkinson

Committee in charge:

    Katherine A. Barbeau, Chair
    Lihini I. Aluwihare
    Peter J.S. Franks
    Ralf Goericke
    B. Gregory Mitchell
    Milton H. Saier

The dissertation of Brian Matthew Hopkinson is approved,

and it is acceptable in quality and form for publication on

microfilm:

_____

_____

_____

_____

_____
<div align="right">Chair</div>

University of California, San Diego

2007

Table of Contents

List of Symbols

α^{Chl} Chlorophyll normalized initial slope of the PE curve

Fe'   All inorganic iron species

FeL   Ligand bound iron forms

$F_v{:}F_m$ Maximum quantum yield of photosystem II

ILI_{chl} Iron limitation index computed from with chlorophyll

ILI_{POC} Iron limitation index computed from particulate organic carbon

ILI_μ Iron limitation index computed from chlorophyll growth rates

$K_{Fe'L}$ Equilibrium constant for ligand complexation with respect to Fe'

μ_{Chl} Chlorophyll derived growth rate

μ_{NO3} Nitrate derived growth rate

p Extent of connection between photosystem II units

P^{Chl}_{max} Chlorophyll normalized maximum photosynthetic rate

σ_{PSII} Effective absorption cross section of PSII

τ Turnover time of first photosystem II electron acceptor

List of Abbreviations

ABC	ATP binding cassette
ACC	Antarctic circumpolar current
BLAST	Basic local alignment search tool
CalCOFI	California cooperative oceanic fisheries investigations
Chl *a*	Chlorophyll *a*
CLE-ACSV	Competitive ligand equilibration adsorptive cathodic stripping voltammetry
ETNP	Eastern tropic North Pacific
FRRF	Fast repetition rate fluorometer
GF/F	Glass fiber filter grade F
HMM	Hidden markov model
HNLC	High nutrient low chlorophyll
HPLC	High preformance liquid chromatography
KN	R/V Knorr
LTER	Long term ecological research
NH	R/V New Horizon
P vs. E	Photosynthesis-irradiance curve
PAM	Pulse amplitude modulation fluorometry
PAR	Photosynthetically active radiation
PC	Peptone casein media
POC	Particulate organic carbon
PON	Particulate organic nitrogen
PSII	Photosystem II
RR	R/V Roger Revelle
RT-Q-PCR	Real time quantitative polymerase chain reaction
SCB	Southern California bight
SCM	Subsurface chlorophll maximum
TAC	2-2-thiazolyazo-*p*-cresol
19-but	19-butanoyloxyfucoxanthin
19-hex	19-hexanoyloxyfucoxanthin

List of Tables

List of Figures

Acknowledgements

I would first like to thank my advisor Kathy Barbeau for all her help and support throughout my graduate work. Though she had trouble understanding why someone with no marine science background would be interested in oceanography, she took me into her lab and provided the right balance of freedom and direction for a PhD student with little background in the field. I would also like to thank my thesis committee: Lihini Aluwihare, Peter Franks, Ralf Goericke, Greg Mitchell, and Milton Saier, whose diverse talents have improved this work.

The Barbeau lab has been an especially harmonious and interesting place to work. I especially want to thank Andrew King, who started his graduate work the same year as I did as the first students in the Barbeau lab. In contrast to my lack of experience, Andrew had been involved in oceanography for many years and has taught me many things, from what a copepod is to the basics of surfing. Kelly Roe has helped me with the practical side of caring for our bacterial pets, and Chris Dupont has introduced me to the world of molecular biology and genomics. Kristin Buck has kept things interesting in our group and provided insight into the life of a post-doc.

Research cruises have been a major part of this research, and they are both a major task and the most fun part of my work. Greg Mitchell was the chief scientist of two long but exciting Antactic cruises which I participated in, and his energy and enthusiasm made them all the more enjoyable. Ralf Goericke was chief scientist on my two calmest and warmest cruises to the eastern tropical North Pacific, which he allowed our group to participate in. Of course the entire Barbeau lab has been essential to all the cruise-based

research and the Mitchell group members (Rick Reynolds, Haili Wang, Brian and Bridget Seegers,) were particularly helpful on the Antartic cruises.

Back on land, I have received assistance learning new techniques from many patient people. Ralf Goericke and his lab have assisted with pigment analysis which was an important part of my work. A short trip to the University of Victoria, to work with Jay Cullen, was essential to learning electrochemical techniques for iron analysis. Rick Reynolds has provided invaluable advice on the esoteric aspects of active fluorescence techniques. The Palenik and Tebo labs, primarily Rhona Stuart and Lisa Sudek, helped me learn to isolate RNA and taught me general techniques in molecular biology. The bioinformatics I was able to learn came primarily from Sheila Podell who was very generous with her time. Terry Gasterland also aided my bioinformatics analyses through her work on the *Microscialla marina* genome, and by providing access to her computational resources.

Two chapters in this dissertation have been published elsewhere. The material in Chapter III was published previously as: Hopkinson, Brian M., B. Greg Mitchell, Rick A. Reynolds, Haili Wang, Karen E. Selph, Christopher I. Measures, Christopher D. Hewes, Osmund Holm-Hansen, and Katherine A. Barbeau. 2007. Iron limitation across chlorophyll gradients in the southern Drake Passage: Phytoplankton responses to iron addition and photosynthetic indicators of iron stress. Limnology and Oceanography 52: 2540-2554. Chapter IV was published as: Hopkinson, Brian M., and Katherine A. Barbeau. 2007. Organic and redox speciation of iron in the eastern tropical North Pacific suboxic zone. Marine Chemistry, 106: 2-17. I was the primary researcher and author of both these papers. Additonally Chapter II has been submitted for publication to

Vita

2001	B.S. (Honors), Chemistry, College of William and Mary
2001-2007	Graduate Student Researcher, Scripps Institution of Oceanography
2002-2005	National Defense Science and Engineering Graduate Fellow
2007	Ph.D University of California, San Diego Scripps Institution of Oceanography

Publications

Hopkinson, B.M., G. Mitchell, R. Reynolds, H. Wang, C. Hewes, C. Measures, O. Holm-Hansen, and K.A. Barbeau. 2007. Iron limitation across chlorophyll gradients in the southern Drake Passage: phytoplankton responses to iron addition and indicators of iron stress. *Limnology and Oceanography* 52: 2540-2554.

Hopkinson, B.M., and K.A. Barbeau. 2007. Organic and redox speciation of iron in the eastern tropical North Pacific suboxic zone. *Marine Chemistry*. 106: 2-17.

Hopkinson, B.M., E.D. Kwee, and S.K. Knudson. 2002. A connection between quantum critical points and classical separatracies of electronic states. *J. Chem. Phys*. 117: 5660-5669.

Fields of Study

Major Field: Oceanography

Studies in Trace Metal Cycling.
Professor Katherine Barbeau

Studies in Biological Oceanography
Professors B. Gregory Mitchell, Ralf Goericke, and Peter Franks

Studies in Microbial Physiology
Professors Margo Haygood, Milton Saier, Lihini Aluwihare, and Brian Palenik

ABSTRACT OF THE DISSERTATION

Oceanographic and ecological consequences of iron localization in

phytoplankton photosystems

by

Brian Matthew Hopkinson

Doctor of Philosophy in Oceanography

University of California, San Diego, 2007

Katherine A. Barbeau, Chair

Iron limits phytoplankton productivity and biomass in significant portions of the global ocean. A number of studies over the past decade have shown that iron's primary role in phytoplankton is as a cofactor in photosynthetic light processesing and electron transport proteins, linking its availability directly to primary productivity. Multiple consequences of this localization were explored in this thesis.

Because photosynthetic iron demands dominate phytoplankton iron requirements, it has been suggested that primary productivity may be co-limited by iron and light when the availability of both factors is reduced. Support for this hypothesis had been previously obtained in iron limited regions with deep mixed layers, but the possibility that iron-light co-limitation may occur outside areas conventionally thought to be iron limited was

explored in Chapter II of this thesis. Phytoplankton, particularly larger diatoms, displayed responses indicative of iron-light co-limited at subsurface chlorophyll maxima in the Southern California Bight and the eastern tropical North Pacific. In these water columns, lack of iron availability limits the growth of larger organisms with consequences for carbon export efficiency and ecosystem structure. The distribution and speciation (redox and organic) of iron in one of these regions, the eastern tropical North Pacific, is discussed in Chapter IV.

Photosynthetic physiology is strongly impacted by iron limitation, due to the high iron content of the photosynthetic apparatus. Assessment of variability in photosynthetic physiological states has proven useful as a diagnostic of iron stresss in laboratory cultures and mesoscale iron addition experiments. In Chapter III, changes in photosynthetic physiology across a gradient in iron stress are examined in relation to experimental responses to iron addition. It was deterimined that in a region of natural iron fertilization in the southern Drake Passage, photosystem II characteristics were correlated with responses to iron addition, and could serve as good indicators of the degree of iron stress in a system.

A disproportionate amount of photosynthetic iron is in the form of heme co-factors, highlighting the potential importance of this form of iron in marine microbial ecosystems. The cycling of heme in the ocean is not well understood, but because it is hydrophobic and photosensitive, direct uptake by bacteria from particulates may be an important pathway of recycling. In Chapter V, the ability of a particle associated bacterium, *Microscilla marina*, to take up heme is discused and a potential heme transport system is identified in its genome. The putative heme transport system is

expressed and upregulated under iron stress and when gowing on heme as an iron source. The genomes of many diverse marine bacteria were searched for similar uptake systems and genes with strong similarity to known heme transporters were identified in alpha- and gamma- proteobacteria. However, no putative heme transporters were identified in cyanobacteria or oligotrophic bacteria such as *Pelagibacter ubique*, suggesting heme is primarily available on particles or in rich environments, in agreement with its chemistry. Further investigations into the uptake capabilities of marine microorganisms may provide additional insights into trace metal cycling.

I

Introduction

Pelagic primary productivity accounts for half of global carbon fixation and its magnitude was long thought to be limited principally by nitrogen and phosphorus availability. However the existence of extensive areas of the ocean with abundant nitrate and phosphate but low productivity and phytoplankton biomass (using chlorophyll as a proxy) demonstrated that these elements could not be the sole factors regulating pelagic productivity. The most prominent explanations for the existence of these High Nutrient Low Chlorophyll (HNLC) regimes were that grazing by zooplankton kept phytoplankton abundance low or that a micronutrient, such as iron, was lacking limiting phytoplankton growth (Martin and Fitzwater 1988; Frost 1991; Cullen 1991). Substantial data and strong personalities supporting the competing theories led to a series of studies investigating the roles of grazing and iron in HNLC regions, culminating in the mesoscale iron enrichment experiments in which tons of iron were added to kilometer size patches of the ocean to assess its biological impact (Martin et al. 1991; Coale et al. 1996; Boyd et al. 2001). The dramatic increase in phytoplankton biomass and productivity observed in these experiments substantiated the claim that iron influences productivity of the in-situ community, and demonstrated iron availability is primarily responsible for the HNLC regions.

Marine iron chemistry

The discovery that iron controls productivity and nutrient drawdown in approximately one third of the ocean has motivated extensive research into the cycling of iron in the ocean and its use by marine microorganisms. In oxic seawater iron is nearly

insoluble with a maximum of approximately 0.3 nM inorganic iron dissolvable in

seawater (Liu and Millero 1999). Consequently iron cannot accumulate in seawater to the

extent that nitrogen and phosphorus do, but instead must be constantly resupplied to

sustain productivity. Riverine inputs and resuspension of shelf sediments add iron to

coastal waters (Johnson et al. 1999; Wu and Luther 1996). These coastal waters have

high iron concentrations such that biota are not iron limited, but iron dynamics within

these waters are beginning to receive more attention since they can serve as iron sources

to oceanic waters. Dust deposition can be an important source of iron to oceanic waters

and it is the lack of significant Aeolian iron supply relative to nutrient input that creates

HNLC regions (Duce and Tindale 1991; Johnson et al 2003). Thus in HNLC waters the

predominant sources of iron are inputs from deep waters and mixing with high iron

coastal waters.

Iron concentrations, however, are not sufficient to understand the cycling and

bioavailability of the element. The form and chemical nature of iron, referred to as its

speciation, impacts iron cycling and is influenced by biological and chemical processes in

the ocean. Through the use of competitive ligand techniques, it is known that dissolved

iron is completely complexed to organic ligands, but these methods provide little

information about the identity of the natural ligands (Rue and Bruland 1995, van den

Berg 1995). There has been speculation that the ligands may be siderophores, iron

binding organic compounds excreted by organisms to complex iron, and the

concentration of ligands has been observed to increase during iron induced phytoplankton

blooms, suggesting a biological source (Rue and Bruland 1997; Martinez et al. 2000).

However a significant portion of the ligands may actually be in the colloidal phase and

are perhaps non-specific metal binding sites rather than compounds excreted intentionally to bind iron (Wu and Boyle 2001). The ligands help solubilize iron and keep it in the dissolved phase, and may influence the bioavailability of iron to organisms depending on the molecular nature of the ligand (Johnson et al. 1997; Hutchins et al. 1999). The redox state of iron will also affect its behavior. Iron (III), the thermodynamically stable form in oxic seawater, is highly insoluble but binds tightly to ligands. The more soluble iron(II) may be formed in surface waters by photochemical or biological reduction, and in anoxic or suboxic regions (Hong and Kester 1986; Barbeau et al. 2001).

Iron in photosynthetic microorganisms

The ability of iron to cycle between Fe(II) and Fe(III) and its abundance during the early evolution of life has made it the most highly required transition metal in most organisms (Ho et al. 2003; Saito et al. 2003). In microorganisms it is used primarily in electron transport proteins, especially those involved in respiration and photosynthesis. Additional important iron containing proteins include nitrate reductase, nitrogenase, certain super oxide dismutases, and catalase. In phytoplankton, photosynthetic reaction centers and electron transport proteins make up most the enzymatic iron (Raven 1990; Sunda and Huntsman 1997; Strzepek and Harrision 2004). When iron concentrations are high, luxury iron uptake and storage in iron binding proteins such as DPS and ferritin occurs, but under low iron conditions, which exist in much of the ocean, iron must be used in metabolic proteins. A detailed study of iron allocation in two marine diatoms showed that nearly all iron was found in photosynthetic proteins under moderate to low iron conditions (Strzepek and Harrison 2004).

Because of the localization of iron in photosynthetic proteins, there is an inherent link between photosynthesis and iron availability. The photosynthetic performance of iron limited phytoplankton is severely altered, and the characteristic photosynthetic properties of iron limitation have been used to diagnose iron stress in the marine environment (Greene et al. 1991; LaRoche et al. 1996; Behrenfeld and Kolber 1999). In particular, patterns of chlorophyll fluorescence in phytoplankton can be used to assess photosynthetic properties, and have proven valuable as signatures of iron stress (Greene et al. 1992; Behrenfeld et al. 2006). Fluorescence of chlorophyll from intact photosystems represents a loss of absorbed light which could otherwise be used for photosynthesis. Analyzing chlorophyll fluorescence at short timescales provides information on the ability of the photosynthetic machinery to absorb and handle light (Krause and Weis 1991; Kolber et al. 1998). In the early mesoscale iron enrichment experiments these methods provided some of the best evidence that the in-situ phytoplankton community was iron limited, and subsequent large scale mapping of photosynthetic properties have revealed the extent of iron limitation in and around HNLC regions (Kolber et al. 1994; Behrenfeld and Kolber 1999; Behrenfeld et al. 2006).

The heavy iron requirement of photosynthetic proteins also complicates growth at low light levels where more photosynthetic proteins are required to harvest light. Although it is chlorophylls and accessory pigments in antennas which actually absorb light, additional iron containing reaction center proteins become needed at lower light as there is a maximal extent to which antanna can be expanded and still efficiently transfer light to the reaction center. The increase in photosynthetic proteins at low light has been shown to drive an increased iron requirement in several marine phytoplankton,

suggesting that low light could exacerbate iron stress (Sunda and Huntsman 1997; Strzepek and Harrison 2004). It has been hypothesized that phytoplankton could become co-limited by iron and light, due to their linked physiology, in situations where both iron and light availability are low (Sunda and Huntsman 1997). Such conditions may be present in the polar oceans where iron concentrations are low and HNLC regimes exist, and strong winds combined with weak stratification create deeply mixed surface layers during much of the year. Several field studies in the North Pacific and subantarctic Pacific have provided support for this hypothesis (Maldonado et al. 1999; Boyd et al. 2001). While iron has been well documented to influence HNLC areas, the potential for iron-light co-limitation to occur deep in the euphotic zone of macronutrient limited water has also been suggested, and field testing of this hypothesis is a focus of this thesis.

Iron acquisition

In order to satisfy their iron needs, microorganisms have devised a range of strategies to acquire the forms of iron most prevalent in their environment. Most organisms have transporters for inorganic iron(III) and frequently iron(II) which can be available in the dissolved phase, but often iron is present in more recalcitrant forms, locked away in minerals, proteins, or organic complexes. To acquire these forms of iron organisms have developed more complicated uptake pathways. Eukaryotic organisms are commonly thought to use reductase based uptake mechanisms whereby enzymatic reduction of iron(III) generates the more soluble and generally more weakly bound iron(II), increasing iron bioavailability (Schroder et al. 2003). The iron(II) is then internalized by a transporter, being reoxidized in the process. These mechanisms are

capable of liberating iron from mineral phases or organic complexes and have been studied in marine diatoms, but may be common in many marine eukaryotes (Maldonado and Price 2001; Shaked et al. 2005; Maldonado et al. 2006). Reductase systems have been most thoroughly investigated because they are the major method of iron acquisition in the yeast *Saccharomyces cervisiae*, a model unicellular eukaryote, but it is very possible that marine organisms have additional uptake pathways adapted to acquire the forms of iron present in the ocean.

Bacteria use siderophore-based uptake mechanisms, excreting these small iron binding compounds which complex iron in the environment, diffusing back to the bacterium for internalization (Nielands 1995). Siderophores were first discovered in pathogenic bacteria which must acquire iron from host proteins, but they are abundant in bacteria from diverse environments including the soil and ocean. Their role in the ocean is not well understood since the dilute nature of the environment would greatly decrease the chance that an excreted siderophore would return to a bacterium capable of using it (Volker and Wolf-Gladrow 1999). However, it may be that siderophores are primarily used by bacteria colonizing particles in the water, where the richer environment could support a greater density of bacteria and allow a greater portion of siderophores to be successfully utilized (Haygood et al. 1993).

Bacteria are also known to have specific transport systems for heme, an abundant form of iron in the host organisms of pathogenic and symbiotic bacteria where these transporters have been best studied. Heme is also likely to be a major form of iron in phytoplankton since photosynthetic proteins are especially rich in heme. Data from iron limited phytoplankton indicate heme would make up 45% of total iron, and recent

measurements of iron replete phytoplankton measured heme as 3-10% of total iron (Strzepek and Harrison 2004; Gledhill 2007). Because heme is relatively hydrophobic and photosensitive it is not likely to make up a significant portion of dissolved iron, but the ability to access heme iron would be beneficial for those bacteria living in close association with phytoplankton or detritus, and perhaps for bacteria in more productive environments where grazing and cell lysis might release heme transiently into the environment. A few studies have investigated the ability of marine bacteria to take up heme and iron bound by other porphyrins (Hutchins, et al. 1999), but the mechanisms involved were not elucidated. The wider use of molecular techniques and availability of genome sequences now allows more thorough characterization of the iron transport capabilities of marine bacteria. In this thesis physiological, molecular, and genomic techniques are employed to investigate heme uptake in marine bacteria, allowing a better understanding of iron cycling in the ocean.

Organization of the dissertation

This dissertation explores varied consequences of the localization of iron in photosynthetic proteins at organismal and environmental levels. The field work presented expands our understanding of the role of iron the oceans and its interaction with light availability, examines iron distributions and speciation in a region where iron-light co-limitation was observed, and contributes to the goal of developing diagnostics of iron stress. The bioavailability and cycling of heme, which is heavily used in photosynthetic proteins, is better defined though studies of a model bacterium and bioinformatic analyses. The work is organized into 5 subsequent chapters:

Chapter II: describes investigations into the roles of iron and light limitation in subsurface chlorophyll maxima outside of classically iron limited regions. Using shipboard iron and light manipulation experiments phytoplankton responses characteristic of iron-light co-limitation were seen at subsurface chlorophyll maxima in the Southern California Bight and the Eastern Tropical North Pacific.

Chapter III: presents results from a study of natural iron fertilization in the southern Drake Passage near the Antarctic Peninsula. Iron addition incubations conducted across a transition from iron limited to iron replete waters helped provide evidence that natural iron fertilization was actually occurring. Relating incubation responses to in-situ photosynthetic properties allowed identification of diagnostics of iron stress.

Chapter IV: discusses iron speciation and distribution in a suboxic zone and the overlying surface waters in the Eastern Tropical North Pacific, where iron light co-limitation was observed. Of particular interest are the measurements of iron(II) in suboxic waters using a sensitive chemiluminescence technique.

Chapter V: describes a study of heme uptake systems in marine bacteria. Physiological characterization of heme uptake was undertaken in the bacterium *Microscilla marina* and a putative heme transport system was identified in the genome of this organism. The genomes of numerous additional marine bacteria were searched for putative heme

transport systems to better understand the distribution of heme uptake capabilities and the cycling of heme in the ocean.

Chapter VI: concludes the thesis summarizing results presented and their significance. The discoveries made in this thesis suggest future work which might be carried out, and these possibilities are discussed in the final chapter.

References

Barbeau, K., E.L. Rue, K.W. Bruland, and A. Butler. 2001. Photochemical cycling of iron in the surface ocean mediated by microbial iron(III)-binding ligands. Nature **413:** 409-413.

Behrenfeld, M.J., and Z.S. Kolber. 1999. Widespread iron limitation of phytoplankton in the South Pacific Ocean. Science **283:** 840-843.

Behrenfeld, M.J., K. Worthington, R.M. Sherrell, F.P. Chavez, P. Strutton, M. McPhaden, and D.M. Shea. 2006. Controls on tropical Pacific Ocean productivity revealed through nutrient stress diagnostics. Nature **442:** 1025-1028.

Boyd, P.W., A.C. Crossley, G.R. DiTullio, F.B. Griffiths, D.A. Hutchins, B. Queguiner, P.N. Sedwick, and T.W. Trull. 2001. Control of phytoplankton growth by iron supply and irradiance in the subantarctic Southern Ocean: Experimental results from the SAZ project. J. Geophys. Res. **106:** 31,573-31,583.

Cullen, J.J. 1991. Hypotheses to explain high-nutrient conditions in the open sea. Limnol. Oceanogr. **36:** 1578-1599.

Duce, R.A. and N.W. Tindale. 1991. Atmospheric transport of iron and its deposition in the ocean. Limnol. Oceangr. **36:** 1715-1726.

Frost, B.W. 1991. The role of grazing in nutrient-rich areas of the open sea. Limnol. Oceanogr. **36:** 1616-1630.

Gledhill, M. 2007. The determination of heme b in marine phyto- and bacterioplankton. Mar. Chem. **103:** 393-403.

Greene, R.M., R.J. Geider, and P.G. Falkowski. 1991. Effect of iron on photosynthesis in a marine diatom. Limnol. Oceanogr. **36:**1772-1782.

Greene, R.M., R.J. Geider, Z. Kolber, and P.G. Falkowski. 1992. Iron-induced changes in light harvesting and photochemical energy conversion processes in eukaryotic marine algae. Plant. Phys. **100:** 565-575.

Haygood, M.G., P.D. Holt, andn A. Butler. 1993. Aerobactin production by a planktonic marine *Vibrio* sp. Limnol. Oceanogr. **38:** 1091-1097.

Ho, T.Y., A. Quigg, Z.V. Finkel, A. Milligan, K. Wyman, P.G. Falkowski, and F.M.M. Morel. 2003. The elemental composition of some marine phytoplankton. J. Phycol. **39:** 1145-1159.

Hong, H., and D.R. Kester. 1986. Redox state of iron in the offshore waters of Peru. Limnol. Oceanogr. **31:** 512-524.

Hutchins, D.A., A.E. Witter, A. Butler, and G.W. Luther III. 1999. Competition among marine phytoplankton for different chelated iron species. Nature **400:** 858-861.

Johnson, K.S., F.P. Chavez, and G.E. Friederich. 1999. Continental-shelf sediment as a primary source of iron for coastal phytoplankton. Nature **398:** 697-700.

Johnson, K.S., V.A. Elrod, S.E. Fitzwater, J.N. Plant, F.P. Chavez, S.J. Tanner, R.M. Gordon, D.L. Westphal, K.D. Perry, J. Wu, and D.M. Karl. 2003. Surface ocean-lower atmosphere interactions in the Northeast Pacific Ocean gyre: aerosols, iron and the ecosystem response. Global Biogeochem. Cycles **17:** doi:10.1029/2002GB002004.

Johnson, K.S., R.M. Gordon, and K.H. Coale. 1997. What controls dissolved iron concentrations in the world ocean? Mar. Chem. **57:** 137-161.

Kolber, Z.S., R.T. Barber, K.H. Coale, S.E. Fitzwater, R.M Greene, K.S. Johnson, S. Lindley, and P.G. Falkowski. 1994. Iron limitation of phytoplankton photosynthesis in the equatorial Pacific Ocean. Nature **371:** 145-149.

Kolber, Z.S., O. Prasil, and P.G. Falkowski. 1998. Measurements of variable chlorophyll fluorescence using fast repetition rate techniques: defining methodology and experimental protocols. Biochim. Biophys. Acta **1367:** 88-106.

Krause, G.H. and E. Weis. 1991. Chlorophyll fluorescence and photosynthesis: the basics. Annu. Rev. Plant Physiol. Plant Mol. Biol. **42:** 313-349.

LaRoche, J., P.W. Boyd, R.M.L. McKay, and R.J. Geider. 1996. Flavodoxin as an in situ marker for iron stress in phytoplankton. Nature **382:** 802-805.

Liu, X. and F.J. Millero. 1999. The solubility of iron hydroxide in sodium chloride solutions. Geochim. Cosmochim. Acta **63:** 3487-3497.

Maldonado, M.T., A.E. Allen, J.S. Chong, K. Lin, D. Leus, N. Karpenko, and S.L. Harris. 2006. Copper-dependent iron transport in coastal and oceanic diatoms. Limnol. Oceanogr. **51:** 1729-1743.

Maldonado, M.T., P.W. Boyd, P.J. Harrison, and N.M. Price. 1999. Co-limitation of phytoplankton growth by light and Fe during winter in the NE subarctic Pacific Ocean. Deep-Sea Res. II. **46:** 2475-2485.

Maldonado, M.T., and N.M. Price. 2001. Reduction and transport of organically bound iron by *Thalassiosira oceanica* (Bacillariophycaea). J. Phycol. **37:** 298-309.

Martin, J.H., and S.E. Fitzwater. 1988. Iron deficiency limits phytoplankton growth in the north-east Pacific subarctic. Nature **331: 341-343.**

Martinez, J.S., G.P. Zhang, P.D. Holt, H.T. Jung, C.J. Carrano, M.G. Haygood, A. Butler. 2000 Self-assembling amphiphilic siderophores from marine bacteria. Science **287:** 1245-1247.

Neilands, J.B. 1995. Siderophores: structure and function of microbial iron transport compounds. J. Biol. Chem. **45:** 26723-26726.

Raven, J.A. 1990. Predictions of Mn and Fe use efficiencies of phototrophic growth as a function of light availability for growth and of C assimilation pathway. New Phytol. **116:** 1-18.

Rue, E.L., and K.W. Bruland. 1995. Complexation of iron(III) by natural organic ligands in the Central North Pacific as determined by a new competitive ligand equilibrium/adsorptive cathodic stripping voltammetric method. Mar. Chem. **50:** 117-138.

Rue, E.L., and K.W. Bruland. 1997. The role of organic complexation on ambient iron chemistry in the equatorial Pacific Ocean and the response of a mesoscale iron addition experiment. Limnol. Oceanogr. **42:** 901-910.

Saito, M.A., D. Sigman, F.M.M. Morel. 2003. The bioinorganic chemistry of the ancient ocean: the co-evolution of cyanobacterial metal requirements and biogeochemical cycles at the Archean-/Proterozoic boundary? *Inorganica Chimica Acta,* **356C**: 308-318.

Schroder, I., E. Johnson, S. de Vries. 2003. Microbial ferric iron reductases. FEMS Microbiol. Rev. **27:** 427-447.

Shaked, Y., A.B. Kustka, and F.M.M. Morel. 2005. A general kinetic model for iron acquisition by eukaryotic phytoplankton. Limnol. Oceanogr. **50:** 872-882.

Strzepek, R.F., and P.J. Harrison. 2004. Photosynthetic architecture differs in coastal and oceanic diatoms. Nature **431:** 689-692.

Sunda, W.G., and S.A. Huntsman. 1997. Interrelated influence of iron, light and cell size on marine phytoplankton growth. Nature **390:** 389-392.

Van den Berg, C.M.G., 1995. Evidence for organic complexation of iron in seawater. Mar. Chem. **50:** 139-157.

Volker, C., and D.A. Wolf-Gladrow. 1999. Physical limits on iron uptake mediated by siderophores or surface reductases. Mar. Chem. **65:** 227-244.

Wu, J., Boyle, E., Sunda, W., Wen, L-S., 2001. Soluble and colloidal iron in the oligotrophic North Atlantic and North Pacific. Science **293:** 847-849.

Wu, J. and G.W. Luther. 1996. Spatial and temporal distribution of iron in the surface water of the northwestern Atlantic Ocean. Geochim. Cosmochim. Acta. **60:** 2729-2741.

II

Interactions between iron and light limitation of phytoplankton at subsurface chlorophyll

maxima in the eastern Pacific

Abstract

The roles of iron and light as limiting and co-limiting factors for phytoplankton growth in subsurface chlorophyll maxima (SCMs) were investigated in mesotrophic to oligotrophic waters of the Southern California Bight and the Eastern Tropical North Pacific using microcosm manipulation experiments. Phytoplankton responses indicative of iron-light co-limitation were found at several SCMs underlying macronutrient limited surface waters in the eastern Pacific. In all experiments responses to iron were observed at elevated light. Iron additions led to a shift in the size and taxonomic structure of the phytoplankton community with large diatoms dominating what was formerly a diverse community of relatively small phytoplankton. The strongest and most ubiquitous responses to iron were found at elevated light, indicating that iron limitation may be especially acute when light levels change rapidly as occurs during eddy events or with strong internal waves. The results show iron influences phytoplankton community structure at SCMs, with consequences for nutrient cycling and carbon export within the lower euphotic zone.

Introduction

It is now well established that iron can control phytoplankton biomass and productivity in High Nutrient- Low Chlorophyll (HNLC) regions, where unused macronutrients are persistently present in surface waters. More recently, the importance of iron availability for phytoplankton has been shown in waters outside of HNLC areas. In coastal upwelling zones, rapid movement of high macronutrient waters into the well-lit

surface layer results in iron limitation when no supplemental iron sources from continental shelf or riverine inputs are available (Hutchins et al. 1998). Such conditions are common off the dry, steep coastlines which characterize major upwelling areas along the coasts of western North and South America, leading to frequent iron limitation in these waters (Hutchins et al. 1998, 2002). In the tropical north Atlantic, nitrogen generally limits phytoplankton growth, but iron, along with phosphorus, limits the rate of nitrogen fixation, indirectly constraining phytoplankton biomass (Mills et al. 2004). It has been speculated that iron may be an important control on nitrogen fixation throughout the oceans due to the high iron requirement of nitrogenase, the key enzyme responsible for the conversion of N_2 to ammonia.

While the nitrogenase enzyme is a significant iron demand for nitrogen fixers, for most photosynthetic organisms the primary use of iron is in photosynthetic proteins (Raven 1990). In marine phytoplankton, recent measurements of iron allocation in the diatoms *Thalassiosira weissflogii* and *T. oceanica* have shown that nearly all cellular iron is localized in photosynthetic light harvesting and electron transport proteins under low iron conditions (Strzepek and Harrison 2004). That this may be true for many phytoplankton taxa is suggested by the increased iron quotas and lowered iron use efficiencies observed in other diatom and dinoflagellate species in response to decreased light levels (Sunda and Huntsman 1997). The increased iron requirements at lower light provide evidence that photosynthetic needs are dictating iron quotas, and for *T. weissflogii* and *T. oceanica*, it has been demonstrated that this is the case (Strzepek and Harrison 2004). The observation that iron requirements increase as light decreases, likely driven by photosystem requirements, has led to the hypothesis that phytoplankton may be

co-limited by iron and light in low light environments (Sunda and Huntsman 1997). In an iron-light co-limited state, growth and photosynthesis are ultimately limited by light processing, but production of photosynthetic proteins required to harvest and process light is constrained by iron availability (Fig. 2.1). It was hypothesized that iron-light co-limitation may occur in low iron regions with deep mixed layers, such as the Southern Ocean, or even in macronutrient-limited, stratified waters, near the base of the euphotic zone (Sunda and Huntsman 1997).

Field research into interactions between iron and light availability has focused on classic HNLC regions in the subarctic North Pacific and the Southern Ocean. Experiments in these regions have shown that limitation or co-limitation by iron and light depends on the local environmental conditions, and high-latitude HNLC regions should not be thought of as exclusively iron limited. An example of iron-light co-limitation was found during the winter in the subarctic North Pacific, where a deep mixed layer (80 m), low incident irradiance, and lack of available iron combined to limit photosynthesis, maintaining low phytoplankton biomass (Maldonado et al. 1999). In the region of the Subantarctic front, it was determined that iron limited growth in an area with a relatively shallow (40 m) mixed layer, but light, in conjunction with iron, controlled growth in an area with deeper (90 m) mixed layers (Boyd et al. 2001). While these studies show iron-light interactions are likely important to consider in high-latitude HNLC regions, there have been no field experiments to assess the potential effect of iron-light co-limitation in the lower euphotic zone in stratified, macronutrient limited waters.

The surface mixed layer is the most accessible strata of the ocean, both to ships and satellites, and often the most productive layer of water columns, but important

biological processes occur within the lower euphotic zone. Through vertical transport mechanisms, new nutrients are introduced and first biologically utilized in the lower euphotic zone, and so ecosystem processes within this layer can affect the fate of newly available nutrients as they are transported toward surface waters. In many water columns the lower region of the euphotic zone is characterized by a subsurface chlorophyll maximum, generally a site of high phytoplankton biomass and productivity, and carbon export (Cullen 1982; Coale and Bruland 1987). SCMs are generated at the interface of the nutrient and light limited portions of the water column, and phytoplankton growth within the SCM is sensitive to adequate acquisition of both light and nutrients (Fig. 2.2.; Cullen 1982; Fennel and Boss 2003).

Knowing the physiological link between iron availability and photosynthesis, we sought to investigate the significance of iron and light as limiting and co-limiting factors within SCMs. Although nitrate is likely to limit growth in the upper portions of the SCM, we suspected that iron may be an important factor deeper in the SCM as light levels decrease and nitrate levels increase, relieving nitrogen stress but exacerbating iron demands (Fig. 2.2). Iron may be especially scarce in this layer when the ferricline is deeper than the nitracline, as is frequently observed (Johnson et al. 1997*b*). Microcosm experiments in which iron and light levels were manipulated were conducted in the southern California Bight and the Eastern Tropical North Pacific. These experiments were used primarily to understand factors limiting the growth and abundance of various phytoplankton in the SCMs, but they may also provide information on the effect of natural iron and light perturbations on the SCM community. Analysis of community responses to changes in light and iron levels suggested that iron-light co-limitation may

be occuring in certain SCMs. In all experiments significant effects of iron were observed when light limitation was relieved. These results provide insight into the likely response of SCM communities to changes in iron or light availability, due to dust inputs of iron, or variability in light levels from doming of isopycnals by upwelling eddies or changes in cloud cover.

Methods

Incubation setup

Incubation experiments were conducted on two cruises in the Southern California Bight (SCB) in November of 2004 aboard the R/V Roger Revelle (incubations denoted RR) and May of 2006 aboard the R/V Knorr (KN incubations), and in the Eastern Tropical North Pacific (ETNP) on an R/V New Horizon cruise in November of 2003 (NH incubation). Locations in the SCB and ETNP where waters were collected for incubation experiments are shown in Fig. 2.3. At each station, water was collected using 12 or 30 L trace metal clean GO-Flo bottles attached to a non-metallic line. Depths for water collection were chosen based on water-column profile data obtained from a CTD cast immediately prior to the GO-Flo cast. The top of the nitracline (1 - 6 μmol L^{-1} NO$_3^-$), within the SCM was targeted as a likely region to find iron stress, since nitrogen limitation was not expected to occur in this layer and light levels were low but still high enough to support phytoplankton growth. Once recovered on-deck, GO-Flo bottles were pressurized with 0.4 μm filtered ultra- high purity nitrogen gas, and water was dispensed within a class-100 laminar flow bench into acid-washed 2.7 or 4 L polycarbonate incubation bottles through acid-cleaned Teflon tubing without pre-screening. Multiple 12

L GO-Flos were required to setup a single incubation, in which case incubation bottles were filled equally from each GO-Flo to ensure uniform initial conditions. Incubations were conducted either in shaded, flow-through, on-deck incubators or, indoors in a temperature-controlled incubator set to 14 ºC to approximate in situ temperatures (13-14 ºC) (Table 2.1). When placed in the flow-through incubators, bottles were sealed in plastic bags to prevent trace metal contamination.

<u>Iron and light manipulations</u>

Filled incubation bottles were randomly assigned in duplicate to the 4 experimental treatments: control (C), added iron (+Fe), increased light (+L), added iron and increased light (+Fe+L). Five nmol L^{-1} iron additions were made during incubation setup from an acidic 100 µmol L^{-1} $FeCl_3$ stock solution. Ambient light levels at the depth of water collection were determined from Photosynthetically Active Radiation (PAR) profiles collected on CTD casts immediately prior to GO-Flo casts for incubation setup. To set light levels for on-deck incubations (NH1, RR4), PAR measurements at depth were converted to percent surface irradiance, and an incubator was shaded with neutral density screening to match this level with the aid of a Biospherical QSL-100 light meter. The lack of spectral correction in these outdoor incubations could potentially impact phytoplankton growth and community structure (Wood et al. 1998). Maximum noon-time irradiances for these treatments were 15-30 µmol photons m^{-2} s^{-1}. A separate incubator was shaded at 3-10 fold higher light level, with maximum noon-time irradiances of 110-130 µmol photons m^{-2} s^{-1}, for increased light treatments. For indoor incubations, the top level of the incubator, closest to the fluorescent lights, was used for high light treatments, and the lower level was used to mimic ambient light levels at depth. Blue stage gels were

used for shading, to achieve desired light intensities and approximate the spectral

distribution of light at depth. The light intensities in the lower level of the incubator were

set to approximately 75% of the maximal noon time irradiance experienced at depth (12-

30 μmol photons m^{-2} s^{-1}), while the upper level was set 3-9 fold higher, at 75-100 μmol

photons m^{-2} s^{-1}. Lights were set to turn on and off at sunrise and sunset, with a half-hour

period in which only half of the lights were on, just after sunrise and prior to sunset.

Details of light intensities for each experiment are given in Table 2.1.

Chlorophyll a (Chl a)

Approximately 100 mL of water was gently filtered onto a GF/F filter, and

extracted for 24 hours in 90% acetone:10% water at 0 - 4 $^{\circ}$C . Fluorescence of the extract

was measured on a Turner 10-AU fluorometer (10-037R filter set) before and after

acidification to determine Chl a (Strickland and Parsons 1972). Eight μm polycarbonate

filters were used to determine size-fractioned Chl a (>8 μm Chl a). Chl a was used to

track phytoplankton growth in the experiments and net Chl a growth rates were

determined by linear regression through natural log transformed Chl a data from the

period of active growth (at least 3 time points) in each experiment. These growth rates

include only increases in excess of grazing rates, which were not assessed, and the

relationship between intrinsic and net growth rates in the experiments is unknown.

Nutrients

Unfiltered water samples were collected in sterile centrifuge tubes and frozen for

later analysis of macronutrients to determine the course of their drawdown during

incubations. Macronutrients (NO_3^-, NO_2^-, PO_4^{3-}, and Si) were determined using standard

colorimetric methods by the Ocean Data Facility at Scripps Institution of Oceanography, or the MSI Analytical Lab at UC Santa Barbara.

Dissolved iron

For iron measurements, water from the GO-Flo bottles used to setup incubations was filtered through an in-line 0.4 μm filter, and stored acidified (pH = 1.8) until analyzed. Iron concentrations from incubations NH1, RR1, RR3, and RR4 were measured by cathodic stripping voltammetry using the 2-(2-thiazolylazo)-*p*-cresol (TAC) ligand method described by Croot and Johansson (2000). Cleaned EPPS buffer was added to water samples to a final concentration of 10 mmol L^{-1}, and the pH of the solution was brought to 8.0 using isothermally distilled ammonia. TAC was then added to 10 μmol L^{-1} and the sample was analyzed on a Metrohm VA663 mercury electrode interfaced to an EcoChemie Autolab PGSTAT30 using a linear sweep waveform. Iron was quantified by 4 standard additions to each sample.

For incubations RR2, KN1, and KN2, iron concentrations were measured with a chemiluminescence detection flow injection analysis system (Bowie et al. 1998; King and Barbeau 2007). Sulfite (2 μmol L^{-1}) was used to reduce all iron in the seawater samples to iron(II), which was then concentrated on a nitriloacetic acid resin column. Iron(II) was eluted from the column with an HCl carrier solution (0.14 mol L^{-1}) and mixed with a basic luminol-ammonia solution to initiate the chemiluminescent reaction for quantification of iron. We have verified the accuracy of our implementations of the TAC electrochemical method and the chemiluinescence method through analysis of the SAFe iron standards. Details of the SAFe standard analyses and additional information on these methods are available in Hopkinson and Barbeau (2007) and King and Barbeau (2007).

POC and PON

Particulate organic carbon (POC) and particulate organic nitrogen (PON) were determined by combustion analysis. Water samples were filtered onto precombusted (450 ºC for 4 hours) GF/F filters and stored in liquid nitrogen. Samples were exposed to fuming HCl overnight to remove inorganic carbon, dried overnight in an oven at 60 ºC, and subsequently analyzed on a Costech 4010 elemental combustion system at the Scripps Institution of Oceanography Analytical Facility.

Pulse amplitude modulated (PAM) fluorometry

Phytoplankton variable fluorescence measurements to assess the quantum yield of photosystem II (PSII) were made using a Walz Xe-PAM fluorometer (Schreiber et al. 1995). Phytoplankton were dark acclimated for approximately half an hour prior to measurement. Probe flashes (2 Hz) from a Xenon lamp were passed through a blue filter (Schott BG39), and further attenuated with a 10% "attenuator" diaphragm plate. Seven hundred ms pulses of actinic light (> 3000 µmol quanta m^{-2} s^{-1}) to saturate photosystem components were supplied by a halogen lamp at 30 s intervals to allow reoxidation of reaction centers and the plastiquinone pool between pulses. Emitted chlorophyll fluorescence was passed through long pass (RG645) and dichroic (R65) filters and measured with a photodiode detector. The described instrument configuration was checked periodically throughout cruises to ensure Xenon flashes were not strongly actinic, and that saturating pulses allowed maximal fluorescence emission to be reached. Initial fluorescence levels (F_o), obtained from the probe flashes alone, and maximal fluorescence (F_m), measured during application of the saturating pulses, were used to calculate F_v:F_m as (F_m-F_o)/F_m.

HPLC pigment analysis

Taxonomically informative phytoplankton pigments were analyzed by high-performance liquid chromatography (HPLC) using a modified version of the method described in Goericke and Montoya (1998). Water samples (~1 L) were gently filtered onto GF/F filters and stored in liquid nitrogen until analyzed. Filters were extracted on ice in 1.5 mL acetone for 0.5 hours, homogenized, and allowed to extract for a further 0.5 hours. Following centrifugation, portions of the extract were mixed with water to produce a 60:40 acetone:water solution, and immediately injected in the HPLC system. Pigments were separated on a 10 cm Alltech Adsorbosphere C8 column, using a gradient between methanol: 0.5 mol L^{-1} aqueous ammonium acetate (75:25) and methanol. Chromatographic peaks were identified by retention time, and quantified by peak area using calibrations determined from pure pigments isolated from algal cultures. This method allows separation of Chl *a* and divinyl Chl *a*, and most of the abundant carotenoids. Lutein and zeaxanthin coelute with this method, but the fraction is referred to as zeaxanthin since it is generally most abundant in oceanic samples.

Phytoplankton cell counts

Microscopic examination of phytoplankton communities from the experiments was conducted to determine the taxa and size of phytoplankton responding to treatments. Fifty mL samples were preserved with ~1 mL sodium borate buffered formalin, concentrated in an Utermohl settling chamber, and counted on an inverted microscope using an ocular micrometer to measure cell sizes. Phytoplankton were classified based on Tomas et al. (1997) into broad, but clearly identifiable groups. At least 100 cells in each group were counted in a sample. The most abundant groups identified were species of

Pseudonitzschia, *Nitzschia*, and *Chaetoceros*, as well as coccolithophores and a miscellaneous class of small pennate diatoms.

Phytoplankton community structure

Pigment signatures and microscopic cell counts were used to assess phytoplankton community structure in incubation experiments. Good agreement was found between the methods where comparisons were possible, providing confidence in their utility as indicators of phytoplankton community structure. While fucoxanthin is present in a number of phytoplankton taxa, a strong correlation between fucoxanthin ($r^2 =$ 0.89, $p < 0.0001$; n = 59) and diatom cell numbers shows diatoms were the major contributors to fucoxanthin concentrations in the experiments. Similarly a strong correlation between coccolithophore numbers and 19-hexanoyloxyfucoxanthin (19-hex) ($r^2 = 0.81$, p < 0.0001, n = 57) indicates coccolithophores are predominately contributing to 19-hex concentrations. Rarely coccolithophores have been reported to produce 19-butanoyloxyfucoxanthin (19-but) (Jeffrey and Wright 1994), but we found only a weak relationship between 19-but and coccolithophore numbers ($r^2 = 0.22$, $p < 0.001$, n = 57). Dominant contributors of 19-but are often *Phaeocystis* sp. or pelagophytes (Jeffery and Wright 1994; Anderson et al. 1996), and while a few *Phaeocystis* colonies were observed in RR1 they were absent from other samples. 19-but is therefore tentatively attributed to pelagophytes. Because cyanobacteria are not enumerable by the microscopic method used, no comparisons can be made with pigment data. However, divinyl Chl *a* (dvChl *a*) can be unambiguously attributed to *Prochlorococcus*.

Statistics

Statistical analyses were conducted on experimental results with JMP 5.1

statistical software (SAS Institute) using tests appropriate for the questions addressed.

The effect of each treatment on Chl *a* growth rate, nitrate drawdown, POC content,

$F_v:F_m$, and %> 8um Chl *a* was assessed using one-way ANOVA and post-hoc Tukey-

Kramer tests. Although these tests assume equal variance among treatments, it was clear

that variance was generally lower in ambient light treatments where less growth occurred.

Consequently selected data from the ambient light treatments was retested without high

light data using one-way ANOVA as noted. To determine whether there was a significant

interaction between iron and light two-way ANOVAs with light and iron as independent

factors were conducted. To assess the effect of iron on Chl *a* and fucoxanthin

concentrations at each light level, Student's *t*-tests were employed. Despite low

replication of each treatment (n = 2) statistical significance ($p < 0.05$) of experimental

results was generally found.

Results

In this first attempt to study iron-light co-limitation at SCMs, we sought to assay a

variety of water columns, from mesotrophic to oligotrophic regions, and sample through

the strong gradients present within SCMs. All experiments showed some characteristic

responses of growth rate, changes in phytoplankton community structure, and physiology

to iron addition though each incubation response was unique in some way. In some

experiments phytoplankton responses to iron were observed at ambient light levels, and

in these experiments strong, immediate responses to iron at elevated light were also

observed (experiments NH1, RR1, RR2, KN1; Table 2.3). In other experiments no

responses were observed at ambient light, but responses to iron were observed in elevated

light treatments after some nutrient drawdown had occurred (experiments RR3, RR4,

KN2; Table 2.3). The differential responses are likely a consequence of varying initial

conditions and stresses between and within the SCMs sampled, potentially depending on

factors which are difficult to constrain in the present study such as the history of each

feature. However, when observed, responses of phytoplankton physiology and

community structure to iron addition were generally similar throughout the experiments,

as discussed in more detail in the following sections.

Initial conditions

Iron and light manipulation experiments were conducted at SCMs in mesotrophic

to oligotrophic waters of the SCB and ETNP. In the SCB where oceanic domains have

been better defined RR1 and RR3 were conducted within the coastal domain while all

other incubations were collected from offshore sites (Fig. 2.3, Hayward and Venrick

1998). All SCMs sampled in this study were also biomass maxima, as indicated by

transmissometer data (data not shown), as opposed to purely Chl a maxima produced by

photoacclimation as often occurs in oligotrophic gyres (Cullen 1982). Water for

experiments was collected from within the SCM, near the top of the nitracline, with

initial Chl a ranging between 0.34-0.92 µg L^{-1}, NO$_3^-$: 0.7-6.3 µmol L^{-1}, dissolved Fe:

0.11-0.32 nmol L^{-1}, and ambient light levels: 0.5-1.2 % surface irradiance (Table 2.1). A

representative water column profile from the station where NH1 was initiated is shown in

Fig. 2.4. This profile demonstrates the relationship between the nitracline and SCM

common to all sites in this study, and shows the approximate gradient of the nitracline at

our study sites. Although the nitracline is relatively steep, we were successful in

capturing the top of it in most incubations (Table 2.1). With the exception of KN1,

phytoplankton communities were typical of those commonly found in the study regions

(Venrick 1998, 2000). At the site of KN1, phytoplankton species at the SCM were typical

of offshore communities, but present at elevated abundances relative to historical data

(*see* Discussion).

Chl a: Concentrations and growth rates

One incubation experiment from the ETNP (NH1) and two from the SCB (RR2,

KN1) showed increases in Chl *a* concentrations and Chl *a* derived growth rates in

response to increased iron at both ambient and elevated light. In these experiments +Fe

and +L treatments resulted in moderate increases in Chl *a* concentrations, but a strong,

synergistic effect of increased iron and light (+Fe+L) led to dramatic increases in Chl *a*

and net phytoplankton growth rates (Fig. 2.5A; Tables 2.2, 2.3). Separation of iron

addition treatments from their respective controls (C, +L) occurred immediately after

growth began. In RR1, an immediate response to iron was seen at elevated light, and

although at ambient light no significant Chl *a* response to iron was seen, responses to iron

were observed in other parameters (Tables 2.2, 2.3, *see* below). In the remainder of the

incubations (RR3, RR4, KN2) no differences between ambient light treatments were

observed in Chl *a* concentrations or growth rates, but at elevated light Chl *a* growth in

+Fe+L treatments eventually outpaced +L treatments, after an initial period in which the

treatments tracked each other (Fig. 2.5B; Tables 2.2, 2.3). Interpretation of Chl *a* results

as a proxy for phytoplankton biomass and growth rate is complicated by differences in

phytoplankton carbon (C):Chl *a* ratios between treatments. As indicated by POC:Chl *a*

(g:g) ratios within our experiments (+Fe+L: 44-51; +L: 77-123), iron stress generally

increases C:Chl, as does higher light intensity (Geider et al. 1998). Additionally, because Chl *a* is a community parameter calculated net community growth rates reflect both growth in response to treatments, and loss by grazing or cell death, particularly of cyanobacteria (*see* below), which may lead to an early drop in Chl *a* in some incubations and lowers net growth rates in these experiments (Fig. 2.5A).

<u>Nutrient drawdown</u>

The macronutrients NO_3^-, NO_2^-, PO_4^{3-}, and Si were measured daily in each incubation, but the results presented will focus on NO_3^- since it was depleted first in incubations where complete nutrient drawdown was reached. At elevated light, nitrate drawdown generally followed Chl *a* increases with faster rates of drawdown occurring in +Fe+L treatments immediately (NH1, RR1, RR2, KN1; Fig. 2.5C), or after some nutrient drawdown occurred and responses to iron were observed in Chl *a* (RR3, RR4, KN2; Fig. 2.5D). Nearly complete drawdown of nitrate was observed in many +Fe+L treatments at which point incubations were harvested to avoid "crashing" of incubations when nutrient exhaustion leads to phytoplankton senescence. Although diatoms came to dominate +Fe+L treatments (*see* below) Si was only exhausted in RR1 concomitantly with nitrate, and remained at concentrations >1 μmol L^{-1} in all other experiments (data not shown). $NO_3^-:PO_4^{3-}$ drawdown ratios approximated Redfield ratios and were not different between treatments (+Fe+L: 15 ± 4; +L: 15 ± 3). Si:NO_3^- drawdown ratios varied widely among experiments and treatments reflecting primarily the abundance of diatoms in each sample, as opposed to the effects of iron on silicification which have been documented (data not shown; Hutchins et al. 1998).

In ambient light treatments, changes in nitrate were generally small but measurable (Table 2.2), though changes in other macronutrients were not resolved (data not shown). No significant differences between treatments were seen. In experiments where differences in Chl a concentration were seen at ambient light (NH1, RR2) expected differences in nitrate drawdown would be relatively small (NH1: 0.1-0.2; RR2: 0.08-0.15; μmol L^{-1} NO_3^-) based on the ratio of nitrate drawdown to Chl a increases observed in elevated light treatments (+Fe+L: 0.6 ± 0.2; +L: 1.2 ± 0.3; μmol L^{-1} NO_3^-: μg Chl a L^{-1}) and maximal Chl a differences between +Fe and control treatments (NH1: 0.16; RR2: 0.13; μg Chl a L^{-1}). However, these differences, especially for NH1, are potentially resolvable and the lack of significant differences in nitrate drawdown suggests some of the Chl a increase in +Fe treatments was due to increasing cellular Chl a quotas after iron addition rather than an increase in phytoplankton biomass.

<u>POC and PON</u>

Initial POC data from several incubations (RR2: 3.4 μmol L^{-1}; KN1: 7.6 μmol L^{-1}) show that only small increases occurred in +Fe and control treatments but significant growth occurred in elevated light treatments (Table 2.2). At ambient light, significantly higher POC concentrations were only observed in +Fe treatments of incubations KN1 and RR4, although because no other responses to iron were observed at ambient light for RR4 this measurement is apparently an anomaly. At elevated light, POC concentrations in +Fe+L treatments were approximately double those of +L treatments, except for RR2 where POC concentrations were similar in both treatments. These observations are consistent with nitrate drawdown in each incubation. In RR1 and RR2, ratios of POC increase: PON increase in +Fe+L treatments (RR1: 12.5; RR2: 10.5 μmol L^{-1}: μmol L^{-1})

were higher than +L treatments (RR1: 8.4; RR2: 7.0), and in excess of expected Redfield

ratios (6.6). In other incubations no differences were seen between +Fe+L and +L

treatments and ratios were closer to Redfield values (+Fe+L: 7.2 ± 0.4; +L: 7.3 ± 1.2).

The previous calculations assume initial POC values were similar to final control

treatment concentrations since initial POC data is lacking for most incubations, but

similar trends are observed in final POC/PON ratios despite the possible complications

from detrital material (RR1 +Fe+L: 9.9, +L: 7.2; RR2 +Fe+L: 8.6, +L: 6.6).

F_v:F_m

PAM fluorometric measurements of F_v:F_m, the maximum efficiency of light

utilization in PSII, were collected daily on all incubations except NH1 (Fig. 2.6; Table

2.4). At ambient light, F_v:F_m remained constant or increased moderately in controls, and

had significantly higher values in +Fe treatments in RR2 and KN1 indicating higher iron

availability led to an increase in photosynthetic efficiency in these incubations where

responses to iron were observed in other parameters at ambient light (Fig. 2.6A; Table

2.4). In RR1, F_v:F_m was also elevated in +Fe treatments compared with controls though

the result was not statistically significant. In experiments RR3, RR4, and KN2 no

differences in F_v:F_m were observed between control and +Fe treatments (Fig. 2.6B; Table

2.4). When light was elevated, F_v:F_m declined relative to initial values in +L treatments in

all experiments for which data is available, but remained constant or increased slightly in

+Fe+L treatments. In incubations where immediate declines in F_v:F_m are observed in +L

treatments a portion of this response may be due to photoinhibition, but the continued

decline of F_v:F_m in +L treatments as growth proceeds is likely caused by increasing iron

stress as available iron is consumed (Fig. 2.6A). In other experiments the drops are

coincident with separation between +L and +Fe+L treatments in several variables indicating Fe stress is the major factor reducing F_v:F_m (Fig. 2.6B). Although nitrate concentrations were low at the start of some experiments, and nearly exhausted in many +Fe+L treatments, no dramatic declines in F_v:F_m were observed in the +Fe+L treatments suggesting nitrogen availability did not have a major impact on photosynthetic efficiency in the experiments (Fig. 2.6).

Phytoplankton community structure

Pigment data showed the initial SCM phytoplankton communities were relatively diverse, with significant amounts of fucoxanthin (diatoms), 19-hexanoyloxyfucoxanthin (19-hex, prymnesiophytes),19-butanoyloxyfucoxanthin (19-but, pelagophytes), and divinyl-Chl *a* (dvChl *a*, *Prochlorococcus* sp.) present and attributable to distinct phytoplankton taxa (Fig. 2.7; see also Fig. 2.10A). At ambient light levels, only fucoxanthin increased in response to iron additions in those incubations where Chl *a* responses were also observed (Table 2.3; Fig. 2.7A). In other experiments, no differences in pigment concentrations were seen at ambient light (Table 2.3; Fig. 2,7C). In all incubations significantly higher levels of fucoxanthin were found in +Fe+L compared to +L treatments when incubations were terminated (Table 2.3; Fig. 2.7A,C). While many taxa other than diatoms contain fucoxanthin, including prymnesiophytes and pelagophytes, they typically have additional accessory carotenoids such as 19-hex or 19-but. In all cases except one (KN1), these pigments did not respond significantly to iron in our experiments, suggesting diatoms were generally the primary taxon affected by iron limitation. Other pigments (19-hex, 19-but) increased in +L and +Fe+L treatments over +Fe and C treatments, but showed no differences between iron treatments, indicating the

net growth rate of phytoplankton containing these pigments was light limited in most incubations (Fig. 2.7A,C). Only in KN1 were significant responses to iron observed in other pigments (Fig. 2.8B). In this incubation 19-hex was slightly elevated in +Fe relative to control treatments, and both 19-hex and 19-but were elevated in +Fe+L treatments compared with +L treatments showing iron has the potential to affect members of the phytoplankton community other than diatoms. The behavior of cyanobacterial pigments (dvChl *a*, zeaxanthin) varied among our experiments though no responses to iron were observed (data not shown). At ambient light levels cyanobacterial pigments were approximately constant in most incubations, however declines were observed in NH1 and KN1. In RR4 increases in dvChl *a* were observed at elevated light, but in many cases (NH1, RR3, RR2, KN1) elevated light levels led to declines in cyanobacterial pigments. Whether this was due to photoacclimation or growth inhibition is unknown. As indicated by pigment signatures, the most prominent change in community structure was a shift to diatom dominance when light and iron availability were increased.

Microscopic analysis of preserved phytoplankton generally confirmed changes in diatom and coccolithophore abundances inferred from pigment data, although some discrepancies were noted, most likely due to changes in cellular pigment contents of phytoplankton between treatments. Diatoms were initially present at low numbers in all incubations except RR1 where *Chaetoceros* were abundant (data not shown; *see* also Fig. 2.10A). At elevated light diatom abundances, especially *Pseudonitzschia* and *Nitzschia*, increased and responded to iron with cell numbers in +Fe+L treatments roughly double those in +L treatments, consistent with POC increases and nitrate drawdown (Fig. 2.7B,D). C and +Fe treatments also had more diatoms relative to initial conditions, and

there were often more diatoms in +Fe treatments though the difference is not statistically

significant in any experiment (Fig. 2.7B). The diatoms were large compared to the

majority of the phytoplankton community with *Pseudonitzschia* cells measured between

20 μm and 100 μm in length, *Nitzschia*: 25-180 μm, miscellaneous small pennates: 6-20

μm, and *Chaetoceros*: 5-25 μm. Coccolithophores also increased at elevated light and

were moderately higher in some +Fe+L treatments compared to +L treatments, although

the differences were not statistically significant in any experiment suggesting at least

some of the increase of 19-hex in +Fe+L treatments of KN1 was due to increased

pigment per cell (Fig. 2.8B). Increases of coccolithphores at ambient light were observed

relative to initial conditions but no responses to iron were seen (Fig. 2.7B,D).

Size fractioned (>8 μm) Chl *a* from the RR experiments showed initial

phytoplankton were mostly less than 8 μm (Table 2.5), except for RR1 which was taken

from a more productive water column with higher initial Chl *a* (Table 2.1) and a greater

proportion of phytoplankton biomass present as larger diatoms. The proportion of Chl *a*

in the >8 μm size class did not change significantly from initial conditions in ambient

light treatments, except in RR1 where a decrease was observed in both +Fe and control

treatments. In contrast, at elevated light the fraction of Chl *a* >8 μm increased moderately

in +L treatments and dramatically in +Fe+L treatments, consistent with microscopic

observations showing larger diatoms grew more rapidly when iron availability was

increased (Table 2.5).

Discussion

These experiments suggest iron availability is an important factor modulating phytoplankton growth and community structure in the SCMs studied, despite macronutrient limitation of the surface waters. Laboratory studies suggesting elevated iron requirements at low light may lead to iron-light co-limitation of phytoplankton growth rates motivated our investigations and experimental design, and two general classes of responses were observed to experimental manipulation of iron and light. In four incubations (NH1, RR1, RR2, and KN1) responses to iron addition were observed at both ambient and elevated light, a combination suggestive of iron-light co-limitation of growth within these SCMs (Tables 2.2, 2.3). In other experiments (RR3, RR4, and KN2) iron had no observable effect on phytoplankton at ambient light, but at elevated light iron addition resulted in faster growth and higher phytoplankton biomass after some nutrient drawdown had occurred. These results indicate light was the proximate factor limiting growth rates at the stratum sampled, but the community was poised for iron limitation if local light levels were to increase due, for example, to passage of an upwelling eddy or generation of strong internal waves.

<u>Iron-light co-limitation</u>

In traditional concepts of growth limitation only one nutrient, the least available, is relevant to understanding constraints on growth rate. More thorough knowledge of autotrophic physiology has revealed that numerous links between nutrients exist, involving acquisition and elemental substitution, which complicates attempts to identify a single limiting nutrient in many situations (e.g., Price and Morel 1990; Sunda and Huntsman 1997). Additionally, in the pelagic marine environment diverse phytoplankton with differing nutrient requirements are typically present, and are

potentially limited by different factors. Taking into account these complications, more recent considerations of nutrient limitation have recognized the existence of co-limitations at the organismal and community level (Arrigo 2005; Saito et al. In press). A cellular level co-limitation by iron and light was hypothesized by Sunda and Huntsman (1997) on the basis of the high iron requirements of photosynthetic reaction center and electron transport proteins. Studies in deeply mixed HNLC waters have provided some evidence that this co-limitation occurs in the field (Maldonado et al. 1999; Boyd et al. 2001). We sought to examine the possibility that iron light co-limitation occurs in SCMs of non-HNLC, stratified waters columns.

In several incubation experiments from the ETNP and SCB (NH1, RR1, RR2, KN1) phytoplankton community responses indicative of iron-light co-limitation were observed. Chl *a* derived growth rates increased in response to elevated light, generally increased in response to added iron, and a synergistic effect on Chl *a* growth rates was observed in response to increased iron and light. Taxaonomic pigment and microscopic data showed diatoms were generally the only taxa to respond to iron at both ambient and elevated light suggesting the co-limitation could be occurring at a cellular level. Because of biases in Chl *a* and carotenoid pigments as an indicator of phytoplankton biomass when light and iron levels are changing, the similar responses of nitrate drawdown, POC increases, and cell numbers to the treatments are notable (Fig. 2.5C; Table 2.2). The lack of a measurable response of POC, cell numbers, or nutrient drawdown to iron addition at ambient light in incubations NH1, RR1, and RR2 is the primary difference between the behavior of these parameters and that of Chl *a*. Phytoplankton biomass may not have increased significantly in +Fe treatments during the

course of these experiments. In these cases it could be argued from a phenomenological perspective that co-limitation of growth rate was not observed because one parameter (Fe) did not produce significant biomass and net growth rate increases on its own.

However, in the context of the hypothesized physiological basis for iron-light co-limitation, additional considerations are relevant. The fact that this co-limitation would operate at a cellular level complicates conclusive demonstration since our data is at a community or multi-species taxonomic level, but several lines of evidence are consistent with a co-limitation due to the need for iron in photosynthetic proteins. A significant interaction effect between iron and light is observed on Chl a growth rates, a result expected under the conceptual model for iron-light co-limitation where the linked physiology of light and iron mean they would be expected to synergistically increase growth rate. Taxonomic pigment data and microscopic cell counts show responses characteristic of co-limitation were generally confined to diatoms. This data rules out the possibility that widely different taxa are independently responding to iron and light, and strongly suggests the interactive effects of iron and light are occurring at a cellular level. Increases in F_v:F_m in response to iron addition at ambient and elevated light demonstrate that added iron was routed to PSII, allowing more efficient light utilization. While this does not rule out the possibility that iron had additional effects on phytoplankton physiology, it does show some added iron was used in the photosynthetic apparatus, as would be expected in an iron-light co-limited state induced by photosynthetic iron requirements. The feature of iron-light co-limitation which is most problematic to demonstrate in our experiments is an increase in growth rate in +Fe treatments.

There is clearly an effect of iron on the phytoplankton community at ambient light as evidenced by increases in Chl a, fucoxanthin, and F_v:F_m, but what is the significance of this data? As discussed above increases in F_v:F_m indicate an increased efficiency of light utilization in PSII, potentially allowing more efficient photosynthesis and higher growth rates. The most conservative interpretation of the Chl a and carotenoid pigments increases in +Fe treatments are that they represent higher cellular pigment contents. Changes in cellular Chl a and accessory pigments reflect acclimation of the photosynthetic apparatus to match light harvesting with requirements for growth (Geider et al. 1998). The increased pigments per cell in conjunction with increased F_v:F_m thus suggest an improved capacity to productively harvest light. Such an adjustment is consistent with the hypothesized physiological basis for iron-light co-limitation, and a modest increase in diatom growth rate may have occurred, but did not produce observably higher biomass for a number of reasons: 1) grazing kept up with relatively small increases in growth rate, 2) because diatoms were only a modest portion of the community, changes in bulk parameters were difficult to detect (and microscopic counts have high variability).

While there is strong evidence that diatom growth rates were iron-light co-limited, it is difficult to conclusively demonstrate iron-light co-limitation of growth rates from these experiments. However, the data show there is a strong effect of iron at elevated light and suggest that iron is an important factor controlling growth rate and community structure at SCMs. Macronutrients are certainly also major determinants of productivity and community structure in these SCMs (Herbland and Voituriez 1979; Cullen 1982), particularly in their upper portions above the nitracline. Iron may have a significant role

within the nitracline where macronutrient limitation is relieved but light levels are low

exacerbating iron stress. Responses characteristic of iron-light co-limitation were

observed in waters with relatively low initial iron concentrations (0.11-0.21 nmol L^{-1}) in

three of the SCMs, but the iron concentration was somewhat higher (0.27 nmol L^{-1}) in the

ETNP which may be due to its location over a suboxic zone (Table 2.1; Deutsch et al.

2001; Hopkinson and Barbeau 2007). Similar behavior of phytoplankton communities in

both the tropical and subtropical Pacific and in waters of varying productivity indicate

iron may be an important factor throughout SCMs in the Pacific where iron supply is

generally low.

<u>Role of iron under changing light levels</u>

Our experiments were designed to test for iron-light co-limitation, but a different

set of responses was found in experiments RR3, RR4, and KN2 where responses to iron

were observed only at elevated light. Lack of responses at ambient light and delayed

onset of iron limitation at high light suggest iron availability was initially higher in these

experiments, and subsequently depleted to limiting concentrations as growth occurred.

Although measured iron concentrations were no different from other experiments (Table

2.1), small changes in iron bioavailability not resolvable by our measurements could have

supported the small amount of growth observed prior to the onset of iron stress (Fig

2.5B,D), given that N:Fe ratios can reach 15,000 for iron limited phytoplankton (Price

2005). Although a response to iron occurred only at elevated light in these experiments,

the effects of iron on phytoplankton physiology and community structure were nearly

identical to those observed on communities where responses suggestive of iron-light co-

limitation were observed. This indicates the net effects of iron limitation on the SCM communities are similar despite initial differences in degree of iron stress (Figs. 2.5, 2.7).

Factors responsible for the differing incubation responses are currently speculative since initial conditions, most notably iron and light levels, were similar. Initial parameters showed no statistically significant differences between incubations where iron-light co-limitation responses were observed and those in which only high light response to iron were found, but because of the limited data set detecting such differences may be difficult. In general, Chl *a* levels were higher and nitrate levels were lower at SCM strata where iron-light co-limitation was observed as compared with incubations where iron responses were observed only at high light (Table 2.1). Links between initial Chl *a* and nitrate concentrations and subsequent response to iron addition may depend on both vertical gradients of iron stress within individual SCMs, and differing iron stress among the SCMs sampled. Strong, coincident gradients in biologically relevant parameters occur within SCMs potentially leading to fine scale changes in proximate limiting factors for phytoplankton growth (Cullen 1982; Fennel and Boss 2003). Higher Chl *a* and lower nitrate levels are found at the top of the nitracline near maximal SCM Chl *a* concentrations, and our results suggest iron-light co-limitation may commonly occur here within the core of the SCM (Fig. 2.2). Further down the water column, nitrate concentrations, which are broadly correlated with iron concentrations (Johnson et al. 1997*a*), increase while Chl *a* declines and light eventually becomes limiting. Incubations in which iron responses were observed only at high light may have originated from this region, suggesting iron stress may arise in this layer if light levels become elevated. The

SCM appears to be a complex feature, with gradients in iron stress overlain on the well known gradients in light and macronutrient limitation (Cullen 1982).

Among SCMs, higher Chl *a* levels are achieved in more productive water columns (Herbland and Voituriez 1979), where macronutrient influxes from below are more rapid and potentially decoupled from iron inputs (aeolian dust, sedimentary fluxes) leading to greater iron stress potentially manifested as iron-light co-limitation at depth. Variability in iron stress among SCMs sampled may also result from differing relationships between the nitracline and ferricline in each water column (Johnson et al. 1997*b*). Iron and nitrate depth profiles are broadly related in oceanic water columns, and in many cases the relationship is very close, but in some water columns there is an offset between the nitracline and the ferricline (Johnson et al. 1997*a,b*). In these waters the ferricline is deeper than the nitracline, possibly due to increased uptake of iron by organisms at depth, or differential rates of remineralization of iron and nitrogen from sinking materials (Frew et al. 2006). Iron stress may develop in the intervening layer giving rise to the iron limitation we observe at the SCM (Fig. 2.2; Johnson et al. 1997*b*).

Although we cannot fully explain the origin of the differing experimental responses, in all incubations the effects of iron on growth and community structure are consistent and dramatic at elevated light (Table 2.2; Fig. 2.7). Consequently, iron limitation may have an especially strong influence on SCMs when light levels change due, for example, to upwelling eddies, internal waves, or changes in cloud cover (Lande and Yentsch 1988; McGillicuddy et al. 1998; Letelier et al. 2004). By lifting the nutricline further into the euphotic zone, mesoscale upwelling eddies effectively raise the local light level of nutrient rich waters, a situation analogous to our +L treatments

indicating iron availability could be an important control on community structure and nutrient cycling within these features. This scenario assumes that eddies act solely to dome isopycnals, preserving relationships between the ferricline and nitracline, which is their effect to a first approximation (McGillicuddy et al. 1998). However eddy doming may also be accompanied by diapycnal mixing or vertical transport complicating a simple model of their biogeochemical impact (McGillicuddy et al. 2007). Eddies are important mechanisms of nutrient supply to oligotrophic regions accounting for about half of new production in the Sargasso sea, but the episodic nature of mesocale eddies complicates efforts to study them (McGillicuddy et al. 1998; Benitez-Nelson et al. 2007).

We encountered an anomalously strong SCM in oligotrophic waters at the edge of the north Pacific gyre from which KN1 was initiated (Fig. 2.9). The SCM phytoplankton community was dominated by flora characteristic of the north Pacific gyre (Venrick 2000; E. Venrick, pers. comm.) which suggests the high biomass was the result of a local nutrient input event, most likely due to isopycnal shoaling. Dramatic iron-light co-limitation of the phytoplankton community was observed at this SCM (Tables 2.2, 2.3; Fig. 2.8A,B). While responses characteristic iron-light co-limitation were usually confined to diatoms in our experiments, pigment data from KN1 indicated that many components of the eukaryotic phytoplankton community were effected by iron in this SCM, including prymnesiophytes and possibly pelagophytes, in addition to diatoms. This further indicates that iron-light co-limitation was especially strong in this stratum (Fig. 2.8B). While available data is insufficient to establish the precise cause of the unusually high SCM biomass at this location, some local process was likely responsible. The observation of strong iron-light co-limitation and significant changes in community

structure in this experiment support our hypothesis that iron availability may be an especially important factor to consider when nutrients are rapidly moved into the lower euphotic zone.

<u>Phytoplankton community responses and environmental relevance</u>

SCM phytoplankton communities in the eastern Pacific were quite diverse containing substantial abundances of cyanobacteria, prymnesiophytes, pelagophytes, and diatoms (Fig. 2.10A). Effects of iron on net growth rates were generally confined to diatoms indicating that iron may be influencing their productivity and abundances within many of the SCMs studied. Comparing pigment distributions in initial SCM phytoplankton communities with +Fe+L treatments shows relief of iron and light limitations led to diatom dominance (Fig. 2.10). Microscopy and size fractioned Chl *a* show these diatoms are large, and most commonly dominated by pennate *Pseudonitzschia* and *Nitzschia* species (Fig. 2.7; Table 2.5), which often respond to iron addition in other iron limited regions (de Baar et al. 2005). However changes in diatom biomass in situ would also likely be influenced by mesozooplankton grazing which is not adequately represented in microcosm experiments. Additionally, microzooplankton grazing may impact taxa differently in situ in comparison with experimental conditions. Despite these caveats, the strong shift towards diatom dominance suggests that a similar shift, though perhaps of lesser magnitude, could occur in situ when limitation by iron and light are relieved.

Because macronutrients, generally nitrogen, control new production in the water columns studied, iron availability would not be expected to affect carbon flux out of the euphotic zone under steady-state conditions (Eppley and Peterson, 1979). However, by

modifying ecosystem structure iron could influence the type of material exported and the efficiency of nutrient export relative to recycling (the *f*-ratio). When iron availability is higher larger diatoms may become more abundant within SCMs changing the size and taxonomic structure of the phytoplankton community, with consequences for ecosystem structure and nutrient cycling. Small phytoplankton are grazed by microzooplankton, routing carbon through the tightly coupled microbial loop where the vast majority of the carbon is remineralized. In contrast larger phytoplankton have higher sinking rates, and are preferentially eaten by metazoan grazers (Michaels and Silver 1988; Boyd and Newton 1999; but see Richardson and Jackson 2007). By enhancing the growth of large diatoms, iron induced shifts in size structure could result in more rapid nutrient export at the SCM, where nutrients first enter the euphotic zone, reducing the *f*-ratio of the system (Eppley and Peterson 1979). Additionally iron availability may modify the type of material exported. In particular larger diatoms sink more rapidly than much of the SCM phytoplankton community and potential changes in food web structure when larger phytoplankton dominate could result in greater production of dense fecal pellets from copepods leading to deeper carbon export (Michaels and Silver 1988). Iron could even increase the magnitude of carbon flux from the system if its availability mediated increases in the C:N ratio of exported material, since N fluxes generally control new and export production in the eastern Pacific (Behrenfeld et al. 2006). In several experiments we did observe marked increases in the C:N ratio of particulate matter under iron replete conditions, suggesting direct export of this material could result in greater carbon export (*see* Results). However, whether this increased C:N ratio would be transmitted through the food web to enhance other routes of carbon export is unknown.

In conclusion, these experiments show iron availability is likely an important factor structuring SCM phytoplankton communities in macronutrient limited water columns of the eastern Pacific. Eukaryotic phytoplankton, principally larger diatoms, showed responses to iron and light manipulations suggestive of iron-light co-limitation, which may be a consequence of the high iron requirements of photosynthetic reaction center and electron transport proteins. Iron availability effected the taxonomic and size structure of the phytoplankton community may modify nutrient and carbon cycling within the SCM, where the majority of new nutrients are introduced to the euphotic zone. Influences of iron on SCM phytoplankton communities was observed in both the ETNP and the SCB which suggests the phenomenon is important in much of the Pacific where aeolian iron supply is low, but whether iron influences lower euphotic zone phytoplankton in other ocean basins remains to be investigated.

Acknowledgments

This chapter was submitted to Limnology and Oceanography as: Hopkinson, Brian M., and Katherine A. Barbeau. Interactions between iron and light limitation of phytoplankton in subsurface chlorophyll maxima of the eastern Pacific.

Table 2.1. Incubation initial conditions. Depth from which incubations were collected and initial water properties are reported, as well as light conditions in situ and during incubation (as percent surface irradiance). The majority of incubations were conducted in an indoor incubator (In), although some were conducted in on-deck flow-through incubators (Out).

Incubation	Depth (m)	NO_3^- (μmol L^{-1})	PO_4^{3-} (μmol L^{-1})	Si (μmol L^{-1})	Fe (nmol L^{-1})	Chl a (μg L^{-1})	Measured Ambient Light	Simulated Ambient Light	Elevated Light	In/Out-doors
NH1	60	0.7	0.5	2.3	0.27 ± 0.08	0.55	1.2	1.5	4.5	Out
RR1	45	3.0	0.5	2.4	0.11 ± 0.02	0.92	0.5	0.6	4.5	In
RR2	50	1.2	0.4	2.6	0.11 ± 0.01	0.35	0.8	0.6	4.5	In
KN1	78	4.1	0.5	5.2	0.21 ± 0.02	0.68	0.7	0.5	3.3	In
RR3	65	6.3	0.8	4.8	0.18 ± 0.04	0.43	0.6	0.5	4.5	In
RR4	50	4.9	0.5	3.6	0.12 ± 0.02	0.38	0.9	0.6	5.9	Out
KN2	77	1.7	0.2	2.7	0.32 ± 0.01	0.34	0.9	1.4	4.4	In

Table 2.2. Incubation responses to iron and light manipulations. Growth rates derived from Chl a (μ_{Chl}), drawdown in nitrate over the course of the experiment (ΔNO_3^-), and particulate organic carbon (POC) concentrations for each treatment are given as the mean of replicate bottles with the standard deviation between replicates reported in parentheses below. Each experiment was analyzed with a one-way ANOVA and post hoc Tukey-Kramer tests to determine significant ($p < 0.05$) differences between treatment means, indicated with different letters. A two-way ANOVA was run on each experiment to determine in which experiments (indicated by *) there was a significant ($p < 0.05$) interaction term between the independent factors iron and light. Finally because variances were lower in ambient light treatments, a t-test was performed only on control and +Fe data and significant ($p < 0.05$) differences between these treatments are indicated with a 't'.

	Ambient- and high-light iron responses				High-light iron response		
	NH1	RR1	RR2	KN1	RR3	RR4	KN2
μ_{Chl} (d^{-1})							
Control	0.16^A	0.00^A	0.08^A	0.01^A	0.08^A	0.02^A	0.17^A
	(0.01)	(0.04)	(0.01)	(0.00)	(0.04)	(0.01)	(0.04)
+Fe	0.22^{A,B,t}	0.03^A	0.13^A	0.05^{A,t}	0.12^A	0.03^A	0.16^A
	(0.01)	(0.08)	(0.03)	(0.02)	(0.02)	(0.04)	(0.00)
+L	0.30^B	0.28^B	0.15^A	0.19^B	0.25^{A,B}	0.16^B	0.39^B
	(0.04)	(0.03)	(0.02)	(0.00)	(0.12)	(0.01)	(0.03)
+Fe+L	0.53^{C,*}	0.60^{C,*}	0.27^B	0.49^{C,*}	0.42^B	0.32^{C,*}	0.70^{C,*}
	(0.04)	(0.00)	(0.01)	(0.03)	(0.01)	(0.04)	(0.04)
ΔNO_3^-							
(μmol L^{-1})							
Control	0.13^A	0.11^A	0.15^A	0.67^A	0.28^A	0.13^A	0.22^A
	(0.01)	(0.05)	(0.02)	(0.06)	(0.02)	(0.10)	(0.06)
+Fe	0.17^A	0.13^A	0.14^A	0.82^A	0.30^A	0.05^A	0.28^A
	(0.03)	(0.23)	(0.02)	(0.07)	(0.01)	(0.09)	(0.00)
+L	0.36^B	1.85^B	0.82^B	1.58^B	1.95^B	0.85^B	1.42^B
	(0.11)	(0.10)	(0.07)	(0.17)	(0.86)	(0.36)	(0.08)
+Fe+L	0.70^{C,*}	3.00^{C,*}	0.99^{C,*}	3.74^{C,*}	4.20^{C,*}	1.22^{C,*}	1.54^B
	(0.02)	(0.01)	(0.02)	(0.32)	(0.21)	(0.16)	(0.00)
POC							
(μmol L^{-1})							
Control	n.d.	9.0^A	5.2^A	9.2^A	5.4^A	3.1^A	n.d.
		(1.3)	(0.1)	(0.1)	(0.4)	(0.1)	
+Fe	n.d.	9.5^A	4.9^A	10.0^{A,B,t}	5.0^A	4.5^{B,t}	n.d.
		(3.3)	(0.4)	(0.2)	(0.8)	(0.3)	
+L	n.d.	21.7^B	12.0^B	12.7^B	13.1^B	6.5^C	n.d.
		(0.8)	(0.1)	(0.3)	(1.8)	(0.3)	
+Fe+L	n.d.	37.1^{C,*}	13.7^{C,*}	24.5^{C,*}	23.1^{C,*}	10.0^{D,*}	n.d.
		(3.7)	(0.1)	(1.4)	(2.7)	(0.7)	

Table 2.3. Effect of iron addition on pigments at each light level. Data are reported as ratios of pigments (μg L^{-1}: μg L^{-1}) to facilitate inter-comparison. Significant differences ($p< 0.05$) between treatments (+Fe vs. Control or +Fe+L vs. +L) are indicated by an asterisk (*), as determined using a one-way ANOVA on the pigment concentrations in each treatment.

	Ambient- and high-light iron responses				High-light iron response		
	NH1	RR1	RR2	KN1	RR3	RR4	KN2
Chl *a* +Fe/C	1.29*	1.31	1.26*	1.32*	1.05	1.29	1.23
	(0.10)	(0.62)	(0.09)	(0.17)	(0.15)	(0.29)	(0.20)
Chl *a* +Fe+L/+L	2.2*	2.8*	1.5*	5.5*	3.0*	2.8*	1.6*
	(0.2)	(0.4)	(0.2)	(1.1)	(1.0)	(0.2)	(0.1)
Fucox +Fe/C	1.43*	1.40	1.38	1.68*	1.08	0.92	0.88
	(0.11)	(0.33)	(0.30)	(0.10)	(0.08)	(0.26)	(0.04)
Fucox +Fe+L/+L	2.16*	1.58*	1.39*	5.82*	3.72*	3.08*	1.95*
	(0.17)	(0.03)	(0.03)	(0.09)	(1.04)	(0.20)	(0.20)

Table 2.4. F_v:F_m at the final time point of incubations except NH1 where variable fluorescence data was not collected. Data are averages and standard deviations (in parentheses) between replicate bottles. Each experiment was analyzed with a one-way ANOVA and post hoc Tukey-Kramer tests to determine significant ($p < 0.05$) differences between treatment means, indicated with different letters.

	RR1	RR2	KN1	RR3	RR4	KN2
Initial	0.50^A	0.48^A	0.60^A	0.53^A	0.51^A	$0.61^{A,B}$
	(0.03)	(0.02)	(0.00)	(0.03)	(0.04)	(0.01)
Control	0.51^A	0.54^B	0.60^A	0.55^A	0.59^B	0.61^A
	(0.02)	(0.01)	(0.01)	(0.01)	(0.01)	(0.04)
+Fe	0.59^A	0.60^C	0.64^B	0.56^A	$0.63^{A,B}$	0.63^A
	(0.01)	(0.01)	(0.01)	(0.01)	(0.01)	(0.00)
+L	0.37^B	0.40^D	0.52^C	0.39^B	0.43^C	0.50^B
	(0.03)	(0.00)	(0.01)	(0.02)	(0.01)	(0.01)
+Fe+L	0.56^A	$0.56^{A,B}$	0.66^B	0.55^A	$0.56^{A,B}$	0.59^A
	(0.01)	(0.01)	(0.01)	(0.02)	(0.01)	(0.01)

Table 2.5. Size Fractioned Chl *a* in select incubations. Values are the mean from replicate bottles with standard deviations between bottles reported below in italics. Each experiment was analyzed with a one-way ANOVA and post hoc Tukey-Kramer tests to determine significant ($p < 0.05$) differences between treatment means, indicated with different letters. For some initial measurements only one sample was taken, and so no standard deviations are available (n.d.) and these data were not included in the ANOVA analysis.

% Chl a >8 µm	RR1	RR2	RR3	RR4
Initial	65^A	6	9	21^A
	(5)	(n.d.)	(n.d.)	(2)
Control	26^B	7^A	12^A	$29^{A, B}$
	(4)	(1)	(0)	(18)
+Fe	25^B	9^A	14^A	$45^{B,C}$
	(17)	(1)	(2)	(1)
+L	67^A	9^A	18^A	$28^{A, B}$
	(11)	(1)	(3)	(5)
+Fe+L	86^A	22^B	34^B	66^C
	(1)	(4)	(4)	(7)

Figure 2.1. Conceptual model of iron-light co-limitation due to iron requirements of the photosynthetic system (Sunda and Huntsman 1997). In this state the ability to process light limits energy generation (represented by electrons: e⁻) and growth, while the availability of iron limits production of photosynthetic proteins (grey ovals in cell membrane) used to process light. Increasing iron or light individually would be expected to increase growth rate, and a synergistic effect should be observed if both variables are increased together.

Figure 2.2. SCMs are formed at the interface of the light limited and macronutrient limited regions of the water column. It was hypothesized that iron-light co-limitation may occur at the top of the nitracline where nitrogen stress is relieved but low light results in high photosynthetic iron requirements. The relationship between the ferricline and nitracline is also an important factor generating iron stress at these depths in the water column. The ferricline is frequently deeper than the nitracline, as diagrammed here, though in some water columns they are coincident (Johnson et al 1997*b*).
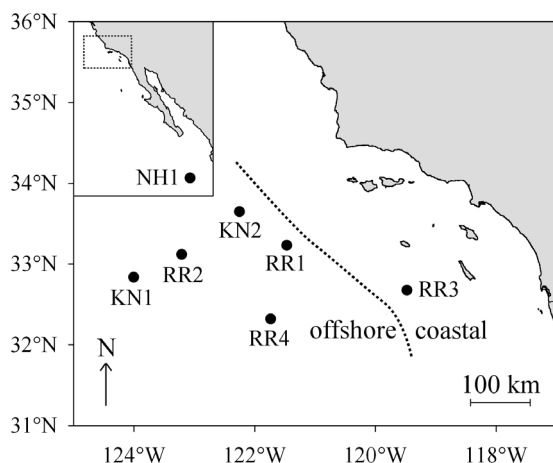
Figure 2.3. A map of the Southern California Bight region where the majority of the incubations were initiated with an inset map of the north east Pacific showing the location of NH1 (17º 24' N, 108º 17' W), and a dotted box around the southern California Bight region. The dotted line in the main map indicates the approximate location of the coastal/offshore boundary coinciding with the inshore edge of the California Current. The boundary was defined based on chlorophyll variability (Hayward and Venrick 1998) and is consistent with patterns in phytoplankton floristics (Venrick 1998). Although this boundary is based on surface characteristics, it is in part the result of subsurface processes and generally corresponds to the point where a stronger inshore shoaling of the nitracline begins (Hayward and Venrick 1998). This boundary is variable depending on the flow of the California Current, and it should be noted that RR1 was initiated at a time of higher productivity from waters more characteristic of the coastal regime.
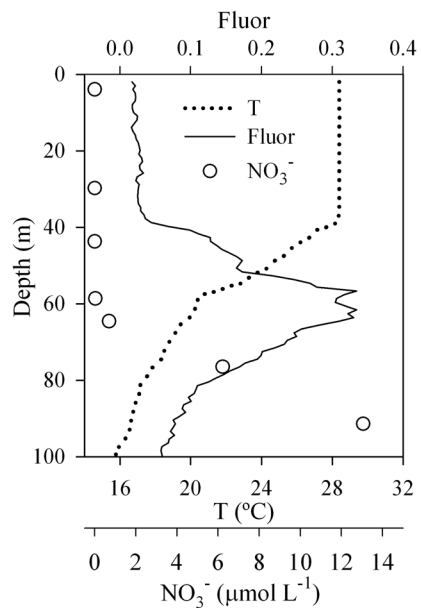
Figure 2.4. Profiles of Chl *a* fluorescence (Fluor, relative units), temperature (T), and nitrate (NO_3^-) at a station (17º 24' N, 108º 17' W) in the eastern tropical North Pacific where NH1 was initiated. SCM and water column structure at this station are typical of the stations sampled in this study. Water for NH1 was collected at 65 m depth, within the SCM, and at the top of the nitracline.
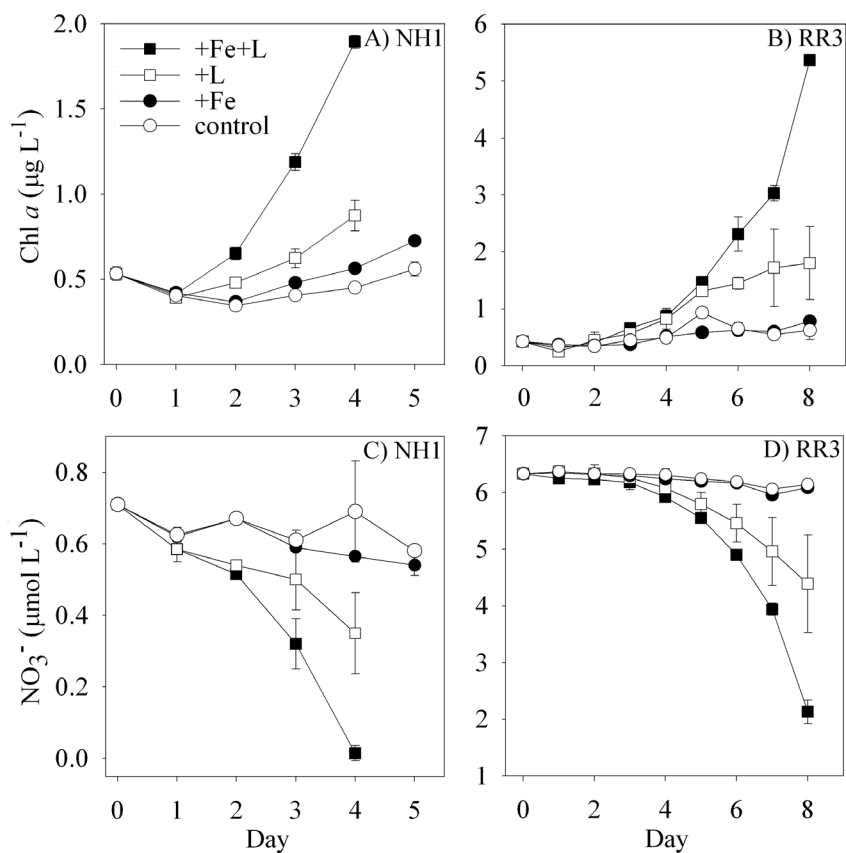
Figure 2.5. (A, B) Chl *a* and (C, D) nitrate data from incubations NH1 (panels A, C) and RR3 (panels B, D), representative of the two general classes of observed: responses to iron at ambient and elevated light (NH1), and delayed responses to iron only at elevated light (RR3). Error bars represent the standard deviation between replicate bottles, and when not visible are smaller than the symbols.
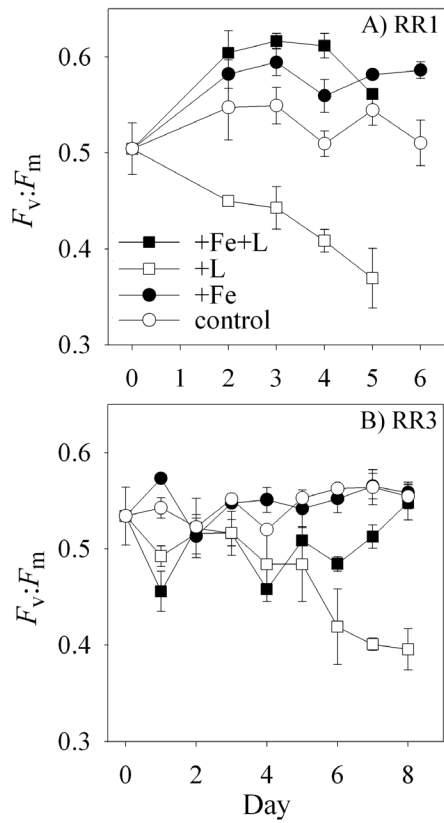
Figure 2.6. Increases in F_v:F_m relative to control and +L treatments were seen in +Fe and +Fe+L treatments in (A) RR1, while in (B) RR3 declines in +L treatments were seen after separation between +Fe+L and +L treatments occurred in other parameters (Fig. 5B, D). Error bars represent the standard deviation between replicate bottles.
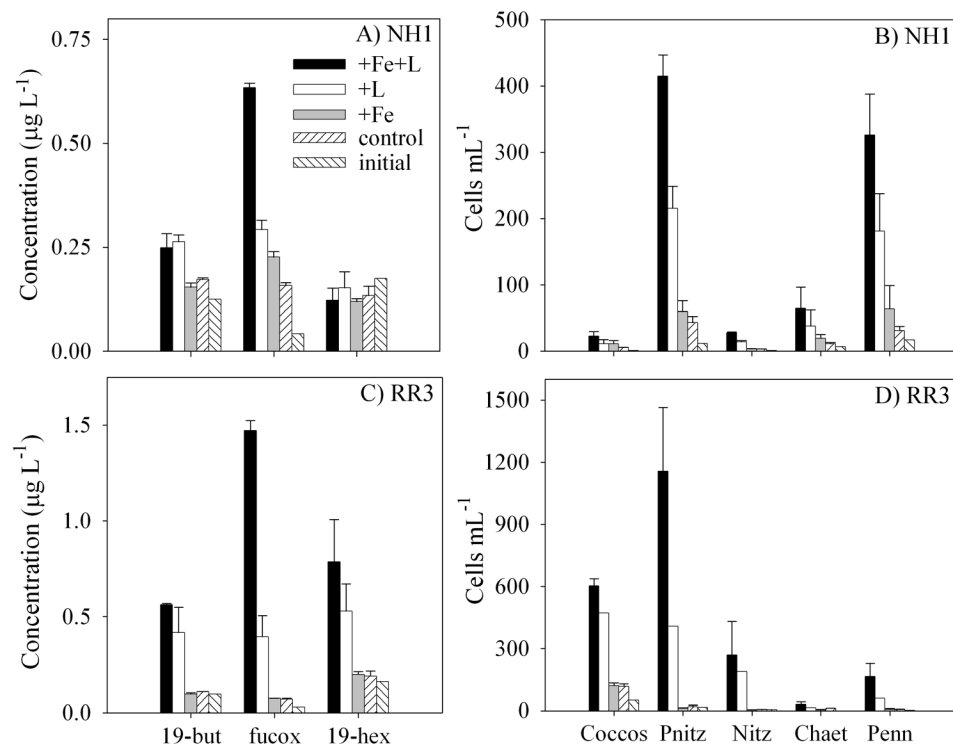
Figure 2.7. Responses of phytoplankton taxa to iron and light manipulations in (A, B) NH1 and (C, D) RR3. Differential responses were observed in the most abundant pigments (panels A, C) 19-butanoyloxyfucoxnathin (19-but) which responded only to light, fucoxanthin (fucox), which responded to iron and light, and 19-hexanoyloxyfucoxanthin (19-hex), which remained constant in NH1, and responded to light in RR3. Microscopic analysis (panels B, D) confirmed that diatoms dominated the response to increased iron and light. Enumerated phytoplankton were grouped into broad classes, the most abundant of which are graphed: Coccolithophores (Coccos), *Pseudonitzschia* species (Pnitz), *Nitzschia* species (Nitz), *Chaetoceros* species (Chaet), and miscellaneous small pennates (Penn). Error bars represent the standard deviation between replicate bottles.
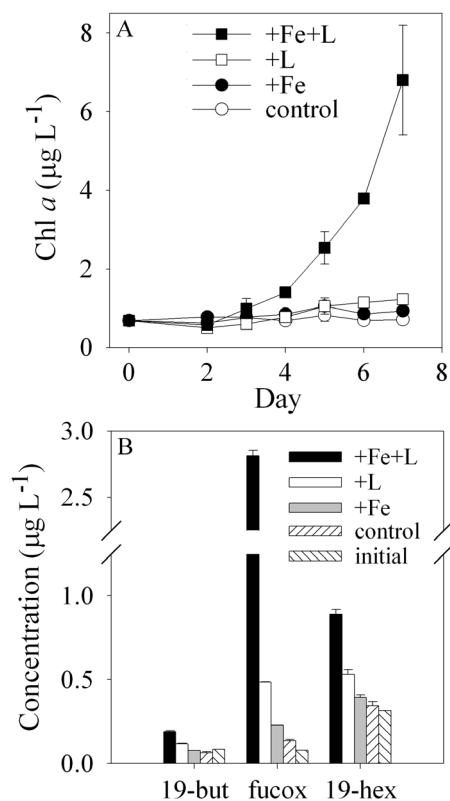
Figure 2.8. Strong effects of iron of the eukaryotic phytoplankton community were observed in incubation KN1, which was initiated from an anomalously strong SCM believed to be the result of a nutrient input event (*see* Discussion). Statistically significant (A) Chl *a* increases were observed in +Fe and +L treatments relative to controls (Table 3). (B) Taxonomic pigments showed that diatoms (fucox), prymnesiophytes (19-hex), and pelagophytes (19-but) all showed responses to iron addition in contrast to other experiments. Error bars represent the standard deviation between replicate bottles.
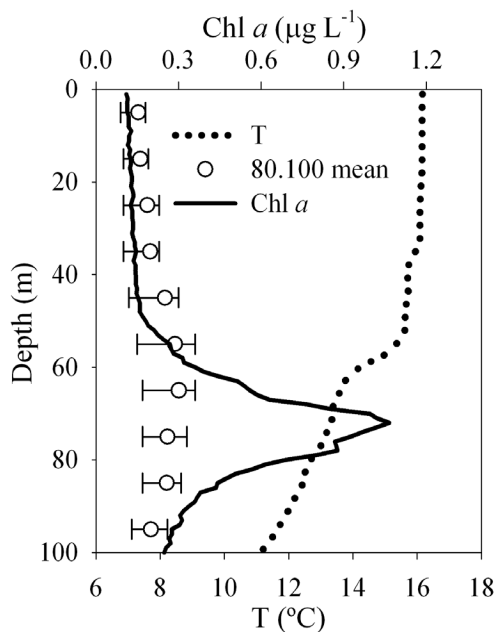
Figure 2.9. An unusually strong SCM where KN1 was initiated. Water column profile of Chl *a* fluorescence (calibrated with discrete Chl *a* samples collected on the CTD cast) and temperature (T) at a station on the edge of the north Pacific gyre (Fig. 2). Maximum Chl *a* concentrations of 1 μg L^{-1} are much higher than typically observed at SCMs this region. Shown for comparison is historical Chl *a* data from CalCOFI station 80.100, the closest station to where KN1 was collected. Chl *a* data collected by the CalCOFI program at station 80.100 quarterly from 1981 to 2005 was binned into 10 m depth intervals, and analyzed. Open circles are the mean value in each depth interval and error bars represent the 75th and 25th percentiles.
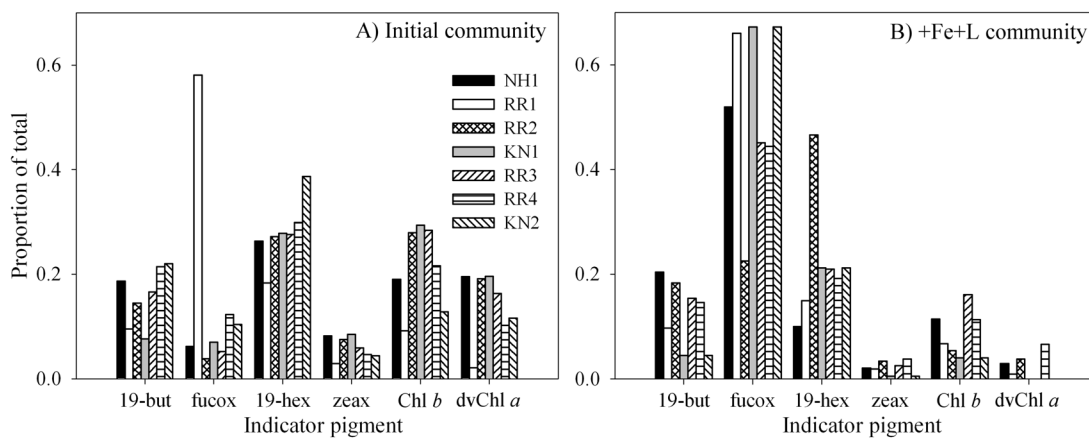
Figure 2.10. A comparison of phytoplankton community structure in (A) initial waters collected for incubation and (B) the final +Fe+L community. As a proportion of the total taxonomically informative pigments shown, fucoxanthin increased dramatically in +Fe+L communities compared to the initial community. The initial community at most stations was fairly diverse as demonstrated by the even distribution of pigments from divergent phytoplankton taxa.

References

Anderson, R.A., R.R. Bidigare, M.D. Keller, and M.Latasa. 1996. A comparison of HPLC pigment signatures and electron microscopic observations for oligotrophic waters of the North Atlantic and Pacific Oceans. Deep Sea Res. II. **43:** 517-537.

Arrigo, K.R. 2005. Marine microorganisms and global nutrient cycles. Nature **437:** 349-355.

Behrenfeld, M.J., K. Worthington, R.M. Sherrell, F.P. Chavez, P. Strutton, M. McPhaden, and D.M. Shea. 2006. Control on tropical Pacific Ocean productivity revealed through nutrient stress diagnostics. Nature **442:** 1025-1028.

Benitez-Nelson, C.R., R.R. Bidigare, T.D. Dickey, M.R. Landry, C.L. Leonard, S.L. Brown, F. Nencioli, Y.M. Rii, K. Maiti, J.W. Becker, T.S. Bibby, W. Black, W.J. Cai, C.A. Carlson, F.Z. Chen, V.S. Kuwahara, C. Mahaffey, P.M. McAndrew, P.D. Quay, M.S. Rappe, K.E. Selph, M.P. Simmons, and E.J. Yang. 2007. Mesoscale eddies drive increased silica export in the subtropical Pacific Ocean. Science **316:** 1017-1021.

Bowie, A.R., E.P. Achterberg, R. Fauzi, C. Mantoura, and P.J. Worsfold. 1998. Determination of sub-nanomolar levels of iron in seawater using flow injection with chemiluminescence detection. Anal. Chim. Acta. **361:** 189-200.

Boyd, P.W., and P.P. Newton. 1999. Does planktonic community structure determine downward particulate organic carbon flux in different oceanic provinces? Deep Sea Res. I **46:** 63-91.

Boyd, P.W., A.C. Crossley, G.R. DiTullio, F.B. Griffiths, D.A. Hutchins, B. Queguiner, P.N. Sedwick, and T.W. Trull. 2001. Control of phytoplankton growth by iron supply and irradiance in the subantarctic Southern Ocean: Experimental results from the SAZ project. J. Geophys. Res. **106:** 31,573-31,583.

Coale, K.H., and K.W. Bruland. 1987. Oceanic stratified euphotic zone as elucidated by ^{234}Th:^{238}U disequilibria. Limnol. Oceanogr. **32:** 189-200.

Croot, P.L., and M. Johansson. 2000. Determination of iron speciation by cathodic stripping voltammetry in seawater using the competing ligand 2-(2-thiazolylazo)-p-cresol (TAC). Electroanal. **12:** 565-576.

Cullen, J.J. 1982. The deep chlorophyll maximum: comparing vertical profiles of chlorophyll *a*. Can. J. Fish. Aquat. Sci. **39:** 791-803.

de Baar, H.J.W., P.W. Boyd, K.H. Coale, M.R. Landry, A. Tsuda, P. Assmy, D.C.E. Bakker, Y. Bozec, R.T. Barber, M.A. Brzezinski, K.O. Buesseler, M. Boye, P.L.

Croot, F. Gervais, M.Y. Gorbunov, P.J. Harrison, W.T. Hiscock, P. Laan, C. Lancelot, C.S. Law, M. Levasseur, A. Marchetti, F.J. Millero, J. Nishioka, Y. Nojiri, T. van Oijen, U. Riebesell, M.J.A. Rijkenberg, H. Saito, S. Takeda, K.R. Timmermans, M.J.W. Veldhuis, A.M. Waite, and C.S. Wong. 2005. Synthesis of iron fertilization experiments: From the iron age to the age of enlightenment. J. Geophys. Res. **110:** C09S16, doi:10.1029/2004JC002601.

Deutsch, C., N. Gruber, R.M. Key, J.L. Sarmiento. 2001. Denitrification and N_2 fixation in the Pacific Ocean. Glob. Biogeochem. Cycles **15:** 483-506.

Eppley, R.W., and B.J. Peterson. 1979. Particulate organic matter flux and planktonic new production in the deep ocean. Nature **282:** 677-680.

Fennel, K., and E. Boss. 2003. Subsurface maxima of phytoplankton and chlorophyll: Steady-state solutions from a simple model. Limnol. Oceanogr. **48:** 1521-1534.

Frew, R.D., D.A. Hutchins, S. Nodder, S. Sanudo-Wilhelmy, A. Tovar-Sanchez, K. Leblanc, C.E. Hare, and P.W. Boyd. 2006. Particulate iron dynamics during FeCycle in subantartic waters southeast of New Zealand. Global. Biogeochem. Cycles **20:** GB1S93, doi:10.1029/2005GB002558.

Geider, R.J., H.L. MacIntyre, and T.M. Kana. 1998. A dynamic regulatory model of phytoplanktonic acclimation to light, nutrients, and temperature. Limnol. Oceanogr. **43:** 679-694.

Greene, R.M., R.J. Geider, Z. Kolber, and P.G. Falkowski. 1992. Iron-induced changes in light harvesting and photochemical energy conversion processes in eukaryotic marine algae. Plant Physiol. **100:** 565-575.

Goericke, R., and J.P. Montoya. 1998. Estimating the contribution of microalgal taxa to chlorophyll *a* in the field – variations of pigment ratios under nutrient- and light-limited growth. Mar. Ecol. Prog. Ser. **169:** 97-112.

Hayward, T.L., and E.L. Venrick. 1998. Nearsurface pattern in the California Current: coupling between physical and biological structure. Deep Sea Res. II **45:** 1617-1638.

Herbland, A., and B. Voituriez. 1979. Hydrological structure analysis for estimating the primary production in the tropical Atlantic Ocean. J. Mar. Res. **37:** 87-101.

Hopkinson, B.M., and K.A. Barbeau. 2007. Organic and redox speciation of iron in the eastern tropical North Pacific suboxic zone. Mar. Chem. **106:** 2-17.

Hutchins, D.A., G.R. DiTullio, Y. Zhang, and K.W. Bruland. 1998. An iron limitation mosaic in the California upwelling regime. Limnol. Oceanogr. **43:** 1037-1054.

Hutchins, D.A., C.E. Hare, R.S. Weaver, Y. Zhang, G.F. Firme, G.R. DiTullio, M.B. Alm, S.F. Riseman, J.M. Maucher, M.E. Geesey, C.G. Trick, G.J. Smith, G.J. Smith, E.L. Rue, J. Conn, and K.W. Bruland. 2002. Phytoplankton iron limitation in the Humboldt Current and Peru Upwelling. Limnol. Oceanogr. **47:** 997-1011.

Jeffrey, S.W., and S.W. Wright. 1994. Photosynthetic pigments in the Haptophyta, p. 111-132. *In* J.C. Green and B.S.C. Leadbeater [eds.], The Haptophyte Algae. Clarendon Press.

Johnson, K.S., R.M. Gordon, and K.H. Coale. 1997*a*. What controls dissolved iron concentrations in the world ocean? Mar. Chem. **57:** 137-161.

Johnson, K.S., R.M. Gordon, and K.H. Coale. 1997*b*. What controls dissolved iron concentrations in the world ocean? Author's closing comments. Mar. Chem. **57:** 181-186.

King, A.L., and K. Barbeau. 2007. Evidence for phytoplankton iron limitation in the southern California Current System. Mar. Ecol. Prog. Ser. **342:** 91-103.

Lande, R., and C.S. Yentsch. 1988. Internal waves, primary production and the compensation depth of marine phytoplankton. J. Plankton Res. **10:** 565-571.

Letelier, R.M., D.M. Karl, M.R. Abbott, and R.R. Bidigare. 2004. Light driven seasonal patterns of chlorophyll and nitrate in the lower euphotic zone of the North Pacific Subtropical Gyre. Limnol. Oceanogr. **49:** 508-519.

Maldonado, M.T., P.W. Boyd, P.J. Harrison, and N.M. Price. 1999. Co-limitation of phytoplankton growth by light and Fe during winter in the NE subarctic Pacific Ocean. Deep-Sea Res. II. **46:** 2475-2485.

McGillicuddy, D.J., A.R. Robinson, D.A. Siegel, H.W. Jannasch, R. Johnson, T.D. Dickey, J. McNeil, A.F. Michaels, and A. H. Knap. 1998. Influence of mesoscale eddies on new production in the Sargasso Sea. Nature **394:** 263-266.

McGillicuddy, D.J., L.A. Anderson, N.R. Bates, T. Bibby, K.O. Buesseler, C.A. Carlson, C.S. Davis, C. Ewart, P.G. Falkowski, S.A. Goldthwait, D.A. Hansell, W.J. Jenkins, R. Johnson, V.K. Kosnyrev, J.R. Ledwell, Q.P. Li, D.A. Siegel, and D.K. Steinberg. 2007. Eddy/Wind interactions stimulate extraordinary mid-ocean plankton blooms. Science **316:** 1021-2026.

Michaels, A.F., and M.W. Silver. 1988. Primary production, sinking fluxes and the microbial food web. Deep Sea Res. A **35:** 473-490.

Mills, M.M., C. Ridame, M. Davey, J. LaRoche, and R.J. Geider. 2004. Iron and phosphorus co-limit nitrogen fixation in the eastern tropical North Atlantic. Nature **429:** 292-294.

Price N.M., and F.M.M. Morel. 1990. Cadmium and cobalt substitution for zinc in a marine diatom. Nature **344:** 658-660.

Price, N.M. 2005. The elemental stoichiometry and composition of an iron-limited diatom. Limnol. Oceanogr. **54:** 1159-1171.

Raven, J.A. 1990. Predictions of Mn and Fe use efficiencies of phototrophic growth as a function of light availability for growth and of C assimilation pathway. New Phytol. **116:** 1-18.

Richardson, T.L., and G.A. Jackson. 2007. Small phytoplankton and carbon export from the surface ocean. Science **315:** 838-840.

Saito, M.A., T. Goepfert, and J.T. Ritt. In press. Some thoughts on the concept of colimitation: Three definitions and the importance of bioavailability. Limnol. Oceanogr.

Schreiber, U., H. Hormann, C. Neubauer, and C. Klughammer. 1995. Assessment of photosystem II photochemical quantum yield by chlorophyll fluorescence analysis. Aust. J. Plant Phys. **22:** 209-220.

Strickland, J.D.H., and T.R. Parsons. 1972. A practical handbook of sea-water analysis, 2nd ed., v. 167. Bulletin of the Fisheries Research Board of Canada.

Strzepek, R.F., and P.J. Harrison. 2004. Photosynthetic architecture differs in coastal and oceanic diatoms. Nature **431:** 689-692.

Sunda, W.G., and S.A. Huntsman. 1997. Interrelated influence of iron, light and cell size on marine phytoplankton growth. Nature **390:** 389-392.

Tomas, C.R. [ed.]. 1997. Identifying marine phytoplankton. Academic.

Venrick, E.L., 1998. Spring in the California Current: the distribution of phytoplankton species, April 1993 and April 1995. Mar. Ecol. Prog. Ser. **167:** 73-88.

Venrick, E.L. 2000. Summer in the Ensenada front: the distribution of phytoplankton species, July 1985 and September 1988. J. Plankton Res. **22:** 813-841.

Wood, A.M., D.A. Phinney, and C.S. Yentsch. 1998. Water column transparency and the distribution of spectrally distinct forms of phycoerythrin-containing organisms. Mar. Ecol. Prog. Ser. **162:** 25-31.

III

Iron limitation across chlorophyll gradients in the southern Drake Passage: Phytoplankton

responses to iron addition and photosynthetic indicators of iron stress

Abstract

Processes influencing phytoplankton bloom development in the southern Drake Passage were studied using ship-board iron enrichment incubations conducted across a surface chlorophyll gradient near the Antarctic Peninsula, in a region of water mass mixing. Iron incubation assays showed that Antarctic Circumpolar Current (ACC) waters were severely iron limited, while shelf waters with high ambient iron concentrations (1 - 2 nmol L^{-1}) were iron replete, demonstrating that mixing of the two water masses is a plausible mechanism for generation of the high phytoplankton biomass observed downstream of the Antarctic Peninsula. In downstream high- chlorophyll mixed waters, phytoplankton growth rates were also iron limited, although responses to iron addition were generally more moderate as compared to ACC waters. Synthesizing results from all experiments, significant correlations were found between the initial measurements of Photosystem II (PSII) parameters (F_v:F_m, σ_{PSII}, and p) and the subsequent responses of these waters to iron addition. These correlations suggest that PSII parameters can be used to assess the degree of iron stress experienced in these waters, and likely in other regions where photoinhibition and nitrogen stress are not confounding factors.

Introduction

Explaining the distribution of phytoplankton biomass in the Southern Ocean has long been a challenge. While the major nutrients which control production throughout much of the world's oceans are plentiful in the Southern Ocean, high phytoplankton biomass is primarily found around or downstream of islands and the continental shelf,

and in the Antarctic Polar Frontal Zone (Sullivan et al. 1993; Holm-Hansen et al. 2005). Attempts to explain the causes of variability in phytoplankton biomass have focused on the availability of iron and light, the two strongest bottom up controls on phytoplankton growth in the Southern Ocean. Well studied seasonal blooms in the Ross Sea and the Antarctic Polar Frontal Zone are controlled by both light and iron availability (Smith et al. 2000; Sedwick et al. 2000). Light limitation prevails throughout the winter and late spring in regions with deep mixed layers (Mitchell et al. 1991). Only at the onset of stratification due to increased heating of surface layers, reduced winds, or melting of sea-ice do blooms begin to form, generally persisting for several weeks (Smith et al. 2000). Iron inputs to surface waters in regions that develop seasonal blooms occur primarily during the winter and early spring from deep mixing and melting of sea ice, and iron levels are relatively high at the beginning of the bloom (Sedwick et al. 2000). This iron is depleted as the growing season progresses to the point that phytoplankton biomass and growth rates become iron limited, leading to bloom decline.

Spring blooms are important phenomena over major areas of the Southern Ocean, but elevated phytoplankton biomass on continental shelves and near islands is more persistent throughout the summer months (Sullivan et al. 1993; Blain et al. 2001). High phytoplankton biomass around islands is especially evident in satellite images, in which low-chlorophyll regions persisting seasonally and inter-annually markedly contrast with high chlorophyll waters around island masses. Because detailed time series and spatial studies of these regions of elevated chlorophyll have primarily been performed using satellite observations, there is limited direct information on the mechanisms responsible for their formation and maintenance. Proximity of these chlorophyll transitions to islands,

the continental shelf, or seamounts suggests natural additions of iron as a potential cause, but changes in light availability due to stratification cannot be ruled out (Sullivan et al. 1993). Examining the influence of the Kerguelen Islands on phytoplankton distributions, Blain et al. (2001; 2007) found elevated levels of iron and chlorophyll in the island wake, but lower chlorophyll and iron outside, suggesting iron supply was responsible for the large phytoplankton blooms in the region. However, light availability was also found to be an important factor controlling phytoplankton biomass in the immediate vicinity of the islands where extremely deep mixed layers, up to 200 m, were found at some stations. By reviewing the literature, Holm-Hansen et al. (2005) showed waters over abyssal plains with low surface chlorophyll have low iron concentrations, while the higher chlorophyll waters found around topographic features including shelves, islands, and seamounts typically have high iron levels greater than 1 nmol L^{-1}, associations consistent with the hypothesized importance of iron in determining Southern Ocean phytoplankton distributions.

A major transition in surface chlorophyll concentration occurs in the southern Drake Passage near the Antarctic Peninsula where an extensive region of low-chlorophyll water, which exists across the eastern South Pacific sector of the Southern Ocean, shifts to high chlorophyll waters which continue across the Scotia Sea to the South Sandwich Islands (Fig. 3.1; Sullivan et al. 1993). On a cruise to study mechanisms responsible for this chlorophyll transition in February and March 2004, the physical, chemical, and biological structure of the transition region was surveyed extensively. It was determined that low chlorophyll ACC waters are funneled through a gap in the Shackleton Transverse Ridge, a bathymetric rise extending off the Antarctic Peninsula perpendicular

to ACC flow, creating a strong current (Zhou et al. unpublished). This jet of ACC water intrudes toward the shelf where mixing with high iron shelf water occurs. Additionally, in the lee of the jet, shelf water is pulled offshore and eddies are generated, leading to further mixing between the two waters. These transport and mixing processes may act as a natural iron fertilization of ACC waters responsible for the elevated chlorophyll in the mixing region and downstream. Herein, we present results from ship-board iron addition experiments conducted across the chlorophyll transition and in nearby shelf waters in order to assess the iron-limitation status of the phytoplankton community in each region. If iron supply induces the southern Drake Passage chlorophyll transition, we hypothesized that iron stress would be reduced across the chlorophyll front and changes in phytoplankton community structure and photosynthetic physiology between low and high chlorophyll waters might be similar to responses observed in ship-board iron addition grow-out experiments. An additional goal of this work was to conduct iron addition experiments across gradients in iron stress in order to determine whether photosynthetic parameters as measured by fast repetition rate fluorometry (FRRF) and photosynthesis vs. irradiance (P vs. E) incubations were robust indicators of iron limitation. Many of these photosynthetic parameters have been shown to be influenced by iron limitation, but have primarily been studied at the extremes of iron limitation or nutrient replete conditions in the field. The heterogeneous and evolving mesoscale structure of the southern Drake Passage presents a natural laboratory to examine the responses of photosynthetic physiology to gradients in iron stress, allowing their utility as indicators of iron stress to be assessed.

Methods

<u>Water type assignments</u>

In the region sampled, ACC and shelf waters were identified as the two primary water types (Zhou et al. unpublished). A mixing index (DW) describing the percent mixture of these two water types was calculated for each station using temperature and salinity characteristics in the upper 50 m of the water column at each station (Zhou et al. unpublished). Because small amounts of shelf water, which might not be resolved with the DW index, could cause large biological responses, we also used biological characteristics (chlorophyll distributions) to define water types. In particular low surface chlorophyll with a deep chlorophyll maximum between 60 – 90 m is typical of low productivity, iron limited ACC waters (Holm-Hansen et al. 2005). For the purposes of this paper, stations with DW < 0.3 were considered 'ACC' when surface chlorophyll was low (~0.1 μg L^{-1}) and a subsurface chlorophyll maximum was present, and 'Mixed' if surface chlorophyll was high (> 0.8 μg L^{-1}) with no subsurface chlorophyll maximum. 'Shelf' stations had DW > 0.85. In figures and tables, these water types are designated 'A' (ACC), 'M' (Mixed), and 'S' (Shelf).

<u>Experimental protocols</u>

Water for experiments was collected using a trace metal clean rosette system consisting of GO-Flo bottles and a CTD mounted on an epoxy coated frame (Measures et al. unpublished). Immediately after the rosette was retrieved, the bottles were pressurized with ultra-high purity nitrogen gas and water was dispensed into acid-washed incubation vessels in a clean environment. Most incubations were conducted in 4 L polycarbonate bottles, except incubation M1 in which 50 L low-density polyethylene carboys were used.

For each experiment two containers were spiked with 5 nmol L^{-1} $FeCl_3$ from an acidified 75 μmol L^{-1} stock solution, and two containers were left unamended as controls. The containers were then sealed and transferred to a temperature-controlled van outfitted with banks of blue-fluorescent lights (Philips TLD 36W/18). Lights were on continuously and the van was maintained at 2-3 °C to replicate ambient temperatures. Incubations from the surface mixed layer were incubated without shading in the van at an irradiance of 140-220 μmol photons m^{-2} s^{-1}, levels saturating for photosynthesis as determined from P vs. E data. For comparison with incubation conditions, characteristics of the in situ light environment were calculated based on mixed layer depths, measured diffuse attenuation coefficients, and the average incident surface irradiance over the cruise.   Incubation light intensities were comparable to the average light intensities experienced by mixed layer phytoplankton (140-250 μmol photons m^{-2} s^{-1}) over the approximately 14 hour photoperiod in our study area, but lower than the 400 - 600 μmol photons m^{-2} s^{-1} maximal light intensity over the photoperiod. However, because incubations were conducted under continuous illumination, time- integrated daily light doses during incubation were roughly double in situ values (Table 3.1). It should be noted that the use of continuous light may have modified phytoplankton community structure, since certain species are known to survive under only a limited range of photoperiod lengths (Timmermans et al. 2001). Incubations from deeper waters were shaded in an attempt to match light levels measured at the sampling depth (30-40 μmol photons m^{-2} s^{-1}), but again because of continuous irradiance during incubation and overestimation of light levels, daily light doses were up to 10 times higher than in situ light levels estimated assuming the deep layers sampled remained at a constant depth and no mixing occurred. Incubations were

sampled every other day. Four liter bottles were sampled under a Class 100 laminar flow hood. Fifty liter carboys were sampled in the incubation van, using a hand vacuum pump and a specially designed sampling cap to prevent contamination.

General

Chlorophyll *a* (Chl *a*) was determined fluorometrically using a methanol extraction method (Holm-Hansen and Reimann 1978). Water was filtered through a GF/F filter, and extracted in methanol overnight at 4°C. Fluorescence of the methanol extracts was measured before and after acidification to determine chlorophyll concentrations. For size fractioned Chl *a*, filters (2 μm or 20 μm) were placed on a wetted filter base of either stainless steel (Millipore) or polystyrene (Nalgene) and filtrate collected in a clean glass or polycarbonate container. 100-150 mL of water was gravity filtered with constant swirling to keep cells suspended, and the filtration was ended when 25-50 mL of seawater remained in the funnel. The filtrate was then passed through a GF/F to catch all particles which were not retained on the 2 μm or 20 μm filters. Chl *a* was measured on the GF/F filters as described above, resulting in concentrations of Chl *a* in the < 2 μm and < 20 μm size fraction. Chl *a* in the <2 μm, 2-20 μm, and >20 μm size fractions was determined by mass balance with total Chl *a*.

Particulate organic carbon (POC) and particulate organic nitrogen (PON) were determined using a CHN elemental analyzer. Samples were collected by filtering 1-2 L of water though a precombusted GF/F filter, and stored in liquid nitrogen until analysis. Nutrients (NO_3, NO_2, NH_3, PO_4, and Si) were analyzed on an autoanalyzer using standard colorimetric methods. Iron measurements were made using a flow injection analysis system as described in Measures, et al. (1995), and detailed analyses of trace metal

distributions in the region will be discussed in Measures et al. (unpublished). Reported

iron concentrations (Table 3.1) are taken from rosette cast profiles immediately prior to

the casts used to collect incubation water at the same station. For most stations these

values should be representative of iron concentrations in incubation source waters.

However, water for incubations A1 and A3 was collected in a region with sharp spatial

gradients in water properties. The relatively high iron concentrations reported for these

incubations (Table 1) are not likely to be representative of actual incubation water based

on the strong responses observed to iron addition and the initial community

measurements of photosynthetic parameters measured on actual incubation waters (see

Results and Discussion).

<u>HPLC pigments</u>

Samples for HPLC analysis of phytoplankton pigments were collected on GF/F

filters and stored in liquid nitrogen until analysis. HPLC analysis of pigments using a C8

column separation method was conducted at CHORS/SDSU (Van Heukelem and Thomas

2001). The CHEMTAX program was used to estimate the contribution of different

phytoplankton taxa to total Chl *a* (Mackey et al. 1996). Taxa known to be present in

Antarctic waters (diatoms, haptophytes, dinoflagellates, cryptophytes, prasinophytes, and

chlorophytes) were included in the analysis using initial pigment ratios for each taxa

determined for Antarctic waters by Wright et al. (1996).

<u>Fast repetition rate fluorometry (FRRF)</u>

A Chelsea Fastracka FRR Fluorometer was used to measure the kinetics of

fluorescence induction and decay on incubation algal assemblages, and the response

fitted to estimate photosystem II (PSII) parameters. All samples were dark acclimated for

at least 1 hour prior to analysis, then circulated through the measurement path of the instrument using a peristaltic pump. The flash protocol consisted of a single turnover saturation phase in which 100 flashlets of 1.46 μs duration were delivered at intervals of 2.8 μs, followed by a relaxation phase consisting of 20 flashlets of the same duration at 51.6 μs spacing. Sets of 15 flash sequences were internally averaged as a single acquisition, and 100 such acquisitions were obtained for each sample and subsequently averaged to obtain high signal to noise fluorescence response curves (Fig. 3.2).

A set of detailed characterization experiments to determine fluorescence baseline and instrument biases were conducted onboard using the identical flash protocol employed for samples, following the procedure described in Laney (2003). Blanks at each gain setting were measured using both de-ionized water (Millipore) and 0.22 μm filtered seawater. While some investigators have reported differences between these blanks (Cullen and Davis 2003), no significant differences were observed in this study. Because of the relatively high chlorophyll concentrations in our incubation samples, the magnitude of the blank was small compared to the measured signal; generally <0.2% and always <4% of the sample maximal fluorescence. Time-dependent responses in fluorescence detection were also assessed and corrected for using measurements of an inert fluorochrome, Rhodamine B.

The averaged fluorescence responses were fitted to the Kolber et al. (1998) physiological model of variable fluorescence using v5 software (Laney 2003). The output included fitted values for the minimal (F_o) and maximal (F_m) fluorescence yields, the effective absorption cross-section for PSII (σ_{PSII}), the connectivity between PSII reaction centers (p), which was allowed to range between 0 and 1, and the turnover time (τ) of

PSII which was modeled as a single exponential decay. F_v:F_m, a measure of the efficiency of photochemistry in PSII, is calculated as $(F_m - F_o)/F_m$. Light intensities in the measurement chamber were calibrated by the manufacturer (Chelsea) in order to calculate absolute values of σ_{PSII}. The model fit for each sample was examined visually to ensure a reasonable coherence with the data, and comparisons between model fits with and without the p parameter confirmed that p was used to compensate for deviations from a Poisson distribution during the rise to F_m (Fig. 3.2). Additionally as shown in Fig. 3.2, samples with larger σ_{PSII} often exhibited reductions in fluorescence towards the end of the saturation flash sequence, in which case only the first 50 saturation flashlets were used as input to the model.

Photosynthesis vs. irradiance

^{14}C photosynthesis-irradiance experiments (P vs. E) were performed in a modified photosynthetron at in situ or incubation van temperature as appropriate for 1-2 hours (Lewis and Smith 1983). Samples were acidified and degassed overnight to remove inorganic ^{14}C, and fixed ^{14}C was measured by liquid scintillation counting. Experimental data were normalized to Chl a and fit to the Platt et al. (1980) model, to calculate α^{Chl}, P^{Chl}_{max}, and the light saturation parameter ($E_k = P^{Chl}_{max}/ \alpha^{Chl}$). The photoinhibition parameter was set to zero if no significant photoinhibition was found.

Flow cytometry

Samples (50 mL) were collected from incubations and stored on ice in the dark until analyzed by flow cytometry within 1- 6 hours of collection. The flow cytometer used was a Beckman-Coulter XL, equipped with a 15 mW 488 nm argon ion laser and mated to an Orion syringe pump for quantitative sample delivery. In order to estimate

phytoplankton biomass, the normalized forward light scatter signature was calibrated for cell size, allowing estimation of a diameter for each particle. Diameters were converted to spherical volumes, with the volumes used to estimate carbon biomass per cell using the Menden-Deuer and Lessard (2000) general equation for protist plankton: $\log \text{pg C cell}^{-1} = 0.860 \times \log(\text{volume}) - 0.583$. Because cells >20 μm in diameter had the maximum forward scatter signal recorded by the flow cytometer, cells in this size range were set equal to the biovolume of 20 μm cells and the calculated biomass from them is considered a conservative estimate.

Iron limitation indices (ILIs)

To quantify the degree of iron stress at each incubation station, the ratio of Chl *a*, POC, or Chl *a* derived growth rate (μ), in iron addition treatments was normalized to the respective value in the control treatments to produce an iron limitation index (ILI): ILI_{Chl}, ILI_{POC}, ILI_{μ} respectively (Table 3.2; similar to Firme et al. 2003). Generally POC samples were only taken on the final day of each experiment (Day 7-14) and so data to compute both ILI_{Chl} and ILI_{POC} were taken from the final time point so that the indices could be compared directly. Growth rates to calculate ILI_{μ} were determined by linear regression through natural log transformed Chl *a* data from the time period of exponential growth.

Results and Discussion

A total of 9 incubations were conducted during the cruise: 4 in ACC waters, 3 in Mixed waters, and 2 on the continental shelf (Fig. 3.1). Upper mixed layer water was used in the majority of the experiments, but two ACC water incubations were from the

subsurface chlorophyll maximum and one Mixed water incubation was taken from the

lower euphotic zone (Table 3.1). Incubation responses varied among the water types, but

in a given water type results from different incubations were similar (Tables 3.2-3.4). A

synthesis of all experimental results is discussed in the following text, and Figures 3.3-3.5

will illustrate one incubation typical of each water type.

ACC water incubations

Phytoplankton assemblages from the extremely low iron (as low as 0.1 nmol L^{-1};

Measures et al. unpublished) and low phytoplankton biomass (0.1 - 0.25 μg L^{-1} Chl a)

ACC waters responded strongly to iron additions, consistent with previous observations

in this region (Helbling et al. 1991). After a two day lag period Chl a began to increase at

a rapid rate in the Fe treatments, but at a much slower rate in the controls, although there

was a consistent increase throughout the control experiments (Fig. 3.3A). POC

concentrations were higher in Fe treatments, although the magnitude of the response was

proportionally less than that of Chl a, as shown by comparisons of ILI$_{Chl}$ and ILI$_{POC}$ for

each experiment (Table 3.2). Cellular Chl a levels are reduced under iron limitation, most

likely accounting for the difference in the magnitude of Chl a and POC responses. Higher

POC:Chl a ratios in controls (184-324 g:g), as compared with Fe treatments (66-132 g:g)

provide support for this interpretation, although it should be noted that detritus and

heterotrophs are included in POC measurements.

Chl a and NO$_3^-$ derived growth rates (μ$_{Chl}$ and μ$_{NO3}$), determined by linear

regression of log transformed data, were similar and clearly affected by iron addition

(Table 3.2). μ$_{Chl}$ values were higher on average than μ$_{NO3}$ for Fe treatments, but lower

than μ$_{NO3}$ for control treatments, which can be attributed to changes in cellular Chl a

content depending on iron availability. Si:NO$_3^-$ drawdown ratios were high in controls, a frequently observed consequence of excess silicification in iron-limited diatoms (Hutchins et al. 1998). In contrast Fe treatments had Si:NO$_3^-$ drawdown ratios near one, the typical ratio observed in nutrient-replete diatoms (Table 3.2). Pigment data indicates diatoms dominated both control and Fe treatments such that bulk nutrient drawdown ratios primarily reflect the activity of diatoms (Table 3.3; Fig. 3.3H). Deviations from Redfield N:P ratios have been observed in some Southern Ocean blooms and incubation experiments, and we also found lower NO$_3^-$:PO$_4^{3-}$ drawdown ratios in the control treatments, possibly due to increased P content of iron stressed phytoplankton (Table 3.2; De Baar et al. 1997; Price 2005). While incubation assemblages do not precisely replicate water column communities, the nutrient depletion processes observed here likely operate in situ as manifested by the large scale depletion of Si relative to NO$_3$ in the Southern Ocean (Sarmiento et al. 2004).

The photosynthetic physiology of the phytoplankton assemblage was assessed at each incubation sampling with FRRF, and less frequently with P vs. E measurements. F_v:F_m, the maximum quantum yield for PSII photochemistry, increased after iron addition to maximum values of 0.36-0.44, but declined toward the end of the experiments presumably due to resumed iron stress after depletion of added iron by uptake, precipitation of iron oxides, or wall adsorption (Fig. 3.3C). The initial increase in control F_v:F_m suggests a slight iron contamination may have occurred, potentially accounting for the small growth observed in the control bottles. The PSII target size, σ_{PSII}, dropped precipitously in both treatments during the first few days of incubation, after which Fe treatments had slightly but consistently smaller σ_{PSII} sizes (Fig. 3.3D) . Because Chl *a*

levels did not change in the first few days of the experiment, and pigment data from several incubations showed only minor changes in community structure after slight increases in Chl *a* (data not shown), the decline in σ_{PSII} presumably occurred prior to major changes in phytoplankton community structure. This suggests a strong physiological acclimation of σ_{PSII} as a result of interactions between changing light and iron availability. The rapid initial drop in σ_{PSII} is probably caused by higher light doses under incubation conditions than were experienced in situ, and smaller σ_{PSII} sizes are commonly found under iron replete conditions. (Greene et al. 1992; Suzuki et al. 2002). The electron transfer rate through PSII, τ^{-1}, increased in both treatments, but to a greater extent in Fe treatments than controls (Fig. 3.3E). *p*, the degree of connection between photosynthetic units, was initially moderately high but dropped off over the course of the incubation in control treatments, while remaining constant in Fe treatments (Fig. 3.3F), consistent with culture studies showing iron limitation reduces *p* (Greene et al. 1992; Vassiliev et al. 1995).

The behavior of P vs. E parameters varied among ACC experiments. The initial slope of the P vs. E curves, α^{Chl}, generally declined during incubations, perhaps due to elevated light doses during incubation, but was often higher at the end of experiments in Fe treatments (Table 3.4). There were no clear trends in the behavior of P^{Chl}_{max}, the maximum rate of photosynthesis, but in three out of four ACC water experiments P^{Chl}_{max} was higher in Fe treatments by the end of the experiment. The normalization of α^{Chl} and P^{Chl}_{max} to Chl a, which changes on a cellular basis depending on iron stress or light level, may obscure cellular photosynthetic responses to iron, but alternative normalization variables including POC and flow cytometry derived carbon biomass are also

problematic because of detrital material included in POC and maximal size estimates available from flow cytometry (see Methods). While results varied significantly between experiments, higher P^{Chl}_{max} and α^{Chl} values generally observed in Fe treatments are consistent with results from laboratory culture experiments testing the effects of Fe limitation on photosynthetic physiology (Greene et al. 1991).

Phytoplankton community and size structure were not significantly different between control and Fe treatments, but shifts to larger sized phytoplankton and diatom dominance were seen compared to the initial community (Table 3.3; Fig. 3.3G,H). As determined by CHEMTAX analysis of HPLC pigment data, diatoms were initially abundant, though variations between experiments were large (Table 3.3). These observations are consistent with historical data showing that diatoms tend to dominate phytoplankton communities in these waters, though in some years flagellate-dominated communities have been observed (Villafane et al. 1995). As is typically observed in iron addition incubations, diatoms came to dominate Fe treatments contributing >80% to Chl a in all cases. However because diatoms were already abundant in initial communities, changes in community structure were less dramatic than is often observed. Diatoms also dominated control treatments, and the lack of difference between Fe and control treatments may be due to various factors including slight iron contamination of controls or effects of bottle confinement on community dynamics. In particular, grazing pressure was likely reduced on larger phytoplankton, such as diatoms, due to under-representation of mesozooplankton. Size-fractioned Chl a and flow cytometry both illustrate the abundance of large cells in initial communities and incubation treatments (Fig. 3.3G; Table 3.3). At more than 50% of total Chl a, the proportion of the initial phytoplankton

community in the >20 µm size fraction is somewhat greater than has typically been found in low chlorophyll Antarctic waters (e.g. Villifane et al. 1995), although methodological differences make comparisons between size-fractioned measurements difficult.

<u>Mixed waters</u>

Although initial phytoplankton biomass was elevated in the Mixed waters (0.8 – 1.4 µg Chl *a* L^{-1}) compared to ACC waters, iron concentrations were similarly low in the 0.1 - 0.3 nmol L^{-1} range (Table 3.1; Measures et al. unpublished). The Mixed water stations where incubations were started were predominantly ACC water (DW < 0.3), well off the shelf break, with apparently only small amounts of shelf water mixed in (Fig. 3.1; Zhou et al. unpublished). Clear responses were observed upon addition of iron to Mixed waters which were qualitatively similar to those in ACC waters, but lesser in magnitude as shown by ILI values computed for each incubation (Table 3.2). Chl *a* and POC increased in both Fe and control treatments, but at a more rapid rate in bottles with added Fe indicating net growth rates in these waters could be iron limited (Fig 3.4A; Table 3.2). Si:NO$_3^-$ drawdown ratios were nearly 2 in control treatments in all Mixed water incubations indicative of iron limited diatom growth, while drawdown ratios in Fe treatments returned to 1 (Table 3.2). Pigment data showed diatoms dominated growth in both control and Fe treatments, and so drawdown ratios should largely reflect diatom physiology (Table 3.3). The response of NO$_3^-$:PO$_4^{3-}$ drawdown ratios to iron addition was not consistent among Mixed water experiments. In two Mixed water experiments, NO$_3^-$:PO$_4^{3-}$ drawdown ratios were lower in control treatments as was found in ACC water incubations. However, one Mixed water experiment did not show a difference in NO$_3^-$:PO$_4^{3-}$ drawdown between treatments.

Photosynthetic parameters in Fe and control treatments diverged, becoming characteristic of iron limitation in controls (Fig. 3.4). F_v:F_m was initially 0.28-0.38, intermediate between the low values found in ACC waters and higher values on the shelf (Table 3.1). In Fe treatments F_v:F_m stayed high throughout the experiment, increasing slightly after iron addition and falling moderately in the final days of the incubation (Fig. 3.4C). F_v:F_m declined in controls over the course of the experiment. Photoinhibition at elevated incubation light levels may have contributed to the decline, but the duration of the decline and strong separation between +Fe and control treatments indicates increasing iron stress in controls was also important. The results suggest the moderately low F_v:F_m in Mixed waters is due to more mild iron stress relative to ACC waters. p roughly followed the behavior of F_v:F_m (Fig. 3.4F), and τ^{-1} increased in Fe treatments, while decreasing in controls, again suggesting relief of iron limitation after supplementation with iron, and increased iron stress in controls as macronutrients are depleted (Fig. 3.4E; Greene et al. 1991; Greene et al. 1992). As in the ACC water experiment, a drop in σ_{PSII} occurred in the first few days of the incubation. However, σ_{PSII} in Fe treatments continued to fall leveling off at a much lower value than the controls, creating greater separation between treatments than seen in ACC experiments (Fig. 3.4D). This may be due to differences in the response of each community to the interacting influences of iron and light, perhaps affected by the initial iron limitation status or community composition of the phytoplankton. P^{Chl}_{max} and α^{Chl} were higher in Fe treatments for incubations M2 and M3 due to declines in control bottles over the course of the incubation which may be the result of the combined effects of increasing iron stress and elevated incubation light doses

(Table 3.3). However in M1 P^{Chl}_{max} and α^{Chl} did not change a great deal during incubation except for a small decline in P^{Chl}_{max} in the Fe treatment.

Large diatoms dominated Mixed waters initially and continued to grow in both control and Fe treatments. Pigment, particle count, and size fractioned Chl *a* data indicated there were only small shifts in community composition and size structure between the initial and final communities, and no differences between control and iron treatments (Fig. 3.4G,H; Table 3.2).

Shelf waters

On the continental shelf, ambient iron concentrations were high (1 - 2 nmol L^{-1}) making iron limitation unlikely (Table 3.1; Measures et al. unpublished). In incubations initiated from shelf waters no differences between control and Fe treatments were observed, even after strong growth and macronutrient drawdown (Fig. 3.5). Chl *a* and POC increased rapidly in all treatments, indicating iron was not limiting in shelf waters, and was present in sufficient quantities to allow macronutrients to be depleted significantly (Fig. 3.5A,B). Initial photosynthetic parameters were characteristic of healthy, growing cells and remained so throughout the incubations. Presumably due to the incubation light regime, τ^{-1} increased and σ_{PSII} decreased during the experiment (Fig. 3.5D,E). $F_v:F_m$ and *p* remained at high values throughout the experiment, and there were no differences between Fe and control treatments for any of the PSII parameters (Fig. 3.5C-F). The size structure of the initial shelf phytoplankton communities was distinctly smaller than ACC and Mixed water despite relatively high biomass, with Chl *a* mostly in the nanoplankton (2 – 20 µm) size class (Fig. 3.5G ; Table 3.3). However, during incubation, microplankton (>20 µm) growth was most rapid, reaching >80% of size

fractioned Chl *a* by the end of the experiments (Fig 3.5G ; Table 3.2). Taxonomic composition of phytoplankton at the start of experiments was variable with diatoms dominating incubation S1, and haptophytes and diatoms in roughly equal proportions in S2, but diatoms were most successful under incubation conditions in both experiments (Fig. 3.5H; Table 3.3).

Despite high iron and macronutrient concentrations, phytoplankton biomass was relatively low on the shelf for the month long duration of our cruise, although at 0.4 – 1.0 µg Chl *a* L^{-1} it was still higher than ACC waters and similar to Mixed waters. Because shelf waters were weakly stratified and deep mixed layers are often observed light availability is a potential constraint on phytoplankton growth (Mitchell et al. 1991). The smaller size of phytoplankton found on the shelf is also consistent with light stress, as smaller phytoplankton with greater surface area to volume ratios are more successful at harvesting light under low-light conditions. However, grazing pressure on larger phytoplankton from abundant krill may also alter the phytoplankton community size structure and potentially limit increases in phytoplankton standing stocks (Haberman et al. 2003). Although we are not able to thoroughly assess limitations on shelf phytoplankton biomass in this analysis, identifying constraints on shelf biomass is important, not only for the shelf ecosystem, but also for understanding conditions allowing bloom development after the mixing of ACC and shelf waters. The lack of significant phytoplankton growth and iron utilization may maintain high iron concentrations on the shelf, allowing shelf waters to serve as an iron source to the ACC (Measures et al. unpublished).

Natural iron fertilization in the Southern Drake passage

These incubation experiments were conducted as part of an interdisciplinary project designed to test the hypothesis that natural iron fertilization of ACC waters is occurring in the Southern Drake passage. The experimental results from our 2004 cruise suggest that phytoplankton growth rate and ultimate biomass, in the absence of other limiting factors, were limited by iron in both the ACC and Mixed waters in the southern Drake Passage, while shelf waters were iron-replete, potentially serving as a source of iron to ACC waters. Because of increased light doses, the continuous photoperiod experienced by phytoplankton in incubations (Table 3.1), and inevitable undersampling and disturbance of the zooplankton community, these incubations, on their own, cannot be used to assess the influence of grazing and light limitation, nor do they replicate in situ community development. However, their utility as assays of iron stress has been validated by mesoscale enrichment experiments (e.g. Coale et al. 2004), and we employ them as a component of a multidisciplinary study to understand regional processes controlling phytoplankton distributions. Our incubation results complement physical data from the study area which show ACC waters are funneled through a gap in the Shackleton Transverse Ridge, a bathymetric rise nearly perpendicular to ACC flow which begins at the tip of the Antarctic Peninsula, creating a strong current which resulted in mixing between ACC and shelf waters in the region to the east of the gap (Measures et al. unpublished; Zhou et al. unpublished; Fig. 3.1). Incubation experiments demonstrate that mixing of a small amount of high iron shelf water with severely iron depleted ACC waters is a plausible mechanism for creation of the higher phytoplankton biomass found downstream in the ACC.

Many of the differences in phytoplankton physiology and community structure between ACC and Mixed waters were replicated by experimental addition of iron to ACC waters, helping support the hypothesis that Mixed water blooms were the result of natural iron additions to ACC waters. The principal distinctive characteristic of Mixed waters, increased phytoplankton biomass, was clearly a response to iron in incubation experiments. Higher Chl *a* and POC concentrations were found in Fe treatments compared with controls in all ACC water experiments (Fig. 3.3; Table 3.2). PSII parameters also showed distinct responses to experimental additions of iron, and similar variations between ACC and Mixed waters were evident (Table 3.1). Near-surface waters collected for incubation experiments initially had higher F_v:F_m and faster electron transfer rates (τ^{-1}) in Mixed waters compared to ACC waters, trends similar to those found in response to Fe addition to ACC waters (Table 3.1; Fig. 3.3). σ_{PSII} sizes were smaller in Mixed waters, and slightly lower σ_{PSII} values were seen in Fe treatments compared to controls in ACC incubations (Table 3.1; Fig 3.3D). Although the PSII parameter trends between control and Fe treatments are clearly similar to the trends between ACC and Mixed waters, the magnitudes are often different, probably due to differences in degree of relief from iron stress and light conditions between natural waters and incubations.

Shifts toward larger phytoplankton and more diatoms in ACC water experiments resulted in a final incubation community more similar to that found in Mixed waters. In three out of four ACC water experiments the initial community was composed of approximately equal proportions of haptophytes and diatoms and had ~50% Chl *a* in the >20 μm size fraction (Table 3.3). By the end of the experiments diatoms dominated, and

>20 μm Chl *a* increased to 75-80%, similar to Mixed waters except for the under-representation of haptophytes in incubations. Although these observations are consistent with the hypothesis that the phytoplankton blooms found in Mixed waters result from natural inputs of iron, the community shift in our iron addition incubations cannot be unambiguously attributed to iron because it was observed in both control and Fe treatments. In summary, however, the characteristic biological features which distinguish Mixed from ACC waters are generally elicited by experimental addition of iron to ACC waters, lending support to the hypothesis that natural iron additions from iron-rich shelf water are responsible for the increased phytoplankton biomass observed in Mixed waters.

<u>Indicators of iron limitation</u>

Development of physiological or chemical diagnostics of nutrient stress has been a continuing goal of the oceanographic community, particularly for iron limitation. Indicators of iron stress have focused on the photosynthetic systems of phytoplankton, which are sensitive to iron stress because of their high iron requirements. A major direction of this research has been the use of active fluorescence methods to probe PSII function. These techniques have proven valuable in field settings for large scale surveys where rapid, repetitive measurements are required (e.g. Behrenfeld and Kolber 1999; Suzuki et al. 2002). However, field studies of phytoplankton photosynthetic physiology have primarily examined the extremes of iron limitation and nutrient replete conditions. In this study, data from iron-addition incubations conducted across a gradient in iron stress are examined for relationships between initial photosynthetic physiological parameters and subsequent responses of phytoplankton to iron addition. This analysis

helps identify and validate the utility of fluorescence and P vs. E derived photosynthetic

physiological parameters as indicators of degrees of iron stress.

Employing ILIs as metrics for iron stress, significant relationships ($p < 0.05$) were

found between initial photosynthetic characteristics and biomass (ILI_{Chl}, ILI_{POC}) and

growth rate (ILI_μ) responses to iron addition (Table 3.5, Fig. 3.6). FRRF derived PSII

characteristics were found to be the best indicators of iron limitation, especially $F_v:F_m$

and σ_{PSII}, which were sensitive to degrees of iron stress (Fig. 3.6). Data from all

incubations were included for regressions with ILI_{Chl} and ILI_μ, but the data point from

incubation A4 was excluded as an outlier for ILI_{POC} correlations. While the value of ILIs

change as incubations develop, and incubations were of different duration, similar

relationships with PSII parameters were found using ILI_{Chl} computed at day 8, 10, and the

final time points, suggesting relationships determined are robust with respect to temporal

changes in ILIs (data not shown). $F_v:F_m$ had significant relationships with all ILIs. While

σ_{PSII} was also well correlated with ILI_{Chl} and ILI_{POC}, the relationship with ILI_μ was

weaker and not quite significant at the 0.05 level. The p parameter had a significant

relationship with ILI_{Chl} (Fig 3.6F), but this may be spurious as there were no clear trends

between p and other ILIs (Table 3.5).

The trends observed are consistent with known effects of iron on PSII

parameters. Strong responses to iron were found when $F_v:F_m$ was low, and numerous

culture and field studies have shown reductions in $F_v:F_m$ under iron stress (e.g. Greene et

al. 1992; Suzuki et al. 2002). The association of larger σ_{PSII} with iron stressed

phytoplankton in our study region is consistent with many field and culture studies

(Greene et al. 1992; Suzuki et al. 2002), though in some cases a decrease in σ_{PSII} with

iron stress has been observed (Vassiliev et al. 1995). Increasing σ_{PSII} may be beneficial under iron stress as an acclimation to maximize light capture with a minimum number of iron containing reaction centers (Greene et al. 1992). Because σ_{PSII}, the functional absorption cross section of PSII, is a product of the optical absorption cross-section of the PSII antennae complex and $F_v{:}F_m$, σ_{PSII} and $F_v{:}F_m$ are not independent parameters (Kolber et al. 1998). However, iron-stress reduced $F_v{:}F_m$, whereas σ_{PSII} increased, indicating variability in the optical absorption cross section under changing iron availability controlled the behavior of σ_{PSII}. Measurement of σ_{PSII} adds additional information to assess iron limitation since σ_{PSII} seems to primarily reflect the optical absorption cross-section in the field data, and correlates with experimental responses to iron addition. While the correlation between p and ILI_{Chl} may have arisen by chance, the negative relationship observed is consistent with limited culture data showing p is lowered under iron stress (Greene et al. 1991; Greene et al. 1992; Vassiliev et al 1995). p is interpreted as a measure of the interconnection between PSII units, although the physiological mechanisms responsible for energy transfer between reaction centers are not well understood (Ley and Mauzerall 1986). Candidate mechanisms, including close physical proximity of reaction centers or sharing of antennae complexes, would be negatively impacted by iron limitation as disconnected pigment-protein complexes accumulate and reaction center density decreases. However, alternative explanations for the p parameter and its variability are possible such as uneven light absorption in densely pigmented cells (Greene et al. 1992), or changing distributions of σ_{PSII} values from different members of the natural phytoplankton community.

Olson et al. (2000) provided the only previous published report of a relationship between initial photosystem parameters and incubation responses to iron addition. They documented a correlation between initial $F_v{:}F_m$ and the response of $F_v{:}F_m$ to iron addition in the western Pacific sector of the Southern Ocean. The relationships we find are similar, but significant in that we find $F_v{:}F_m$ can be used to predict biomass and net-growth rate limitation by iron. Additionally, the linear relationships found between ILIs and $F_v{:}F_m$ and σ_{PSII} as opposed to threshold responses, indicate that these parameters are capable of resolving degrees of iron stress (Fig. 3.6). This ability to distinguish degrees of iron limitation is important since many systems, including the region of our study and some eastern boundary current systems such as the California Current, are subject to different levels of iron stress with varying consequences for the ecology and biogeochemistry of the waters (Hutchins et al. 1998; Firme et al. 2003).

Other parameters which are known to be influenced by iron stress, did not have significant relationships with ILIs, suggesting other environmental factors had stronger influence on them in this system. Although culture studies show they can be sensitive to iron limitation, the P vs. E parameters, α^{Chl} and P^{Chl}_{max}, had no relationship with degree of iron limitation (Table 3.5). τ^{-1} was generally smaller at ACC stations, and responses of τ^{-1} to iron addition were observed, but correlations between ILIs and τ^{-1} were not significant (Table 3.5). Additionally, no significant correlations were found between iron concentrations and ILI_{Chl} or ILI_{POC}, and although a significant correlation occurred between ILI_μ and iron concentrations, this regression was leveraged solely by the high iron concentrations on the shelf and cannot be considered a useful relationship without data from locations with intermediate iron concentrations. In our study region a

disconnect between iron concentrations and iron stress, except at the most general level, likely occurs because introduced iron is rapidly taken up in Mixed waters. Thus the rate of nutrient supply, which is often difficult to determine, is frequently more important than nutrient concentrations, again emphasizing the need for alternative indicators of nutrient stress.

The observed relationships between PSII parameters and incubation responses to iron addition suggest phytoplankton iron stress is an important control on photosynthetic physiology in the southern Drake Passage. These correlations do not imply causation, but instead may reflect a co-dependence of ILIs and PSII parameters with iron availability in the waters. Likely biochemical consequences of iron stress can be used to rationalize these trends by analogy with responses to iron stress observed in culture experiments. However other possible confounding factors should be considered before concluding our correlations do reflect the influences of iron. Nitrogen stress is known to affect PSII in ways similar to iron stress, but nitrate levels were high throughout the region, greater than 20 µmol L^{-1}. Because iron is involved in nitrate uptake, as a cofactor in nitrate reductase (Maldonado and Price 1996), low iron could indirectly result in nitrogen stress reducing photosynthetic competency, but even if this were the case nitrogen stress would reflect lack of iron and not invalidate the interpretation of our correlations between ILIs and PSII parameters. High light levels can also influence PSII parameters, but different trends might be expected if photoinhibition were a strong influence. High light generally decreases $F_v:F_m$ and σ_{PSII} together due to damage of PSII reaction centers and the need to reduce antennae size to limit light capture, although it is possible that photoinhibition may increase σ_{PSII} if reaction centers are damaged but light

harvesting proteins are not reduced, effectively increasing the ratio of antennae to reaction center proteins (Kolber et al. 1988; Falkowski and Kolber 1995). We find increased σ_{PSII} where F_v:F_m is low, a combination observed under iron stress. Diel cycles in F_v:F_m have been observed in the field due to photoinhibition and iron stress, potentially influencing the relationships we determined (Behrenfeld and Kolber 1999). Our incubations were generally set up around mid-day and there was no consistent bias in setup time for any one water type, ruling out time of day as confounding factor. Other studies have found that phytoplankton community structure can be an important control on σ_{PSII}, and possibly influence other PSII parameters (Moore et al. 2006). However in the southern Drake Passage we did not find any relationships between the proportion of diatoms or haptophytes in a community and σ_{PSII} or F_v:F_m (all r^2 values < 0.17, p values > 0.3, $n=9$). Iron appears to be the primary control on PSII parameters at the depths examined, leading to the observed relationships between these parameters and ILIs, which may be useful for evaluation of iron stress in our study region.

In conclusion, our incubation results support the hypothesis that mixing between iron limited ACC waters and iron replete shelf waters occurring in the southern Drake Passage creates the high phytoplankton biomass observed downstream of the mixing region. Iron addition experiments showed ACC waters were strongly iron limited while shelf waters with 1 - 2 nmol L^{-1} dissolved iron were iron replete. Shelf iron and the physical processes responsible for its introduction into iron limited waters, as opposed to atmospheric inputs or upwelling of deep iron, are likely important for development of the

large blooms observed downstream of islands and continental protrusions in the Southern Ocean (Sullivan et al 1993).

Using our results from iron addition experiments conducted throughout a region of strong mixing between iron limited and iron replete waters, relationships between degree of iron stress and photosynthetic physiology were found. These results indicate iron affects certain PSII parameters in this region of the Southern Ocean and measurement of these parameters can be used to accurately infer iron stress. Other factors known to influence PSII characteristics, including light and nitrogen stress, did not exert strong effects on PSII parameters of natural populations at the depth horizons sampled during our study. Because nitrate levels are high throughout the Southern Ocean and mixed layers are generally relatively deep minimizing photoinhibition, the essential conclusion that PSII parameters reflect degree of iron stress may apply to much of the Southern Ocean.

Acknowledgments

Table 3.1. Incubation source waters and station parameters. Relevant station data and initial parameters for each incubation including water type, depth of sampling for incubation setup, iron concentrations, Chl a, and mixed layer depth (MLD). Average daily light doses within the mixed layer or depth of sampling (In situ light) are presented for comparison with daily light doses while incubated (Inc. light). Initial PSII parameters (F_v:F_m, σ_{PSII} (x10^{-20} m^2 photon^{-1}), τ^{-1}, and p) measured on waters collected for incubation are reported. Station numbers (Sta. no.) are included to facilitate comparisons with other papers published from this study.

Inc	Water type	Sta. no.	Depth	MLD (m)	Fe (nmol L^{-1})	Chl a (µg L^{-1})	F_v:F_m	σ_{PSII}	τ^{-1} (s^{-1})	p	In situ light (mol m^{-2} d^{-1})	Inc. light (mol m^{-2} d^{-1})
A1	ACC	27	25	43	0.48*	0.15	0.22	913	182	0.36	11.3	16.0
A2	ACC	55	20	58	0.14	0.10	0.23	915	40	0.37	9.8	18.8
A3	ACC	27	85	43	0.48*	0.27	0.27	1035	162	0.33	0.3	2.5
A4	ACC	55	85	58	0.12	0.17	0.30	963	70	0.24	0.5	3.2
M1	Mixed	42	25	48	0.09	0.79	0.28	820	455	0.31	6.7	16.0
M2	Mixed	64	20	38	0.11	0.87	0.34	775	401	0.36	8.3	12.0
M3	Mixed	64	50	38	0.31	1.41	0.38	758	388	0.34	0.3	2.9
S1	Shelf	3	20	31	1.74	0.90	0.50	815	164	0.42	9.1	18.8
S2	Shelf	57	20	50	1.59	0.44	0.42	558	412	0.40	8.0	18.8

*May not be representative of iron concentrations in incubation water. See Methods.

Table 3.2. Basic incubation responses. Growth rates determined from Chl *a* increases (μ_{Chl}) and nitrate drawdown (μ_{NO3}) for control (C) and iron addition (Fe) treatments, POC levels, iron limitation indices (ILIs), and nutrient drawdown ratios ($\mu mol\ L^{-1}$: $\mu mol\ L^{-1}$) from each incubation. The length of each incubation (t_f) is also reported. 'No data' (nd) indicates sufficient nutrient data was not available to compute NO_3 derived growth rates or nutrient drawdown ratios from these incubations (A2, A4).

Inc	t_f (d)	μ_{Chl} (d⁻¹)		μ_{NO3} (d⁻¹)		POC (μmol L⁻¹)			ILI_{Chl}	ILI_{POC}	ILI_μ	Si:NO_3^- drawdown		NO_3^-:PO_4^{3-} drawdown	
		C	Fe	C	Fe	t_0	C	Fe				C	Fe	C	Fe
A1	12	0.14	0.39	0.12	0.29	3.8	19	54	7.4	2.9	2.9	2.06	0.97	10.3	13.2
A2	14	0.15	0.32	nd	nd	2.8	17	43	6.0	2.6	2.1	nd	nd	nd	nd
A3	11	0.18	0.47	0.25	0.37	4.5	20	66	10.0	3.3	2.6	2.73	1.17	9.7	14.4
A4	14	0.14	0.34	nd	nd	3.2	16	104	11.7	6.5	2.4	nd	nd	nd	nd
M1	13	0.11	0.24	0.18	0.25	9.6	39	76	3.4	2.0	2.3	1.82	0.98	14.9	13.5
M2	11	0.08	0.23	0.14	0.29	5.7	34	90	4.3	2.6	2.7	1.73	0.94	10.7	12.7
M3	7	0.17	0.34	0.20	0.31	11	41	62	3.0	1.5	1.9	1.94	1.12	9.9	12.2
S1	12	0.19	0.21	0.30	0.31	11	52	52	1.2	1.0	1.1	1.06	0.84	14.6	15.2
S2	14	0.37	0.42	0.40	0.40	4.0	117	139	1.3	1.2	1.1	0.82	0.77	10.6	11.0

Table 3.3. Community structure response in incubations. Data are averages and standard deviations from all incubations in a given water type. Size fractioned data are percent of Chl *a* in each size class, and taxonomic divisions are percent contribution to total Chl *a* determined with CHEMTAX. Haptophytes (Hapt.) and diatoms comprised the majority of the community in all incubations.

Water type	Sample	<2 μm	2-20 μm	>20 μm	Hapt.	Diatoms
	t_0	15 ± 7	31 ± 9	54 ± 3	48 ± 25	48 ± 26
ACC	C	4 ± 1	20 ± 5	76 ± 5	9 ± 6	89 ± 8
	Fe	1 ± 1	21 ± 3	79 ± 3	4 ± 1	91 ± 5
	t_0	4 ± 1	20 ± 4	76 ± 5	27 ± 6	72 ± 6
Mixed	C	2 ± 1	22 ± 10	76 ± 11	22 ± 10	76 ± 11
	Fe	1 ± 1	20 ± 8	79 ± 8	9 ± 4	86 ± 6
	t_0	14 ± 6	68 ± 22	17± 16	24 ± 8	64 ± 20
Shelf	C	1 ± 1	15 ± 4	84 ± 4	5 ± 7	81 ± 7
	Fe	0 ± 0	15 ± 3	85 ± 3	8 ± 11	77 ± 10

Table 3.4. P vs. E data. The initial slope of P vs. E curves, α^{Chl} (mg C • mg Chl a^{-1} • h^{-1} • (μmol photons • m^{-2} • h^{-1})$^{-1}$), and the maximum rate of photosynthesis, P^{Chl}_{max} (mg C • mg Chl a^{-1} • h^{-1}) from all incubations at the initial time point (t_0), and final time point for the control (C) and Fe treatment (Fe). Only one replicate from each treatment was sampled.

Incubation	α^{Chl}			P^{Chl}_{max}		
	t_0	C	Fe	t_0	C	Fe
A1	0.012	0.006	0.007	0.80	0.50	0.70
A2	0.031	0.010	0.013	0.35	1.00	0.90
A3	0.018	0.006	0.011	0.84	0.33	0.54
A4	0.004	0.007	0.017	0.23	0.78	1.13
M1	0.009	0.005	0.006	1.01	1.08	0.69
M2	0.014	0.003	0.007	0.99	0.37	0.74
M3	0.025	0.007	0.012	0.86	0.20	0.72
S1	n.d.	0.013	0.011	n.d.	0.91	0.80
S2	0.013	0.009	0.010	0.54	0.93	0.80

Table 3.5. Regression relations with ILIs, percent of variance explained (r^2), and significance level (p). Relationships significant at the 0.05 level are in bold.

	ILI_{Chl}		ILI_{POC}		ILI_μ	
	r^2	p	r^2	p	r^2	p
$F_v{:}F_m$	**0.44**	**0.05**	**0.69**	**0.01**	**0.58**	**0.02**
τ^{-1}	0.36	0.08	0.15	0.33	0.02	0.74
p	**0.52**	**0.03**	0.24	0.22	0.29	0.13
σ_{PSII}	**0.66**	**0.01**	**0.56**	**0.03**	0.40	0.06
α^{Chl}	0.01	0.96	0.08	0.62	0.01	0.81
P^{Chl}_{max}	0.02	0.90	0.16	0.39	0.24	0.18
Fe	0.32	0.12	0.42	0.08	**0.65**	**0.01**
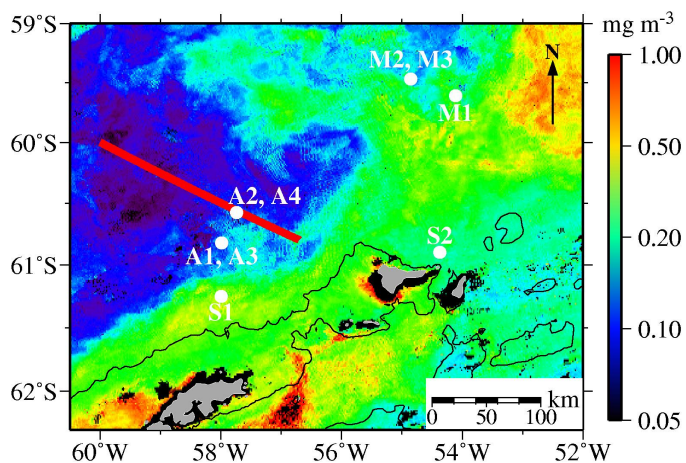
Figure 3.1. Satellite chlorophyll image of the study region with locations of incubation experiments overlain. The satellite image is a MODIS chlorophyll composite from January-March 2004 spanning the time of our study. Low chlorophyll, iron-limited ACC waters are in the west and shelf waters are in the south around the South Shetland Islands, with a region of mixing between these two waters to the east where chlorophyll is high. A deep gap between the southern end of the Shackleton Transverse Ridge (red line) and the continental shelf (delineated by the 500 m isobath; black line) creates a jet of ACC water which leads to mixing between ACC and shelf waters (Zhou et al. unpublished).
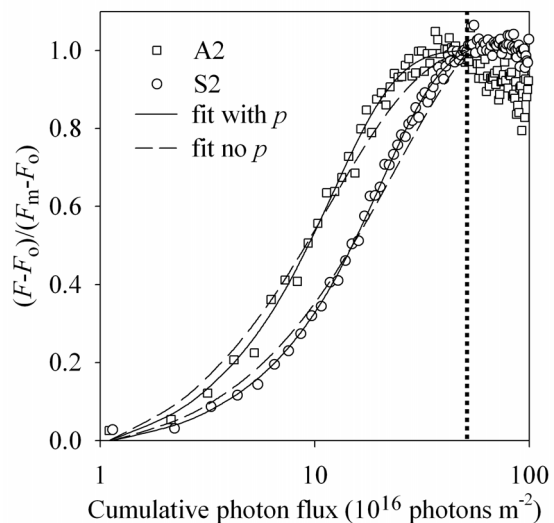
Figure 3.2. Representative fluorescence response data from initiations of incubations A2 and S2 plotted to highlight the differences in σ_{PSII} between iron limited (A2) and replete (S2) waters as well as the effect of the p parameter on fits to the Kolber et al. (1998) model. Runs of the v5 fitting software with and without the p parameter demonstrate that the data are better fitted with the p parameter due to lowered fluorescence early in the flash sequence, but later, a more rapid rise in fluorescence than would be expected without photosystem connectivity. Note that reductions in fluorescence towards the end of the flash sequence were observed when σ_{PSII} was large (e.g., A2), in which case only data from the first 50 flashlets (before the dotted line) were fit.
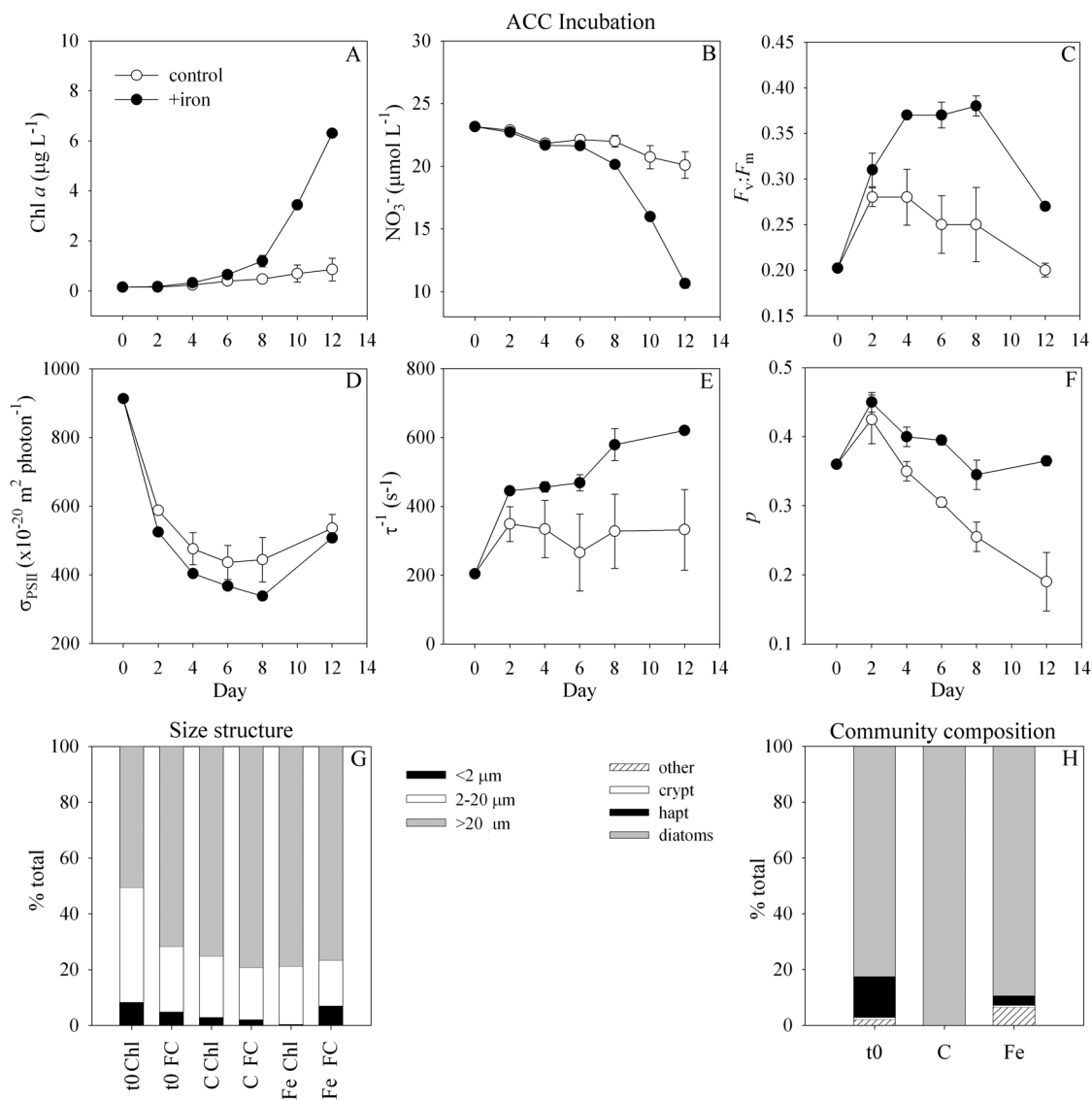
Figure 3.3. (A-H) Results of a typical incubation (A1) from ACC surface waters. Error bars (A-F) are standard deviations between duplicate bottles. Size structure (G) was determined using both size-fractioned Chl *a* (Chl) and flow cytometry (FC) at the initiation of the experiment (t0), and the final time-point in control (C) and Fe treatments (Fe). Phytoplankton community composition (H) was determined from CHEMTAX analysis of pigments taken from the initiation of the experiment and the final time-point. The 'other' category includes dinoflagellates, prasinophytes, and chlorophytes, which rarely contributed substantially to total biomass individually. Size (G) and community structure (H) data are the averages from duplicate bottles.
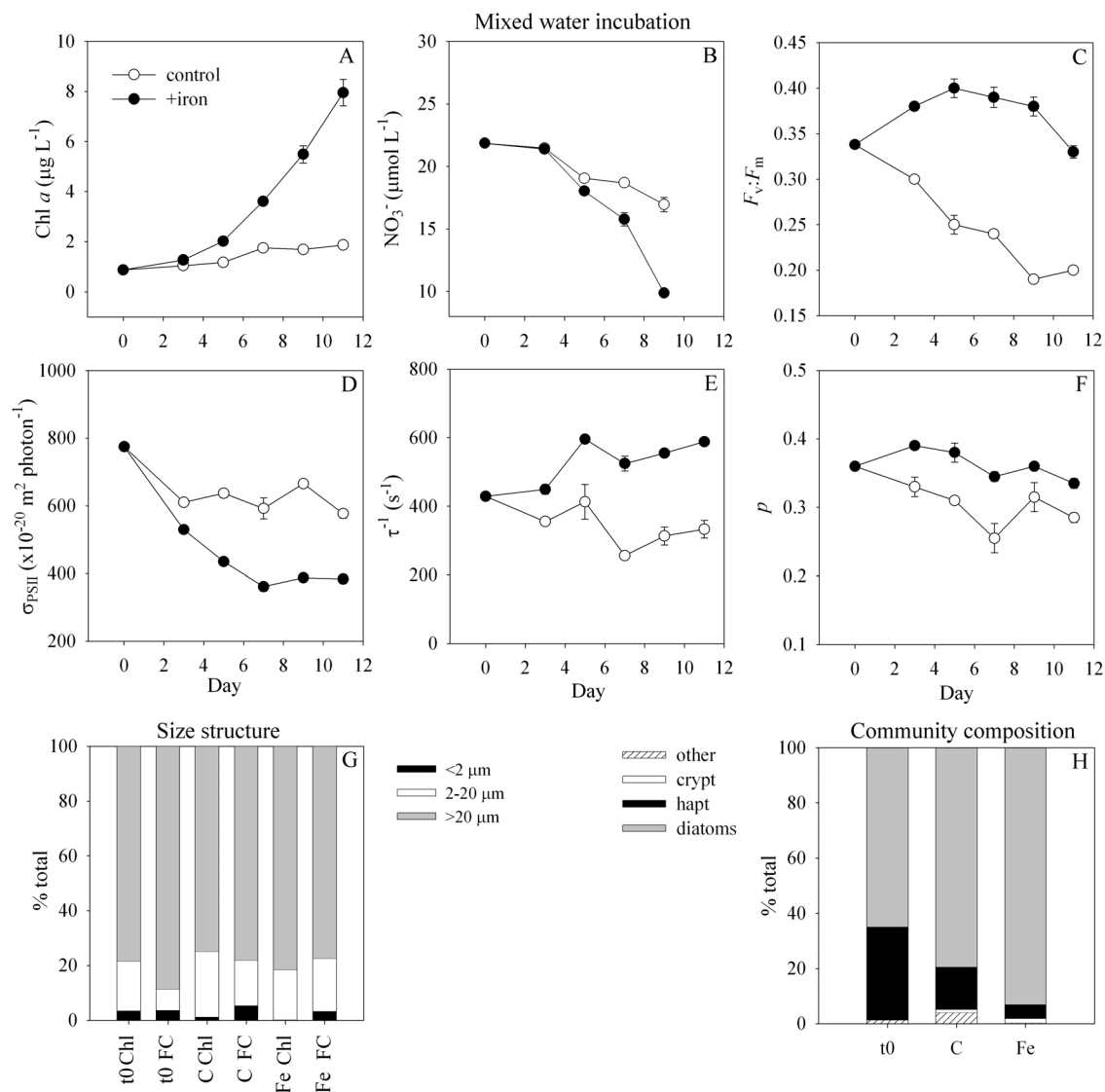
Figure 3.4. (A-H) Incubation (M2) results from a Mixed water experiment. Error bars (A-F) are standard deviations between duplicate bottles. Size (G) and community structure (H) show data from initial and final time-points, as described in detail in the caption to Fig. 3.
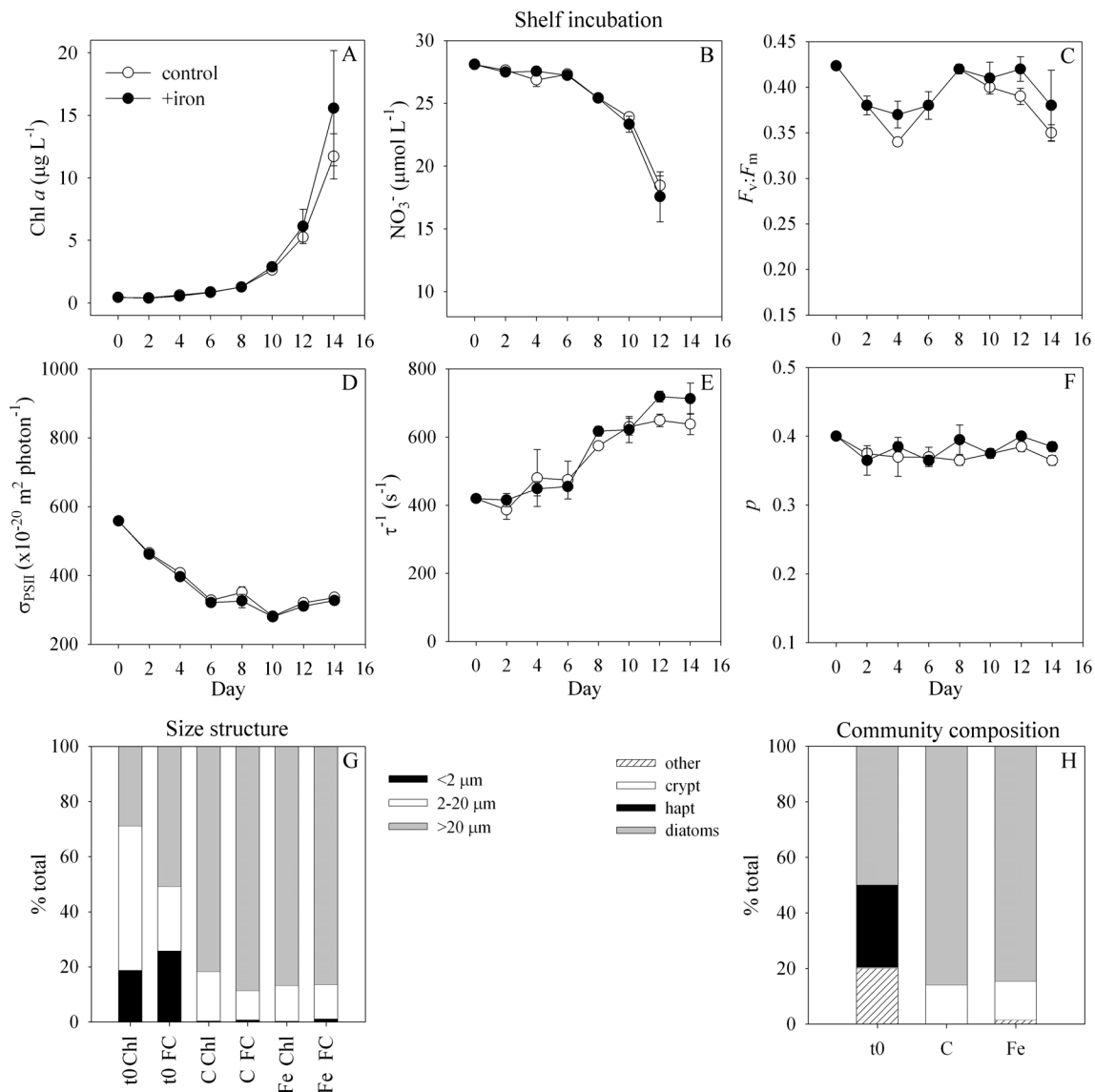
Figure 3.5. Incubation (S2) results from a shelf experiment. Error bars (A-F) are standard deviations between duplicate bottles. Size (G) and community structure (H) show data from initial and final time-points, as described in detail in the caption to Fig. 3.
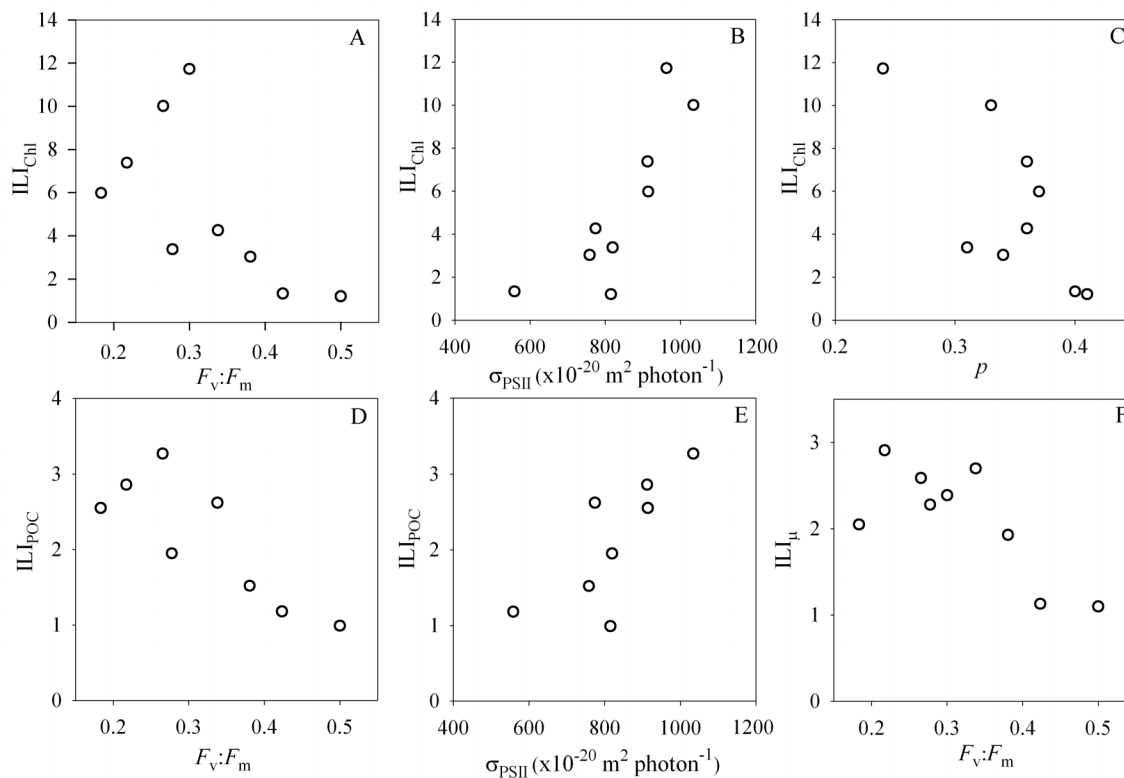
Figure 3.6. Indicators of iron limitation. (A, B, C) Plots of iron limitation indices (ILIs) determined from chlorophyll (ILI$_{Chl}$), (D, E) POC (ILI$_{POC}$), and (F) growth rate (ILI$_{\mu}$) responses to iron in incubation experiments, versus PSII characteristics for which significant linear regression relationships were found. ILI and PSII data used to construct plots are presented in Tables 1 and 2, and regression statistics are summarized in Table 5.

References

Behrenfeld, M.J., and Z.S. Kolber. 1999. Widespread iron limitation of phytoplankton in the south Pacific Ocean. Science **283:** 840-843.

Blain, S., P. Treguer, S. Belviso, E. Bucciarelli, M. Denis, S. Desare, M. Fiala, V.M. Jezequel, J. Le Fevre, P. Mayzaud, J.C. Marty, and S. Razouls. 2001. A biogeochemical study of the island mass effect in the context of the iron hypothesis: Kerguelen Islands, Southern Ocean. Deep-Sea Res. I **48:** 163-187.

Blain, S., B. Queguiner, L. Armand, S. Belviso, B. Bombled, L. Bopp, A. Bowie, C. Brunet, C. Brussaard, F. Carlotti, U. Christaki, A. Corbiere, I. Durand, F. Ebersbach, J.-L. Fuda, N. Garcia, L. Gerringa, B. Griffiths, C. Guigue, C. Guillerm, S. Jacquet, C. Jeandel, P. Laan, D. Lefevre, C. Lo Monaco, A. Malits, J. Mosseri, I. Obernosterer, Y.-H. Park, M. Picheral, P. Pondaven, T. Remenyi, V. Sandroni, G. Sarthou, N. Savoye, L. Scouarnec, M. Souhaut, D. Thuiller, K. Timmermans, T. Trull, J. Uitz, P. van Beek, M. Veldhuis, D. Vincent, E. Viollier, L. Vong, and T. Wagener. 2007. Effect of natural iron fertilization on carbon sequestration in the Southern Ocean. Nature **446:** 1070-1074.

Coale, K.H., K.S. Johnson, F.P. Chavez, K.O. Buesseler, R.T. Barber, M.A. Brzezinski, W.P. Cochlan, F.J. Millero, P.G. Falkowski, J.E. Bauer, R.H. Wanninkhof, R.M. Kudela, M.A. Altabet, B.E. Hales, T. Takahashi, M.R. Landry, R.R. Bidigare, X. Wang, Z. Chase, P.G Strutton, G.E. Friederich. M.Y. Gorbunov, V.P. Lance, A.K. Hilting, M.R. Hiscock, M. Demarest, W.T. Hiscock, K.F. Sullivan, S.J. Tanner, R.M. Gordon, C.N. Hunter, V.A. Elrod, S.E. Fitzwater, J.L. Hones, S. Tozzi, M. Koblizek, A.E. Roberts, H. Herndon, J. Brewster, N. Ladizinsky, G. Smith, D. Cooper, D. Timothy, S.L. Brown, K.E. Selph, C.C. Sheridan, B.S. Twining, and Z.I. Johnson. 2004. Southern Ocean Iron Enrichment Experiment: Carbon cycling in high- and low-Si waters. Science **304:** 408-414.

Cullen, J.J., and R.F. Davis. 2003. The blank can make a big difference in oceanographic measurements. Limnol. Oceanogr. Bull. **36:** 1578-1599.

De Baar, H.J.W., M.A. van Leeuwe, R. Scharek, L. Goeyens, K.M.J. Bakker, and P. Fritsche. 1997. Nutrient anomalies in *Fragilariopsis kerguelensis* blooms, iron deficiency and the nitrate/phosphate ratio (A.C. Redfield) of the Antarctic Ocean. Deep-Sea Res. II **44:** 229-260.

Falkowski, P.G., and Z. Kolber. 1995. Variations in chlorophyll fluorescence yields in phytoplankton in the world oceans. Aust. J. Plant. Physiol. **22:** 341-355.

Firme, G.F., E.L. Rue, D.A. Weeks, K.W. Bruland, and D.A. Hutchins. 2003. Spatial and temporal variability in phytoplankton iron limitation along the California coast and

consequences for Si, N, and C biogeochemistry. Global Biogeochem. Cycles **17**, 1016, doi:10.1029/2001GB001824

Greene, R.M., R.J. Geider, and P.G. Falkowski. 1991. Effect of iron limitation on photosynthesis in a marine diatom. Limnol. Oceanogr. **36:** 1772-1782.

Greene, R.M., R.J. Geider, Z. Kolber, and P.G. Falkowski. 1992. Iron-induced changes in light harvesting and photochemical energy conversion processes in eukaryotic marine algae. Plant. Physiol. **100:** 565-575.

Haberman, K.L., R.M. Ross, and L.B. Quetin. 2003. Diet of the Antarctic krill (Euphausia superba Dana): II. Selective grazing in mixed phytoplankton assemblages. J. Exp. Mar. Biol. Ecol. **283:** 97-113.

Helbling, E.W., V. Villafane, and O. Holm-Hansen. 1991. Effect of iron on productivity and size distribution of Antarctic phytoplankton. Limnol. Oceanogr. **36:** 1879-1885.

Holm-Hansen, O., and B. Riemann. 1978. Chlorophyll *a* determination: improvements in methodology. OIKOS **30:** 438-447.

Holm-Hansen, O., M. Kahru, and C.D. Hewes. 2005. Deep chlorophyll a maxima (DCMs) in pelagic Antarctic waters. II. Relation to bathymetric features and dissolved iron concentrations. Mar. Ecol. Prog. Ser. **297:** 71-81.

Hutchins, D.A., G.R. DiTullio, Y. Zhang, and K.W. Bruland. 1998. An iron limitation mosaic in the California upwelling regime. Limnol. Oceanogr. **43:** 1037-1054.

Kolber, Z., J. Zehr, and P. Falkowski. 1988. Effects of growth irradiance and nitrogen limitation on photosynthetic energy conversion in photosystem II. Plant Physiol. **88:** 923-929.

Kolber, Z.S., O. Prasil, and P.G. Falkowski. 1998. Measurements of variable chlorophyll fluorescence using fast repetition rate techniques: defining methodology and experimental protocols. Biochim. Biophys. Acta **1367:** 88-106.

Laney, S.R. 2003. Assessing the error in photosynthetic properties determined by fast repetition rate fluorometry. Limnol. Oceanogr. **48:** 2234-2242.

Lewis, M.R., and J.C. Smith. 1983. A small volume, short-incubation-time method for measurement of photosynthesis as a function of incident irradiance. Mar. Ecol. Prog. Ser. **13:** 99-102.

Ley, A.C., and D.C. Mauzerall. 1986. The extent of energy transfer among Photosystem II reaction centers in *Chlorella*. Biochim. Biophys. Acta **850:** 234-248.

Mackey, M.D., D.J. Mackey, H.W. Higgins, and S.W. Wright. 1996. CHEMTAX – a program for estimating class abundances from chemical markers: application to HPLC measurements of phytoplankton. Mar. Ecol. Prog. Ser. **144:** 265-283.

Maldonado, M.T., and N.M. Price. 1996. Influence of N substrate on Fe requirements of marine centric diatoms. Mar. Ecol. Prog. Ser. **141:** 161-172.

Measures, C.I., J. Yuan, and J.A. Resing. 1995. Determination of iron in seawater by flow injection analysis using in-line preconcentration and spectrophotometric detection. Mar. Chem. **50:** 3-12.

Menden-Deuer, S., and E.J. Lessard. 2000. Carbon to volume relationships for dinoflagellates, diatoms and other protist plankton. Limnol. Oceanogr. **45:** 569-579.

Mitchell, B.G., E.A. Brody, O. Holm-Hansen, C. McClain, and J. Bishop. 1991. Light limitation of phytoplankton biomass and macronutrient utilization in the Southern Ocean. Limnol. Oceanogr. **36:** 1662-1677.

Moore, C.M., D.J. Suggett, A.E. Hickman, Y.N. Kim, J.F. Tweedle, J. Sharples, R.J. Geider, and P.M. Holligan. 2006. Phytoplankton photoacclimation and photoadaptation in response to environmental gradients in a shelf sea. Limnol. Oceanogr. **51:** 936-949.

Olson, R.J., H.M. Sosik, A.M. Chekalyuk, and A. Shalapyonok. 2000. Effects of iron enrichment on phytoplankton in the Southern Ocean during late summer: active fluorescence and flow cytometric analyses. Deep-Sea Res II **47:** 3181-3200.

Platt, T.C., C.L. Gallegos, and W.G. Harrison. 1980. Photoinhibition of photosynthesis in natural assemblages of coastal marine phytoplankton. J. Mar. Res. **38:** 687-701.

Price, N.M. 2005. The elemental stoichiometry and composition of an iron-limited diatom. Limnol. Oceanogr. **50:** 1159-1171.

Sarmiento, J.L., N. Gruber, M.A. Brzezinski, and J.P. Dunne. 2004. High-latitude controls of thermocline nutrients and low latitude biological productivity. Nature **427:** 56-60.

Sedwick, P.N., G.R. DiTullio, and D.J. Mackey. 2000. Iron and manganese in the Ross Sea, Antarctica: Seasonal iron limitation in Antarctic shelf waters. J. Geophys. Res. **105:** 11,321-11,336.

Smith, W.O., J. Marra, M.R. Hiscock, and R.T. Barber. 2000. The seasonal cycle of phytoplankton biomass and primary productivity in the Ross Sea, Antarctica. Deep-Sea Res. II **47:** 3119-3140.

Sullivan, C.W., K.R. Arrigo, C.R. McClain, J.C. Comiso, and J. Firestone. 1993. Distribution of phytoplankton blooms in the Southern Ocean. Science **262:** 1832-1837.

Suzuki, K., H. Liu, T. Saino, H. Obata, M. Takano, K. Okamura, Y. Sohrin, and Y. Fujishima. 2002. East-west gradients in the photosynthetic potential of phytoplankton and iron concentration in the subarctic Pacific Ocean during early summer. Limnol. Oceanogr. **47:** 1581-1594.

Timmermans, K.R., M.S. Davey, B. van der Wagt, J. Snoek, R.J. Geider, M.J.W. Veldhuis, L.J.A., Gerringa, and H.J.W. de Baar. Co-limitation by iron and light of *Chaetosceros brevis*, *C. dichaeta* and *C. calcitrans* (Bacillariophyceae). Mar. Ecol. Prog. Ser. **217:** 287-297.

Van Heukelem, L., and C.S. Thomas. 2001. Computer-assisted high-performance liquid chromatography method development with applications to the isolation and analysis of phytoplankton pigments. J. Chromatogr. A **910:** 31-49.

Vassiliev, I.R., Z.S. Kolber, D. Mauzerall, V.K. Shukla, K. Wyman, and P.G. Falkowski. 1995. Effects of iron limitation on photosystem II composition and energy trapping in Dunaliella tertiolecta. Plant Physiol. **109:** 963-972.

Villafane, V.E., E.W. Helbling, and O. Holm-Hansen. 1995. Spatial and temporal variability of phytoplankton biomass and taxonomic composition around Elephant Island, Antarctica, during the summers of 1990-1993. Mar. Biol. **123:** 677-686.

Wright, S.W., D.P. Thomas, H.J. Marchant, H.W. Higgins, M.D. Mackey, and D.J. Mackey. 1996. Analysis of phytoplankton from the Australian sector of the Southern Ocean: comparisons of microscopy and size frequency data with interpretations of pigment HPLC data using the 'CHEMTAX' matrix factorisation program. Mar. Ecol. Prog. Ser. **144:** 285-298.

IV

Organic and redox speciation of iron

in the eastern tropical North Pacific suboxic zone

Abstract

The organic and redox speciation of iron was examined in the strongly layered upper water column of the eastern tropical North Pacific, including oxic and suboxic waters, in a region 100-1300 km offshore. Suboxic conditions ($[O_2] < 5$ µM) were found to affect the organic speciation of iron, and reduced dissolved iron, Fe(II), was present in the suboxic zone, but conditions were not sufficiently reducing to convert all iron to Fe(II). Dissolved iron concentrations in the suboxic zone were similar to concentrations found in oxic regions.

Using a competitive ligand exchange-adsorptive cathodic stripping voltammetry (CLE-ACSV) method, natural ligands were found to have distinct characteristics in the oxic and suboxic waters with stronger ligands found in the suboxic zone. It is unusual to find stronger ligands below the euphotic zone, but their strength, $logK_{Fe'L}$=12.1-12.8, is within the range determined for surface ligands in other regions. These strong ligands may be the result of the unique chemistry of the suboxic zone stabilizing reduced or labile compounds, or they may be actively produced by microbes to enhance iron uptake. No onshore-offshore trends in ligand strength or concentration were detected suggesting the ligands may result from the inherent chemistry of the suboxic zone or production from denitrifiers, rather than the resident suboxic zone population of *Prochlorococcus* which were more abundant nearshore.

A luminol-chemiluminescence based flow injection analysis (FIA) technique capable of detecting picomolar concentrations of Fe(II) was used to assess the redox state of iron in the suboxic zone and overlying oxic waters at a station 1300 km offshore. An

elevated signal equivalent to 0.12-0.15 nM Fe(II), 21-24% of dissolved iron, was found

only in the suboxic waters. Oxidation kinetics suggest that this Fe(II) is most likely

produced by an *in-situ* process, as opposed to being transported from shelf sediment. The

luminol-chemiluminescence Fe(II) method was systematically tested for inferences from

reduced species potentially present in the suboxic zone to validate our Fe(II) results.

Several species, V(IV) and V(III), produced significant signals, but considerations of the

reducing state of the suboxic zone make it unlikely that reduced V is present. With

additional information on the identity of the suboxic zone species provided by analysis of

signal decay rate, it was determined that Fe(II) was the most reasonable source of the

signal, and at minimum the chemiluminescence data allows us to set limits on the Fe(II)

concentration in the offshore suboxic water column.

 Introduction

Iron is widely recognized as an important factor controlling productivity,

phytoplankton community composition, and nitrogen fixation in oceanic systems (Coale

et al. 1996; Mills et al. 2004). The supply of bioavailable iron for marine organisms is

influenced by its complex chemistry including low aqueous solubility, several oxidation

states, and association with natural ligands. Characterization of iron concentration and

speciation in the field has been instrumental in shaping our understanding of iron

biogeochemistry and iron limitation in the marine environment, from the initial

recognition that iron concentrations are in the nanomolar range, to more recent

developments regarding complexation to organic ligands and colloidal iron phases (e.g.

Martin et al. 1990; Rue and Bruland 1997; Wu et al. 2001). Many studies on iron

distributions and speciation have been conducted throughout the world's oceans with emphasis on environments with significant areal extent such as the open ocean gyres and HNLC regions, or high productivity like the Peru Upwelling (e.g. Rue and Bruland 1995; Wu et al. 2001). Few studies have attempted to describe iron speciation in oceanic regions with suboxic waters, despite the possible importance of redox transformations to iron biogeochemistry, and the requirement of iron for denitrification (Hong and Kester 1986; Landing and Bruland 1987; Rue et al. 1997; Witter et al. 2000).

Herein we describe a field study of iron concentrations and speciation in the eastern tropical North Pacific (ETNP), a strongly stratified system with a prominent water column suboxic zone. The combination of high surface productivity and unventilated mid-waters creates a thick layer of suboxic water in both the eastern Pacific and the Arabian Sea (Wyrtki 1962). In these regions oxygen has been depleted by heterotrophic consumption to less than 5 μM, and use of NO_3^- as a final electron receptor has begun (Cline and Richards 1972). Under these conditions redox transformations of a number of elements, such as nitrogen, manganese, and chromium, occur which have significant impact on their biogeochemical cycling (Deutsch et al. 2001; Murray et al. 1981; Rue et al. 1997). The extent to which iron is impacted *in-situ* by suboxic conditions in the water column is still being evaluated and is a focus of this work.

Iron concentrations and some aspects of speciation have been examined in the suboxic zones of the eastern Pacific and Arabian Sea. Dissolved iron concentrations in suboxic zones have been measured in a few locations, and have been found to be similar to or somewhat elevated in comparison with oxic waters (Landing and Bruland 1987; Witter et al. 2000). In addition to measuring iron concentrations, a variety of different

techniques have been used to provide information about aspects of iron speciation including ligand complexation and redox state. Witter et al. (2000) used an electrochemical competitive ligand exchange technique and found iron(III) binding ligands in the Arabian Sea suboxic zone at higher concentrations than is found in most oxic regions. To examine the redox state of iron, Hong and Kester (1986) measured iron(II) using a ferrozine chelator method in nearshore waters with high total iron. They found extremely high levels of iron(II), up to 40 nM, in the suboxic waters over the shelf-break off Peru suggesting iron(II) may be prevalent throughout the suboxic zone. However, in the eastern tropical North Pacific (ETNP), an area more typical of open-ocean suboxic zones, Landing and Bruland (1987) found no evidence of *in-situ* reduction of iron(III) to iron(II) based on ratios of acid-leachable to refractory particulate iron.

Work on iron concentrations has been conducted in both major suboxic regions, the Arabian Sea and the ETNP. However measurements of iron speciation in these environments have been more limited, and in particular have not used techniques to examine iron's redox state and natural iron-binding ligands in the same location. In this work, we combine measurements of dissolved iron with analysis of iron(III)-binding ligands and limits on iron(II) concentrations to provide a more comprehensive picture of iron speciation in an open-ocean suboxic zone and compare this to the oxic waters immediately overlying the suboxic layer.

Sampling and Methods

<u>Sampling</u>

The eastern tropical North Pacific (ETNP) is an area with an intense oxygen minimum zone (OMZ) in midwaters. Oxygen concentrations fall to 0.5-2 µM at the core of the OMZ where active water column denitrification and redox transformations of trace elements occur (Cline and Richards 1972; Rue et al. 1997). On an onshore-offshore transect starting near Manzanillo, Mexico in November, 2003, we collected vertical profiles at four stations extending from the surface mixed layer into the OMZ. All samples were collected and processed using trace-metal clean techniques. Samples were collected with 12L Teflon-lined Go-Flo bottles on synthetic, non-metallic line. The bottles were individually attached to the synthetic line and triggered at depth using Teflon coated messengers. Once on-board, the bottles were pressurized with 0.4 µm filtered, Ultra High Purity (UHP) nitrogen gas and the water was dispensed through Teflon tubing into a Class 100 Laminar flow hood, or for iron(II) analysis, into a glove bag filled with 0.4 µm filtered UHP nitrogen. Samples for dissolved iron were filtered in-line through precleaned Millipore 0.4 µm Isopore filters into acid-cleaned low-density polyethylene (LDPE) bottles and were immediately acidified with 6N Ultrex HCl to pH=1.8. Samples for iron-binding ligands and iron(II) were similarly filtered though 0.4 µm filters, but dispensed into Teflon (FEP) bottles. Iron(II) samples were processed immediately as described below, while samples for iron(III)-binding ligands were frozen without acidification until analysis onshore.

<u>Dissolved iron analysis</u>

Samples for dissolved iron were analyzed by cathodic stripping voltammetry using a modified version of the 2-(2-thiazolylazo)-p-cresol (TAC) ligand method described by Croot and Johansson (2000). Samples were stored acidified for more than a

year to ensure iron had been freed from all ligands. For analysis, TAC was added at a final concentration of 10 μM, followed by the EPPS buffer (10 mM), and finally the pH was brought up to 8.0 using Q-NH$_3$. Adjustment of the pH as the last step should help avoid loss of iron to natural ligands or by precipitation. The electrochemical analysis was performed on an Autolab PGSTAT30 (EcoChemie) connected to a hanging mercury drop electrode (Metrohm VA663), and analyzed using a linear sweep waveform as described in Croot and Johansson (2000). All chemicals were purchased from Sigma-Aldrich in the highest purity available. A 1 M stock solution of EPPS buffer was cleaned by passing through a column of Chelex-100 ion exchange resin, and Q-NH$_3$ was produced by isothermal distillation. Iron concentrations were quantified with 4 standard additions.

The validity of this method was tested by measuring the SAFe (Sampling and Analysis of Fe) surface and deep iron standards. Our results on triplicate measurements of each standard were 0.10 ± 0.02 nM for the surface sample (bottle #279), and 0.92 ± 0.04 nM for the deep sample (bottle #285), which agree well with the consensus values of 0.095 ± 0.024 nM for the surface standard and 0.90 ± 0.09 nM for the deep standard (K. Johnson, personal communication; SAFe standards and further information are available by contacting 'requestsafestandard@ucsc.edu'). Replicate dissolved iron analyses were run on all samples from stations 15 and 21 to determine errors associated with the measurement method. The average standard deviation was 0.025 nM, and no single set of replicates had a standard deviation greater than 0.07 nM.

Iron Binding Ligands

The concentration and strength of dissolved iron-binding ligands on samples collected from the ETNP were determined using the TAC competitive ligand exchange-

adsorptive cathodic stripping voltammetry (CLE-ACSV) method of Croot and Johansson (2000). CLE-ACSV involves a competition between natural seawater ligands and an added electrochemically active ligand (TAC in this case) for added iron. Through measurement of the amount of electrochemically active ligand bound to iron at a range of iron concentrations, the concentration and binding strength of natural ligands can be inferred. To conduct the CLE-ACSV measurements, frozen seawater samples were thawed at room temperature overnight at which point 15 mL sub-samples were dispensed into 60 mL Teflon bottles. EPPS buffer (10 mM) was added to bring the pH to 8.0 and iron spikes from 0 – 5 nM were added to titrate the natural ligands. After allowing the natural ligands to equilibrate with the added iron for one hour, the competing ligand, TAC (10 μM), was added and allowed to equilibrate for one hour more. The sample was then measured on the voltammetric apparatus using a 10 minute deposition time and the linear sweep wave form. Addition of reagents to the titration samples were staggered so that equilibration times were constant. Current measurements were converted to TAC-labile iron concentrations using the sensitivity calculated at the highest iron additions, where natural ligands should be saturated. Because weak ligands may not be completely saturated, this method may lead to an underestimation of the sensitivity (Turoczy and Sherwood 1997). However, the ligand concentrations we determined were small (~ 1 nM) relative to the range of our titration (5 nM added Fe), and underestimation should be minimal.

The relatively short (one hour) equilibration time used in our titration experiments was chosen based on tests showing that 1 hour was sufficient to achieve an apparent equilibrium between TAC and natural ligands, and short enough to avoid loss of added

iron to the walls (Cullen et al. 2006, J. Cullen, personal communication). There has

recently been debate as to whether equilibrium is actually achieved after the several hour

equilibration time typically used in ligand titration experiments (Town and van Leeuwen

2005; van den Berg 2005). While this debate continues, it is certainly true that there are a

wide range of dissociation constants among all known iron binding ligands, and all

methods currently used may be prone to overestimation of ligand strengths if very slow

dissociating ligands are present in seawater. While shorter equilibration times are

theoretically more susceptible to overestimation of ligand strength, the results of Cullen

et al. (2006, personal communication) indicate our measurement method should be

equivalent to the 5 to 16 hour equilibration times commonly used in CLE-ACSV

experiments (e.g. van den Berg 1995; Croot and Johansson 2000; Witter and Luther

2000)

Ligand concentrations and strengths were determined from the titration data using

a Langmuir linearization. Plots of *Fe'/FeL* vs. *Fe'* were constructed as described in van

den Berg (1982) and Ruzic (1982) where *Fe'* represents all inorganic forms of Fe(III) and

FeL stands for Fe(III) bound to natural iron binding ligands (Fig. 4.2). The side reaction

coefficient used for complexation of *Fe'* by TAC was $\alpha_{Fe'(TAC)_2} = 250$ (Croot and

Johansson 2000). The slope, *m*, of a linear fit to the data was used to determine the total

ligand concentration, [L] ([L]=1/m), and the y-intercept, y_o, was used to calculate the

conditional stability constant, $K_{Fe'L}$, ($K_{Fe'L}$= [L]/y_o) (Fig. 4.2.). Conditional ligand

strengths are valid for the experimental condition of the medium, and have been reported

with respect to Fe' as opposed to Fe^{3+}. Errors in ligand concentration and binding strength

were determined from the standard error in linear regression estimates of *m* and y_o. For

three linearizations with small y_o's (very strong ligands), the standard error in y_o exceeded

its value. This translates to an infinite error in the upper limit of $K_{Fe'L}$, and indicates the

ligands are nearly too strong to calculate binding strengths for using our CLE-ACSV

method. When plotting these data points, arrows are used instead of error bars to indicate

an upper limit of the ligand strength is uncertain (Fig. 4.4). The transformed titration data

was fit well by a line in all profiles except at Station 19 where errors in the fits were

larger than at other stations. In the interest of consistency the data from these samples

was transformed using the same Langmuir linearization used for the other samples.

<u>Chemiluminescence methods</u>

<u>Instrumentation for Fe(II) determination</u>

Fe(II) concentrations were determined using the FeLume system developed by

D.W. King (Waterville Analytical). The FeLume is a flow injection analysis system. For

Fe(II) analysis, an alkaline luminol reagent is mixed with the Fe(II)-containing solution,

resulting in luminol oxidation with concurrent chemiluminescent emission. The mixing

and reaction take place in a spiral flow cell positioned in front of a photomultiplier tube

(PMT). The set-up of the instrument was similar to that described in Rose and Waite

(2001) - i.e. the sample and luminol reagent were continually mixed in the flow cell by

omitting the injection valve, and the sample line was kept as short as possible and by-

passed the peristaltic pump, going instead directly into the flow cell. In this way the time

for sample to enter the flow cell was minimized (approx. 3 seconds). Samples for Fe(II)

analysis were obtained via Go Flo casts into oxic and suboxic zone waters. Once GoFlos

were on deck, they were immediately pressurized with filtered N_2 gas and water was

dispensed via Teflon tubing through an in-line 0.4 µm polycarbonate filter membrane and

directly into a laminar flow hood, where analysis with the FeLume was performed immediately. For suboxic zone samples, the pressurized Teflon line led directly from the in-line filter into a glove bag filled with N_2 gas. Once bubbles were flushed from the line, samples were taken directly for Fe(II) analysis, by running the FeLume sample tube into the sampling container inside the glove bag. No corrections have been made to our measured Fe(II) concentrations for oxidation loss. For samples in the oxygenated water column, none of our Fe(II) measurements were above background, so correction is not necessary. For samples in the suboxic zone, signals were generally at least 10x above background. We expect oxidative losses would have been insignificant given that oxygen contamination and temperature changes in the GoFlo bottles were minimal over the time frame between getting the bottles back on deck and analysis (Time frame between bottle retrieval and analysis was generally between 10 and 20 minutes, low O_2 concentrations were confirmed by Winkler titration of dissolved oxygen in the GoFlo water, and temperatures were periodically confirmed by direct measurement from the sample line.) In addition, duplicate and triplicate samples determined 5-10 minutes apart did not show signs of signal loss. The relatively low pH of the suboxic zone water (about 7.5) ensured that, even if fully oxygenated and warmed to 20 °C, Fe(II) half-life would be on the order of 30-45 minutes (Millero et al. 1987; Millero and Sotolongo 1989).

The luminol formulation which we used in this work was similar to that employed by Croot and Laan, 2002. 0.13 g luminol sodium salt (Sigma-Aldrich) and 0.53g K_2CO_3 (Sigma-Aldrich) were dissolved in 10 mL of Milli-Q water to make a concentrated luminol stock. 5 mL luminol stock, plus 5 mL 10 M HCl (Ultrex), plus 22 mL concentrated NH_4OH (Optima) was then diluted to 500 mL with Milli-Q water. This

reagent was allowed to sit overnight before use. The FeLume instrument was calibrated

daily by the method of standard additions, adding known concentrations of Fe(II) (0.1,

0.2, 0.4, 0.8 nM) to the standard matrix. For standard additions, a 0.01 M primary Fe(II)

stock solution was made just prior to the 1 month cruise by dissolving $Fe(NH_4SO_4)_2 \cdot$

$6H_2O$ in 0.1 M Ultrex HCl. Secondary Fe(II) standards (10 μM and 1 μM) were made

up in 0.01 M Ultrex HCl on the ship just prior to calibration analysis each day. For the

standard addition matrix we used either 0.4 μm filtered surface seawater or 0.4 μm

filtered suboxic zone water (from 200 m depth). Filtered suboxic zone seawater which

had been held in the dark at least 8 hours was used to provide a blank measurement. We

found no difference between oxic and suboxic water blanks. Blank values averaged 127 $\pm$

24 counts/200 ms, and were constant over the course of several days during which the

field measurements were made. Detection limits for all standard addition runs were

consistently below 0.05 nM. Errors were determined as the standard deviation of

duplicate or triplicate samples. FeLume standard additions typically exhibited curvature

as has been shown previously (Rose and Waite 2001, 2002). Data were fit with a

quadratic function in Microsoft Excel.

Interference tests

The FeLume system was designed to measure Fe(II), and potential interferences

from metals likely to be present in oxic waters have been tested extensively (Seitz and

Hercules 1972; O'Sullivan et al. 1995). These tests have demonstrated that despite the

reduction in signal caused by metals such Mn(II) and Cu(II), the method is relatively

specific for Fe(II) which can be quantified accurately as long as standard additions are

done (O'Sullivan et al. 1995). However, the possibility of other reduced species, which

may be present in the suboxic zone, producing a signal has not been systematically tested.

We tested reduced species which are known to be present or could be present in

the suboxic zone to determine whether they would interfere with our attempts to measure

Fe(II). Elements to be tested were chosen based on the criteria that they 1) occur at

significant, >100 pM, concentrations, in deep waters as reported in Nozaki (2001), and 2)

have at least one redox couple which occurs between pE_{cond} 12.6 and -3. The first

criterion is based on the fact that Fe(II) is very efficient at initiating the light generating

reaction of luminol, and so interfering species would have to be present at similar

concentrations to generate a conflicting signal (Rose and Waite, 2001). The second

criteria was chosen because although it is difficult to define a definite pE_{cond} for the

suboxic zone, the conditions are somewhere between oxic, pE_{cond}=12.6, and anoxic,

pE_{cond}= -3, since oxygen has been depleted but free sulfide is not present (Therberge et al.

1997). Redox reactions which occur in the suboxic zone are likely to have pE_{cond}'s

between these potentials. Most studies suggest a pE_{cond} in the range of 8-6 for the

suboxic zone, but we chose to consider elements with a much wider range of redox

couples to cover more possibilities (Rue et al. 1997). To the best of our knowledge, we

tested reduced species of all the elements which met the above criteria except uranium,

which is not commercially available in a reduced state. The pE_{cond} of the UO_2^{2+}/U^{4+}

couple is quite reducing (-0.78), and although we were not able to test its interference

directly, the reduced species is unlikely to be present in the suboxic zone based on

thermodynamic considerations. Many of the arguments in section the discussion about

the likelihood of reduced V in the suboxic zone apply to U, since neither is reduced until

nearly sulfidic conditions, nor are they required by most organisms for cellular metabolism. Mo(V) was tested due to Mo's similarities to V which was found to be a potential interference. Additionally, Co(II) was run since it reacts with luminol, and recent studies have shown Co concentrations are higher in suboxic zones (up to 300 pM) (Saito et al. 2004). At concentrations potentially found in the suboxic zone, neither Mo(V) nor Co(II) produced signals strong enough to cause an interference.

Values of pE_{cond} for redox couples were calculated for the pH (7.5) and temperature (11 °C) conditions characteristic of the suboxic zone using equation 16 of Turner et al. (1981) with a few exceptions described below. pE_{cond} values incorporate the influence of hydrolysis and inorganic complexation for most species using stability constants from Turner et al. (1981) and $E°$ values from Vanysek (2004). For V, pE_{cond}'s incorporate the effects of hydrolysis but not inorganic complexation, and the relevant data was obtained from Wanty and Goldhaber (1992). For Mo an $E°$ value for the $H_2MoO_4/Mo_2O_4^{2+}$ couple from Bard et al. (1985) was used to compute the $MoO_4^{2+}/Mo(V)$ couple listed in Table 1 which incorporates the effects of suboxic zone pH and temperature on pE_{cond}, but not hydrolysis or inorganic complexation. The pE_{cond} for $CoOOH(s)/Co^{2+}$ is based on the value from Moffett and Ho (1996) adjusted to the temperature and pH conditions of the suboxic zone.

The reduced species tested are listed in Table 4.1. The FeLume was configured as described above for Fe(II) field measurements. Compounds to be tested were purchased in the highest purity grade available from Aldrich and based on the reported impurities Fe contamination is not an issue. Fresh solutions were made up immediately prior to tests since many of the reduced species degrade. Seawater solutions of each compound were

run on the FeLume at three different concentrations chosen based on the concentrations of each element present in seawater (Nozaki 2001). While most compounds did not produce any signal above background, V(IV) and V(III) reacted with luminol as has been found by other investigators, and must be considered as potential interferences in the determination of Fe(II) (Table 4.1, see Discussion ; Pilipenko et al. 1975). Cu(I) produced a small signal at 1 nM, not significant enough to cause a problem for Fe(II) determination, and the signal actually declined below baseline at higher concentration ruling it out as a possible interference. A small signal was also observed from Co(II), but this signal was weak enough that it could not be a significant interference.

Other investigators have tested the effects of organic ligands on Fe(II) measurements using luminol-chemiluminescence methods, and we did not repeat these tests. Ussher et al. (2005) showed that strong Fe(II) and Fe(III) binding compounds changed the apparent redox state of Fe as determined using a luminol method. For some ligands including siderophores and EDTA, it was shown that organically complexed Fe(II) was not detectable by the luminol Fe(II) method. The extent to which organic complexation influenced our Fe(II) concentrations is difficult to assess without more detailed studies.

<u>Decay rates</u>

Reduced species other than Fe(II) which may be present in the suboxic zone were found to produce a chemiluminescence signal in the FeLume. The decay times of species which pose significant interference problems, V(IV) and V(III), were measured and compared with decay times of the signal measured in the field in an attempt to identify which reduced species was present in the suboxic zone.

The decay time of the field signal from the suboxic zone was measured on a freshly collected suboxic sample. Immediately after initial measurement of the signal in the fresh suboxic sample, the suboxic zone water was rapidly oxygenated, and decay of the signal was monitored over 75 minutes, when it returned to near baseline values. Throughout the decay measurement pH was stable at 7.55, and the temperature stabilized at 20.1 °C after five minutes. The suboxic water was fully oxygenated by shaking the water in a 500 mL bottle with atmospheric air in the headspace. To ensure that the sample was fully oxygenated we verified our shaking procedure using the Winkler titration method. Measuring decay on a sample equilibrated with atmospheric air allowed us to easily compare decay rates measured in the field to decay experiments done in the laboratory.

At a later date, we measured the decay of Fe(II), V(IV), and V(III) for comparison with field data. Stock solutions of Fe(II), V(IV), and V(III) were made up in 1% HCl immediately prior to the decay experiment. Suboxic zone seawater collected on the cruise was used in all experiments. Small aliquots of the acidic stock solutions added to the suboxic seawater did not effect the pH which was constant at 7.5, and temperature was maintained at 20.1 °C using a water bath. Decay of the reduced species was measured over 90 minutes or until the chemiluminescence signal returned to background levels. Decay rates were determined several times for each species at a range of relevant concentrations, 0.2-1.2 nM for Fe(II), 10-40 nM for V(IV), and 5-40 nM for V(III). Each species followed a pseudo-first order decay rate as shown by plots of the natural log of concentration versus time for selected experiments in figure 4.3. No systematic change in decay rate with concentration was found, but there was some variability in decay rates

especially between rates determined on different days. This could be due to H_2O_2

contamination, and this variability is incorporated in our estimate of decay rates by

averaging several runs and reporting standard deviations (see Discussion)

Results and Discussion

<u>Iron Concentrations</u>

Profiles of dissolved iron concentrations were measured at four stations from the

surface mixed layer into the core of the suboxic zone on a transect heading offshore from

Manzanillo in November 2003. Surface layer concentrations were consistently low, but in

deeper waters iron concentrations were elevated nearshore, up to 1.2 nM, and gradually

decreased offshore to around 0.6 nM (Fig. 4.4). No evidence was found to suggest

suboxic conditions offshore enhanced iron concentrations since the concentrations were

comparable to those found in oxic waters at similar distances offshore (Johnson et al.

2003). The same conclusion was reached by Landing and Bruland (1987), who measured

similar iron concentrations both in the suboxic zone of the ETNP and in oxic water of the

North Pacific. In the Arabian Sea, Witter et al. (2000) observed iron concentrations in the

suboxic zone of 1.2 – 2.6 nM. However, the high values they observed were not confined

to the suboxic zone, and in fact are not unusual in the Arabian Sea because of the

proximity to arid land and consequent dust inputs of iron (Measures and Vink 1999;

Witter et al. 2000)

A trend of decreasing metal concentration with distance offshore, as we observed

in our data, is typical for particle reactive trace elements such as iron, aluminum, and

manganese (Landing and Bruland 1987; Measures and Vink 1999). Inputs from riverine,

sedimentary, or atmospheric sources generally elevate trace metal levels nearshore. These high concentrations are attenuated offshore by particle scavenging and mixing with open ocean waters depleted of trace metals. In the eastern tropical South Pacific (ETSP), upwelling of suboxic water in contact with reducing sediments was determined to be the mechanism behind the >15 nM Fe observed in coastal surface waters and subsurface waters in contact with sediments contained >50 nM dissolved iron (Bruland et al. 2005). Surrounding deserts and suboxic bottom water are similarities between the ETSP and ETNP, making sedimentary and atmospheric iron sources the most likely cause of iron enrichment nearshore in the ETNP. The loss of iron from the ETNP suboxic zone as waters move offshore is most likely due to scavenging processes. This suggests a significant portion of the iron in the suboxic zone is present as particle reactive Fe(III) rather than soluble Fe(II). Alternatively, nearshore waters may contain Fe(II) which is gradually oxidized to Fe(III) and scavenged.

Iron(III) Binding Ligands

At all depths we found concentrations of strong iron binding ligands that exceeded the concentration of dissolved iron such that at equilibrium nearly all Fe(III) would be bound to these ligands (Fig. 4.4). The upper water column of the ETNP is an extremely stratified system with distinct biological and chemical conditions in each vertical layer which may affect ligand characteristics. At the time of our sampling the surface mixed layer had a low phytoplankton standing stock (chl a ~0.1ug/L) dominated by cyanobacteria and subject to high light intensities (Goericke et al. 2000). Immediately below the mixed layer, was a strong subsurface chlorophyll maximum with higher phytoplankton biomass composed of both eukaryotes and cyanobacteria, at lower light

levels (Goericke et al. 2000). Ligand characteristics were similar in both the mixed layer and the subsurface chlorophyll maximum, despite the gradients in light intensity and phytoplankton community structure (Fig. 4.4).

Differences in ligand strengths were observed however between the oxic waters and the suboxic water which began at the base of the euphotic zone. Stronger ligands ($logK_{Fe'L}$=12.1-12.8) were observed within the suboxic zone relative to the mixed layer and subsurface chlorophyll maximum at three out of four stations. However, we note that while ligand strengths are generally higher in the suboxic zone, the errors at some depths are moderately large and may obscure deviations from the general trend. Our results contrast with ligand studies from regions with oxic water columns where ligand strengths have generally been found to remain constant with depth, for example in the Mediterranean Sea, or to decrease at depth as has been observed in the Pacific Ocean (van den Berg 1995; Rue and Bruland 1995). In our offshore transect, the one profile where trends in ligand strengths with depth were not as clear was Station 19. The titration data for these samples were not fit as well in the Langmuir transformations to determine ligand concentration and binding strength, resulting in larger errors and perhaps obscuring ligand trends. Because true equilibrium may not have been established in our ligand titrations (see Methods), natural ligands which have slower dissociation constants may be confused with thermodynamically stronger ligands. Thus the suboxic zone ligands may actually be slower to dissociate bound iron rather than thermodynamically stronger, but in either case there are indications of ligands with distinct characteristics in the suboxic zone. The differences observed in ligand characteristics between the oxic and suboxic waters could result from the distinct chemistry of the suboxic zone, or its unique

biological community composed of a nearly mono-algal population of *Prochlorococcus* and denitrifying bacteria (Goericke et al. 2000).

One possibility to explain the apparently stronger ligands at depth is biological production of iron chelators, such as siderophores, to aid uptake. The unusual population of *Prochlorococcus*, which form the secondary fluorescence maximum just below the oxic-suboxic interface, live at extremely low light levels and require additional iron for photosystem use (Sunda and Huntsman 1997). Production of iron binding ligands for uptake or to sequester iron from other organisms may be a strategy used by *Prochlorococcus* to secure additional iron. However, *Prochlorococcus* were much more abundant in the suboxic zone nearshore, while ligand characteristics showed no major onshore-offshore gradients indicating a source other than *Prochlorococcus* (Fig. 4.4). Another possible source of iron binding ligands are denitrifiers, which require iron for denitrification enzymes (Granger and Ward 2003). No direct measure of the biomass of denitrifiers or rate of denitrification from our study is available to compare with ligand distributions, but the secondary particle maximum in the suboxic zone, which is believed to be created by denitrifying bacteria, was recorded in transmissometer profiles and serves as an index of denitrifier biomass (Garfield et al. 1983). Suboxic zone *Prochlorococcus* partially obscure denitrifiers in the upper portion of the secondary particle maximum, which extends from the oxic-suboxic interface to ~350 m, but transmissometer data from below the *Prochlorococcus* maxima, showed that the bacterial portion of the secondary particle maximum was strong throughout our transect (Fig. 4.4). Offshore decline in denitrifier biomass is not as strong as the decline in suboxic zone

Prochlorococcus, making denitrifiers a more likely source for the ubiquitous iron binding ligands if they are produced by resident organisms.

Rather than being actively produced to bind iron, ligands measured in the suboxic zone could also be bacterial exudates produced for purposes other than iron acquisition, or as a byproduct of the breakdown of organic matter. Bacteria and phytoplankton release organic compounds into surrounding water for diverse reasons including as grazing deterrents, antibiotics, and to reduce the toxicity of trace metals (Moffett and Brand 1996; Long and Azam 2001). Released organic compounds or their degradation products may coincidentally bind iron. Additionally, iron binding ligands could result from partial decomposition of organic matter exported from the euphotic zone. Both these processes occur in oxic waters as well, but labile or reduced iron binding compounds produced could be more stable or longer lived under suboxic conditions.

It has also been proposed, based on data from diverse regions, that ligand concentrations are higher in regions where iron inputs or concentrations are higher (Witter et al. 2000). Such a relationship could be caused by production of ligands in response to inputs of iron as has been observed in mesoscale iron addition experiments (Rue and Bruland 1997; Croot et al. 2001) At a given station our data support this observation as ligand concentrations track the increase in iron with depth, and overall in our study area ligand concentrations were relatively low, perhaps due to low iron inputs in the region. However, we found no significant onshore-offshore trend in ligand concentrations in contrast to dissolved iron.

The numerical concentration and strength of natural ligands determined varies significantly depending on methods used by different investigators. Different competitive

ligands have different analytical windows and require higher or lower pH's which will affect natural ligand binding. Beyond variations in analytical method, data collected can be transformed in a variety of ways to extract a ligand concentration and strength. These considerations mean that while comparisons between investigators of trends derived from a single data set may be robust, comparisons of actual ligand concentrations and strengths must be done cautiously. Generally the conditional stability constants ($\log K_{Fe'L}$) that we measured in the ETNP were in the range found by other investigators (e.g. Rue et al. 1995; Witter et al. 2000; Boye et al. 2005). Our surface ligand strengths are similar to those found in most other work in oxic seawaters, but consistently in the middle to lower end of the range. The most interesting observation in our study was the strength of the suboxic zone ligands, similar to those observed by Witter et al. (2000), which were stronger than oxic zone ligands and at the higher end of the range of strengths found by other investigators in surface waters (Rue and Bruland 1995; Boye et al. 2005). At $\log K_{Fe'L}$ = 12.1-12.8, their strength approached that of the class of strong iron binding ligands, L_1 ($\log K_{Fe'L}$=13.2), described by Rue and Bruland (1997) with strengths similar to isolated marine siderophores.

Fe(II) concentrations

No direct measurements of Fe(II), the reduced state of iron, have been made in the open-ocean regions of a suboxic zone. Measurements made near the coast of Peru found Fe(II) levels up to 40 nM, and at some locations nearly all dissolved Fe was Fe(II), suggesting Fe(II) may also be a significant portion of dissolved iron offshore (Hong and Kester, 1986). However, examining ratios of acid leachable to refractory particulate Fe, Landing and Bruland (1987) found no evidence for *in-situ* reduction of Fe as they did for

Mn, but this does not rule out the presence of Fe(II) from a low level of Fe(II) production

or Fe(II) which originated in coastal waters and was transported offshore. In this work a

chemiluminescence method capable of detecting picomolar Fe(II) concentrations was

used to directly measure Fe(II) in the offshore regions of the ETNP suboxic zone (Rose

and Waite, 2001; Croot and Laan, 2002).

At the furthest offshore station (Station 21), 1300km from the coast, a profile

from the surface to the core of the suboxic zone was analyzed with the

chemiluminescence method for Fe(II). Signals were detected in all of the samples from

within the suboxic zone but immediately above the suboxic zone, in the oxygen gradient,

signals returned to background (Fig. 4.5). If these signals are interpreted as being solely

from Fe(II), Fe(II) concentrations would be 0.12–0.15 nM or 21-24% of total dissolved

iron. These measurements set an upper limit to Fe(II), but the signal may not be due

exclusively to Fe(II). Below we consider potential interferences, the likelihood that they

were present in the suboxic zone, and argue that the observed signal was due primarily to

Fe(II).

Validity of the chemiluminescence method in suboxic seawater

The chemiluminescence technique used in this study is based upon the rapid

reaction of Fe(II) with O_2 which occurs at high pH in the flow cell. This reaction

produces superoxide which reacts with luminol giving off light (Rose and Waite 2001).

The technique was developed for measuring Fe(II) in oxic seawater, and reaction

conditions have been optimized to be sensitive and selective for Fe(II) by increasing the

pH and excluding hydrogen peroxide from the reagents (Seitz and Hercules 1972). Many

trace metals present in oxic waters including, Mn(II), Cu(II), Co(II), Cr(III), and Ni(II)

have been shown to be unreactive under conditions used to measure Fe(II) (O'Sullivan et al. 1995). However, more exotic species potentially present in suboxic environments have not been systematically tested. We conducted tests of most elements with a redox couple between oxic and anoxic conditions and present at concentrations greater than 100 pM in seawater, in order to determine whether their reduced forms produced light under the conditions we used to measure Fe(II) in the field. Two reduced forms of vanadium, V(III) and V(IV), were found to initiate the luminol reaction, and thus are potential interferences in the determination of Fe(II) (Table 4.1; Pilipenko et al. 1975).

Although V(III) and V(IV) can produce a chemiluminescence signal it seems unlikely that these species were present in the suboxic environment at concentrations sufficient to produce the signal we observed. The pE_{cond} of the V(V)/V(IV) and V(V)/V(III) couples (pE_{cond}= -3.1 ; -2.7 respectively) show that thermodynamically the reduced species would not be expected until anoxic conditions are reached. Removal of V from seawater has been observed in anoxic waters and strongly reducing sediments, but not in suboxic waters (Emerson and Huested 1991; Nameroff et al. 2002). In a study to assess the redox state of the ETNP suboxic zone, Rue et al. (1997) determined the redox states of a suite of trace element redox couples spanning pE_{cond} of ~12 to 0. They found full reduction of iodate to iodide (pE_{cond}=11.8), but only partial reduction of Cr(VI) to Cr(III) and Se(VI) to Se(IV) (pE_{cond}= 8.4 ; 7.4 respectively), and concluded that the trace elements examined behaved according to thermodynamic predictions based on the NO_3^- /NO_2^- couple (pE_{cond}= 7.3) controlling the suboxic zone pE. Based on the redox state of other trace element couples it seems unlikely that V(IV) or V(III) was present in the suboxic zone.

Interpreting elemental behavior based on purely thermodynamic considerations can be misleading, especially for biologically active elements. While V is not generally required for cellular metabolism, V(V) can be used as an oxidant for respiration by certain metal-reducing bacteria (Carpentier et al. 2003). Similar bacteria may exist in the marine environment, but use of oxidants is predictably ordered by energy yields of the reactions (Froelich et al. 1979). With sufficient NO_3^-, a much better oxidant, available it is unlikely that V(V) is being reduced for respiratory use. Reduction of V(V) by bacteria produces V(IV), which our chemiluminescence instrument is not very sensitive for. To produce the observed chemiluminescence signal ~10 nM V(IV) would need to have been present in the suboxic zone, and while small amounts of V(IV) might be produced in microenvironments, such large amounts of a reactive species would not be expected to accumulate due to both oxidation and scavenging onto particles (Wehrli and Stumm 1989). The chemiluminescence technique is more sensitive to V(III), and ~3 nM V(III) could have created the signal we detected in the suboxic zone, but V(III) is highly insoluble, particle reactive, and unstable even at low oxygen levels (Wanty and Goldhaber 1992). V(III) is rarely found in the natural environment and even in sediments it is thought to be formed by slow reduction of V(IV) with sulfide (Wanty and Goldhaber 1992).

Additional evidence as to the identity of the species responsible for the chemiluminescence signal is provided by the oxic decay rate of the signal. As described in the methods, the rate of decay of the chemiluminescence signal from the suboxic zone was measured on a sample which had been fully oxygenated. The main oxidants of Fe(II)

in natural waters are O_2 and hydrogen peroxide, H_2O_2, and the decay rate of Fe(II) by

these oxidants can be described by :

$$\frac{-d[Fe(II)]}{dt} = k_1[Fe(II)][O_2][OH^-]^2 + k_2[Fe(II)][H_2O_2][OH^-] \quad (1)$$

where the rate constants k_1 and k_2 are functions of temperature and ionic strength

(Millero et al. 1987; Millero and Sotolongo 1989). If all factors except Fe(II) are kept

constant the rate expression becomes:

$$\frac{-d[Fe(II)]}{dt} = k_{app}[Fe(II)] \quad (2)$$

Under these conditions simple exponential decay is expected with a pseudo-first order

rate constant, k_{app}, and a plot of *ln[Fe(II)]* vs. time (*t*) should yield a straight line. As

shown for the field signal, in figure 4.6, an initial rapid drop in signal is observed

producing a non-linearity in the *ln(signal)* vs. *t* plot, but after this drop the decay becomes

nearly linear corresponding to pseudo-first order decay. The pseudo-first order decay

rate, k_{app}, calculated from a linear fit to the field decay data was 1.7×10^{-2} min^{-1}. This

decay constant was calculated using the raw instrument signal assuming that the

instrument response was linearly related to the concentration of the unknown species

producing the signal. (At the relatively low signal levels observed in the suboxic zone

deviations from non-linearity are minor for the possible sources of the signal, Fe(II),

V(III), and V(IV), and should not present a problem in this discussion.)

Comparisons of the field decay rate with literature values and decay rates

determined in our lab for Fe(II), V(III), and V(IV) under conditions replicating the field

experiment are shown in Table 4.2 (see Methods). The decay rate of the field species falls

within the range of Fe(II) oxidation rates from literature sources and is close to the value

determined in our lab experiments. Unfortunately, analysis of decay rates does not help

distinguish Fe(II) from V(IV) as their decay rates are nearly identical, but it does rule out

the possibility of V(III) being the source of the suboxic zone signal since its decay rate is

more than an order of magnitude faster than the field decay rate. Our laboratory decay

rates of Fe(II) and V(IV) are somewhat faster on average than the field decay rate. An

uncontrolled parameter which may account for this discrepancy is the concentration of

H_2O_2 in both our field sample and laboratory experiments. The field decay experiment

was performed on a freshly collected trace-metal clean sample from suboxic zone waters

and significant H_2O_2 contamination was unlikely. While the concentration of H_2O_2 was

not measured, concentrations of H_2O_2 are extremely low in deep oxic waters, 0.5-2nM

(Yuan and Shiller 2004). If the concentration of H_2O_2 in the suboxic water is similar to

that in deep oxic waters our observed decay rate would agree well with the Fe(II) decay

rate at low H_2O_2 predicted from the literature (Table 4.2; Millero et al. 1987; Millero and

Sotolongo 1989). On the other hand, our laboratory experiments were conducted with

suboxic zone water which had been stored in a cold room for approximately 1 year. Use

of water collected from the suboxic zone helped to control for variables such as salinity,

pH, and potentially other unknown or difficult to replicate factors such as the presence of

organic ligands which may affect oxidation rate. However, other investigators have found

H_2O_2 contamination from laboratory air, and our water may have had increased H_2O_2

levels compared with the field experiment, speeding up the rate of Fe(II) decay (King et

al. 1995). Overall the observed field decay rates are close to the rates of decay expected

for Fe(II), and although V(IV) cannot be ruled out as an interference based on analysis of

decay rates, considerations of the reducing level of the suboxic zone discussed above make it unlikely that V(IV) was present in the suboxic zone.

Decay rates of Fe(II) in suboxic waters may also have been affected by natural organic ligands which, depending on their identity, may accelerate or retard oxidation. Strong Fe(III) binding ligands such as siderophores and EDTA generally accelerate the rate of decay. Our CLE-ACSV measurements indicate free strong Fe(III) binding ligands existed in the suboxic zone, and may increase the rate of Fe(II) oxidation, potentially accounting for the non-linearity observed in our signal decay measurements. No information is available on natural Fe(II) ligands and no methods yet exist for their measurement, but if present they can stabilize Fe(II), even completely preventing its oxidation. The chemiluminescence signal returned to near background in our experiments precluding extreme stabilization by Fe(II) ligands, but more subtle stabilization may have slowed decay. In spite of the many factors which may influence decay, the field signal decay rate closely matched that of inorganic Fe(II).

We acknowledge that our chemiluminescence measurements cannot be definitively attributed to Fe(II), but when thermodynamics and decay rates of possible interferences are considered, Fe(II) emerges as the most likely source of the chemiluminescence signal. In the future, use of a coupled column separation-chemiluminescence detection method may be valuable to verify these results, though column methods may also be subject to biases and artifacts (Croot and Laan 2002). However, for subsequent discussion here it will be assumed that the chemiluminescence signal we observed in the suboxic zone was exclusively due to Fe(II).

Fe(II) sources and sinks

While the presumed redox state of the suboxic zone, pE ~7, indicates iron should

be in its oxidized form, Fe(II) represents 21-24% of total dissolved iron present in the

suboxic zone at the station sampled (Fig. 4.5). No Fe(II) was detected in the oxygen

gradient, but Fe(II) was detected just below the oxic-suboxic interface when nitrite is

detected and remained essentially constant over the upper part of the suboxic zone where

we sampled. Consideration of possible sources and sinks of this Fe(II) provide a better

understanding of the likely origin and cycling of Fe(II) in the suboxic zone. Fe(II) could

be a product of *in-situ* processes such as normal metabolic cycling or microbial

respiration using Fe(III), or it could result from offshore transport of Fe(II) produced in

reducing sediments on the shelf. The half-life of Fe(II) is extended under suboxic

conditions where lower pH (7.5), temperature (11.6 ^{o}C), and O_2 (0.5-2μM), compared to

surface waters, all combine to decrease the oxidation rate of Fe(II) (Millero et al. 1987;

Morrison et al. 1999). Using the equations of Millero et al. (1987) for oxidation of Fe(II)

by O_2, the half-life of Fe(II) under suboxic zone conditions would be 8-30 days

depending on the O_2 concentration which is the most uncertain parameter. However,

H_2O_2 is an important oxidant of Fe(II), and the predicted half-life of Fe(II) would be

significantly shorter if H_2O_2 was present in the suboxic zone. There have been no direct

measurements of H_2O_2 in the suboxic zone, but if concentrations are similar to deep oxic

waters, 0.5-2 nM, the half-life of Fe(II) would be 0.16-0.65 days (Millero and Sotolongo

1989; Yuan and Shiller 2004). The suboxic zone half-life is substantially longer than

what would be expected in the surface, or even the oxygen gradient where Fe(II) was

absent. The Fe(II) half life would be only 70 minutes at 25 μM O_2 and 6 nM H_2O_2, the

estimated conditions of the lowest sample in the O_2 gradient where no Fe(II) was detected.

In contrast to the half-life of Fe(II) in the suboxic zone, the characteristic time (T_k) for transport of Fe(II) from the coast based on horizontal eddy diffusivity is approximately 32 years ($T_k=D^2/K_H=(1300km)^2/5.14x10^4$ km^2/yr = 32.8 years)(Okubo, 1971). Sluggish advective transport, which contributes to the formation of the suboxic water mass, means that even if deep waters are moving as fast as surface waters, 2-4 cm/s, it would still take 1-2 years for coastal waters to reach Station 21, where Fe(II) was measured (Kessler 2002). The time required to transport Fe(II) from coastal sedimentary sources is much larger than the estimated half-life of Fe(II) in the suboxic zone, indicating that an *in-situ* process is required. It is unlikely that Fe(II) is produced by microbial respiration using Fe(III), since NO_3^- is still available for respiration and no evidence of in-situ reduction of particulate Fe was observed in contrast to particulate Mn (Landing and Bruland 1987).

The most likely source of Fe(II) is simply the normal metabolic processes which regularly cycle iron between redox states when it is used in electron transport proteins. Cellular iron is a mix of Fe(II) and Fe(III) and grazing or viral lysis will release this Fe into the surrounding waters (Hutchins and Bruland, 1994). It is difficult to estimate an Fe(II) production rate in the suboxic zone because so many of the important processes and parameters are unknown. To match oxidative loss of Fe(II), calculated to be 0.16 nM/day if literature decay rates (for 2 μM O_2, 0.5 nM H_2O_2) are applied to measured suboxic zone Fe(II) concentrations, the 1.5 nM particulate iron measured in the suboxic zone by Landing and Bruland (1987) would have to turnover every few days to support

the observed Fe(II) concentrations (Millero et al. 1987; Millero and Sotolongo 1989). Unfortunately, there is no good estimate of what portion of this particulate iron is Fe(II), nor what portion is mineral or organismal, making a more accurate estimate of the necessary turnover time impossible. None-the-less, the point of this exercise is to demonstrate that ecologically reasonable turnover times of particulate iron could account for the dissolved Fe(II) measured in the suboxic zone.

Sinks for Fe(II) include oxidation to Fe(III) and uptake by microorganisms in the suboxic zone. Since Fe(II) is more kinetically labile and more weakly bound to known Fe(III) chelators such as siderophores, it is thought to be a more bioavailable form of Fe (Sunda 2001). This Fe(II) could be an important source of bioavailable iron to *Prochlorococcus* and denitrifiers living in the suboxic zone especially if the strong Fe(III) binding ligands prohibit uptake of Fe(III) by certain taxa. However, there is certainly the possibility that strong Fe(II) organic ligands, such as thiols, also exist and reduce bioavailability, but Fe(II) ligands have not yet been investigated. As discussed above Fe(II) oxidation by oxygen still occurs in the suboxic zone but at a much reduced rate. The life time of Fe(II) may also be affected by other factors which have not been well characterized such as complexation by organic ligands or sulfide. Slightly elevated levels of metal-complexed sulfide were measured in the Arabian suboxic zone and complexation and stabilization of Fe(II) by sulfide could occur in the ETNP (Therberge et al. 1997). Rose and Waite (2002) found that Fe(II) oxidation rates could be accelerated by the presence of strong Fe(III) ligands under oxic conditions, but our measurements indicate that Fe(II) and excess strong Fe(III) binding ligands can co-exist in suboxic waters. *In-situ* processes best explain the presence of Fe(II), but our understanding of

Fe(II) life time and bioavailability is limited by lack of information on Fe(II) ligands or direct measurements of *in-situ* half-life.

Conclusion

Iron is present in the oxic and suboxic layers of the ETNP at concentrations similar to those found in oxygenated water columns. Reducing shelf sediments or atmospheric deposition elevate iron concentrations closer to land but as the waters are transported offshore concentrations are reduced by half over the span of our transect. Fe(III) binding ligands are present at all depths, but are particularly strong in the suboxic zone, a feature not present in oxic regions. These ligands could be a byproduct of the unique chemistry of the suboxic zone which may allow reduced or labile compounds to persist, or they may be actively produced by *Prochlorococcus* and denitrifiers living in the suboxic zone. Although the ligands are stronger at depth, their strength ($logK_{cond}=$ 12.1-12.8) is within the range found in other regions of the ocean (Rue and Bruland 1995; Witter et al. 2000; Boye et al. 2005)).

An extremely sensitive chemiluminescence technique was used to measure Fe(II) in the suboxic zone (Rose and Waite 2001). Concentrations of 0.12-0.15nM, or 21-24% of dissolved iron were measured, but interpretation of the chemiluminescence signal was complicated by the possibility of interferences from other reduced species. We found that V(IV) and V(III) can react with luminol to produce a chemiluminescence signal under the same conditions as Fe(II). Considerations of the thermodynamics and kinetics of these possible interfering species indicate that Fe(II) is the most reasonable source of the chemiluminescence signal, and at a minimum the measurements set upper limits on the

concentration of Fe(II). This study highlights the need to thoroughly consider the system under analysis when interpreting chemiluminescence results, as has been advised previously (Rose and Waite 2001). The Fe(II) is most likely produced *in-situ* by normal cellular processes, but accumulates to high levels because of slower oxidation times under suboxic conditions.

A better picture of iron speciation in the suboxic zone is relevant to understanding the processes occurring within the suboxic zone and the oxic water column above. Iron is required for denitrification and for the photosynthetic apparatus of *Prochlorococcus* growing in the weak light available at the top of the suboxic zone. Strong iron binding ligands complex Fe(III) in the suboxic zone which may enhance or diminish iron bioavailability depending on their nature and the organisms involved. Despite the presence of excess strong Fe(III) binding ligands, substantial concentrations of Fe(II) exist in the suboxic zone possibly stabilized by organic ligands or small amounts of sulfide (Therberge et al. 1997). Unfortunately there is presently very little information on organic Fe(II) ligands in oxic or suboxic waters. Iron redox and organic speciation is significantly affected by suboxic conditions, but conditions are not so reducing that iron is fully reduced to Fe(II), nor does iron accumulate in the suboxic zone.

experiments and interference tests. We also thank Whitney King for assistance and advice with Fe(II) measurements. This research was funded by NSF grant OCE-0220959 to K. Barbeau.

This chapter was published previously as: Hopkinson, Brian M., and Katherine A. Barbeau. 2007. Organic and redox speciation of iron in the eastern tropical North Pacific suboxic zone. Marine Chemistry 106: 2-17.

Table 4.1. Results of interference tests. FeLume signals are reported relative to signal of 1nM Fe(II).

Redox Couple	pE_{cond}	Seawater Concentration (nM)	Compound tested	FeLume Signal		
				1 nM	10 nM	100 nM
[a]IO_3^-/I^-	11.8	500	KI	0	0	0
$HCrO_4^-/Cr^{3+}$	8.4	4	$CrCl_3 \bullet 6H_2O$	0	0	0
SeO_4^{2-}/SeO_3^{2-}	7.4	2	Na_2SeO_3	0	0	0
[a]NO_3^-/NO_2^-	7.3	2000^b	$NaNO_2$	0	0	0
MnO_2/Mn^{2+}	6.8	0.8	$MnCl_2 \bullet 4H_2O$	0	0	0
Cu^{2+}/Cu^+	6.8	2	CuCl	0.03	-0.02	-0.04
$CoOOH(s)/Co^{2+}$	3.8	0.1	$CoCl_2 \bullet 6H_2O$	0.01	0.06	0.36
$Sb(V)/Sb(III)$	3.4	2	$Sb(CH_3CO_2)_3$	0	0	0
Fe^{3+}/Fe^{2+}	1.9	0.7	$Fe(NH_4SO_4)_2 \bullet 6H_2O$	1	11	495
$H_3AsO_4/HAsO_2$	-1.6	20	$NaAsO_2$	0	0	0
VO^{2+}/V^{3+}	-2.7	40	VCl_3	0.15	0.76	5.9
VO_2^+/VO^{2+}	-3.1	40	$VOSO_4$	0.03	0.20	0.48
$MoO_4^{2-}/Mo(V)$	-6.1	100	$MoCl_5$	0	0	0

[a] concentrations tested of these compounds were 100 nM, 1 μM, 10 μM

[b] approximate concentration of NO_2^- in the suboxic zone.

Table 4.2. Decay rates of field species, Fe(II), and reduced V for comparison. Sources: (1) Millero, et al., 1987; (2) Millero and Sotolongo, 1989.

Species	k_{app} ($\times 10^{-2}$ min^{-1})	Conditions	Source
Field Signal	1.7	ETNP sample + O_2	This study
Fe(II)	2.7 ± 0.7	Lab decay	This study
V(IV)	2.5 ± 0.7	Lab decay	This study
V(III)	25.7 ± 0.4	Lab decay	This study
Fe(II)	1.5	Predicted, 2nM H_2O_2	1,2
Fe(II)	2.7	Predicted, 10nM H_2O_2	1,2
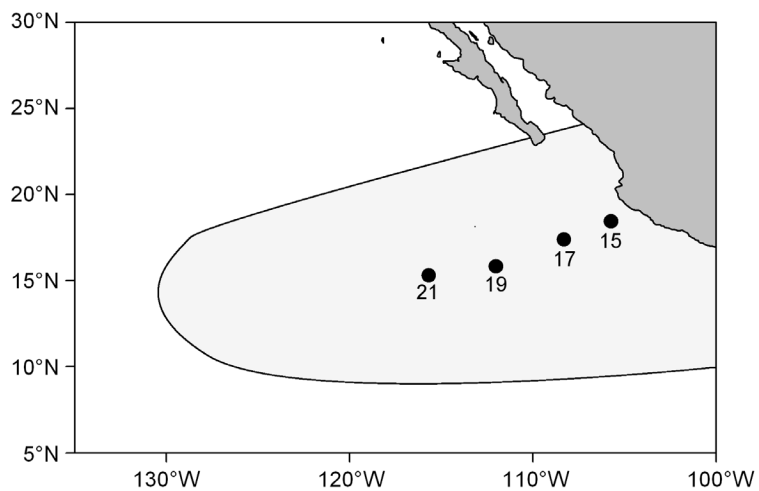
Figure. 4.1. A map of stations occupied during November 2003 cruise, and approximate extent of the suboxic zone (lightly shaded area) based on Wyrtki (1967) and Deutsch, et al. (2001). Station numbers used throughout the text are indicated on the map.
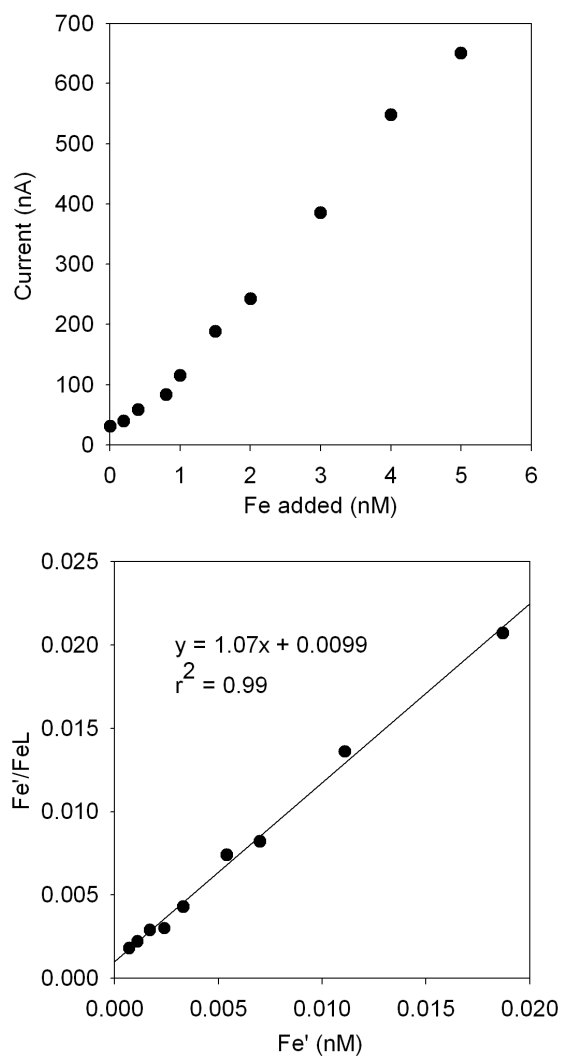
Figure. 4.2. A CLE-ACSV titration from Station 21 190m depth, top, and the Langmuir linearization with best fit line, below.
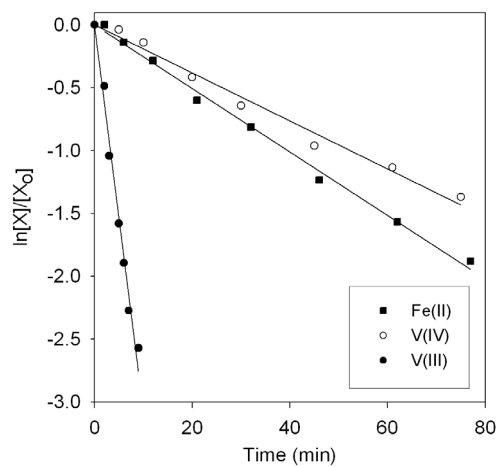
Figure. 4.3. Results of selected decay experiments of Fe(II), V(IV), and V(III), plotted to show pseudo-first order decay kinetics. The solid lines are linear regressions through the data.
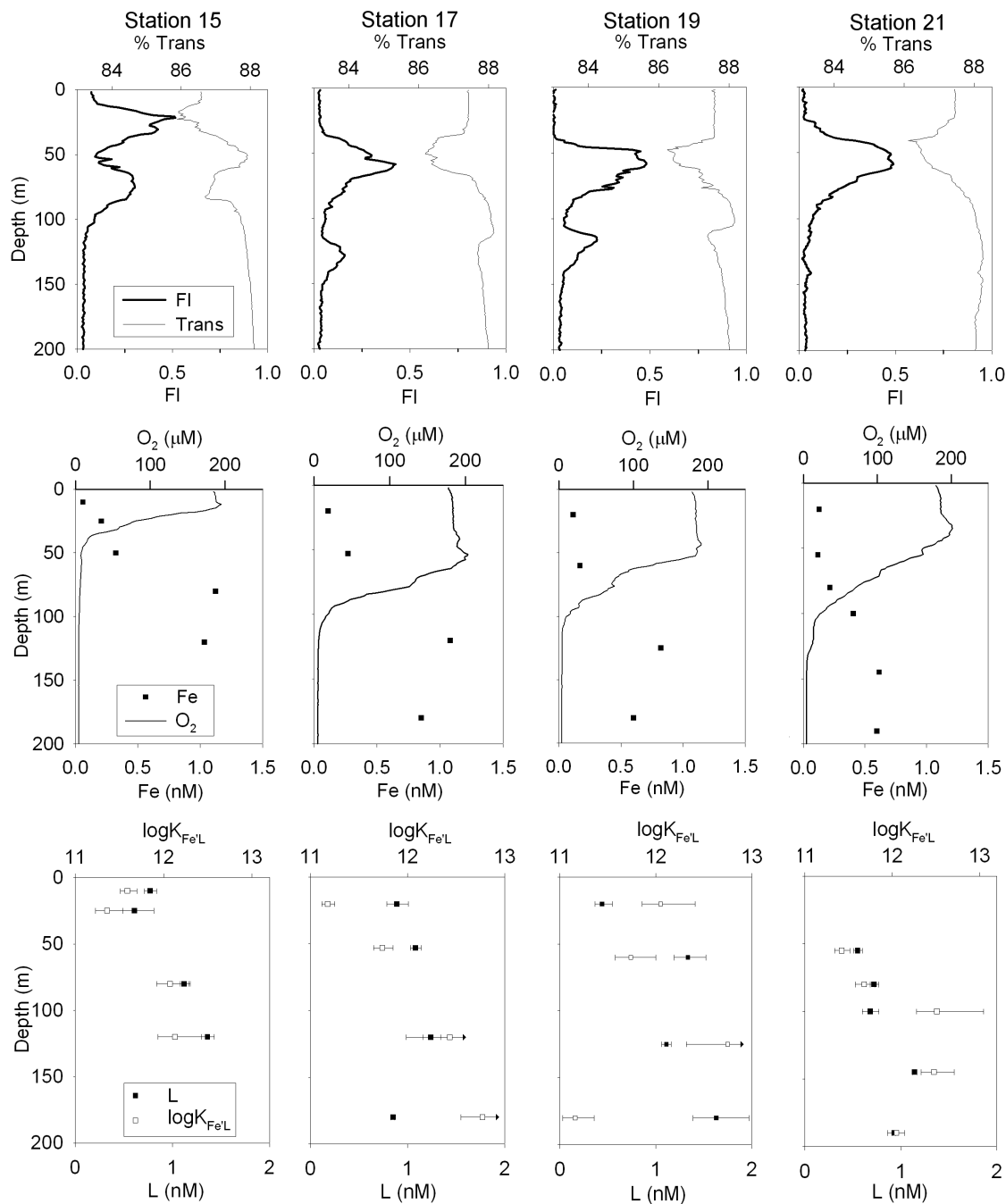
Figure. 4.4. Profiles of dissolved iron concentrations (Fe), iron binding ligands (L), and their conditional stability constants ($logK_{Fe'L}$) shown with reference to aspects of the biological (fluorescence (Fl), % beam transmission (% Trans)) and chemical (O_2) structure of the water column. Arrows, in place of error bars, on certain $logK_{Fe'L}$ values indicate an upper limit cannot be placed on these ligand strengths (see Methods).
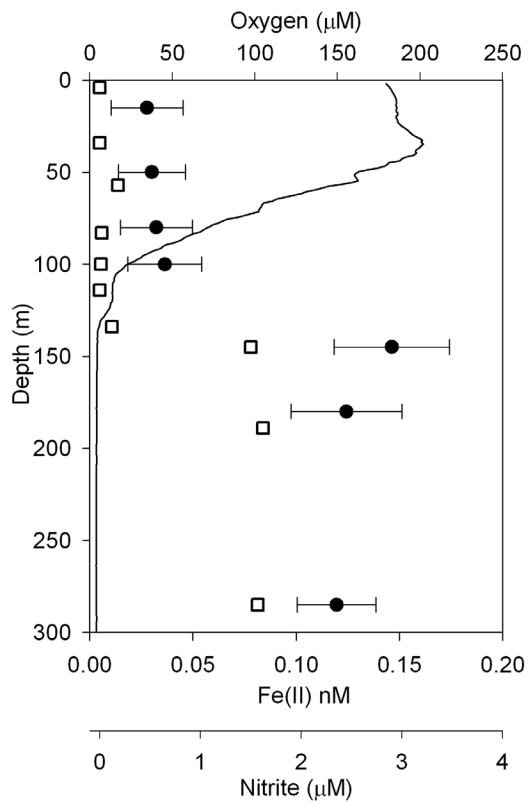
Figure. 4.5. Profile of Fe(II) (●), NO_2^- (□), and O_2 (solid line) at Station 21. Fe(II) is present in the suboxic zone where NO_2^- occurs, but is undetectable in the oxycline and surface waters.
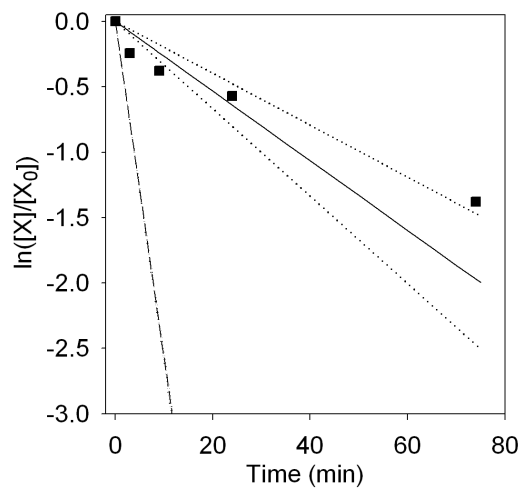
Figure. 4.6. Decay of field signal (■) compared to laboratory-determined decay rates of Fe(II) and V(IV) (solid line) and V(III) (dashed line). Laboratory-determined rates are an average of three to four replicates with the dotted lines representing the standard error. Only one line is shown for Fe(II) and V(IV) because their decay rates are nearly identical.

References

Bard, A.J., R. Parsons, and J. Jordan (Eds.), 1985. Standard potentials in aqueous solution. IUPAC, New York.

Boye, M., J. Nishioka, P.L. Croot, P. Laan, K.R. Timmermans, and H.J.W. de Baar. 2005. Major deviations of iron complexation during 22 days of a mesoscale iron enrichment in the open Southern Ocean. Mar. Chem. **96:** 257-271.

Bruland, K.W., E.L. Rue, G.J. Smith, and G.R. DiTullio. 2005. Iron, macronutrients and diatom blooms in the Peru upwelling regime: brown and blue waters of Peru. Mar. Chem. **93:** 81-103.

Carpentier, W., K. Sandra, I. De Smet, A. Brige, L. De Smet, and J. Van Beeumen. 2003. Microbial reduction and precipitation of vanadium by *Shewanella oneidensis*. Appl. Environ. Microbiol. **69:** 3636-3639.

Cline, J.D., and F.A. Richards. 1972. Oxygen deficient conditions and nitrate reduction in the eastern tropical North Pacifc. Limnol. Oceanogr. **17:** 885-900.

Coale, K.H., K.S. Johnson, S.E. Fitzwater, R.M. Gordon, S. Tanner, F.P. Chavez, L. Ferioli, C. Sakamoto, P. Rogers, F. Millero, P. Steinberg, P. Nightingale, D. Cooper, W.P. Cochlan, M.R. Landry, J. Constantinou, G. Rollwagen, A.Trasvina, and R. Kudela. 1996. A massive phytoplankton bloom induced by an ecosystem-scale iron fertilization experiment in the equatorial Pacific Ocean. Nature **383:** 495-501.

Croot, P.L., and M. Johansson. 2000. Determination of iron speciation by cathodic stripping voltammetry in seawater using the competing ligand 2-(2-Thiazolylazo)-*p*-cresol (TAC). Electroanalysis **12:** 565-576.

Croot, P.L., A.R. Bowie, D.F. Russell, M.T. Maldonado, J.A. Hall, K.A. Safi, J. La Roche, P.W. Boyd, and C.S. Law. 2001. Retention of dissolved iron and Fe(II) in an iron induced Southern Ocean phytoplankton bloom. Geophys. Res. Lett. **28:** 3425-3428.

Croot, P.L., and P. Laan. 2002. Continuous shipboard determination of Fe(II) in polar waters using flow injection analysis with chemiluminescence detection. Anal. Chim. Acta **466:** 261-273.

Cullen, J.T., B.A. Berquist, and J.W. Moffett. 2006. Thermodynamic characterization of the partitioning of iron between soluble and colloidal species in the Atlantic Ocean. Mar. Chem. **98:** 295-303.

Deutsch, C., N. Gruber, R.M. Key, and J.L. Sarmiento. 2001. Denitrification and N_2 fixation in the Pacific Ocean. Glob. Biogeochem. Cycles **15:** 483-506.

Emerson, S.R., and S.S. Huested.1991. Ocean anoxia and the concentrations of molybdenum and vanadium in seawater. Mar. Chem. **34:** 177-196.

Froelich, P.N., G.P. Klinkhammer, M.L. Bender, N.A. Luedtke, G.R. Heath, D. Cullen, P. Dauphin, D. Hammond, B. Hartman, and V. Maynard. 1979. Early oxidation of organic matter in pelagic sediments of the eastern equatorial Atlantic: suboxic diagenesis. Geochim. Cosmochim. Acta **43:** 1075-1090.

Garfield, P.C., T.T. Packard, G.E. Friedrich, and L.A. Codispoti. 1983. A subsurface particle maximum layer and enhanced microbial activity in the secondary nitrite maximum of the northeastern tropical Pacific Ocean. J. Mar. Res. **41:** 747-768.

Goericke, R., R.J. Olson, and A. Shalapyonok. 2000. A novel niche for *Prochlorococcus sp.* in low-light suboxic environments in the Arabian Sea and the Eastern Tropical North Pacific. Deep Sea Res. **47:** 1183-1205.

Granger, J., and B.B. Ward. 2003. Accumulation of nitrogen oxides in copper-limited cultures of denitrifying bacteria. Limnol. Oceanogr. **48:** 313-318.

Hong, H., and D.R. Kester. 1986. Redox state of iron in the offshore waters of Peru. Limnol. Oceanogr. **31:** 512-524.

Hutchins, D.A., and K.W. Bruland. 1994. Grazer-mediated regeneration and assimilation of Fe, Zn, and Mn from planktonic prey. Marine Ecol. Prog. Ser. **110:** 259-269.

Johnson, K.S., V.A. Elrod, S.E. Fitzwater, J.N. Plant, F.P. Chavez, S.J. Tanner, R.M. Gordon, D.L. Westphal, K.D. Perry, J. Wu, and D.M. Karl. 2003. Surface ocean-lower atmosphere interactions in the Northeast Pacific Ocean Gyre: aerosols, iron, and ecosystem response. Glob. Biogeochem. Cycles **17:** doi:10.1029/2002GB002004.

Kessler, W.S. 2002. Mean three-dimensional circulation in the Northeast Tropical Pacific. J. Phys. Oceanogr. **32:** 2457-2471.

King, D.W., H.A. Lounsbury, and F.J. Millero. 1995. Rates and mechanism of Fe(II) oxidation at nanomolar total iron concentrations. Envrion. Sci. Technol. **29:** 818-824.

Landing, W.M., and K.W. Bruland. 1987. The contrasting biogeochemistry of iron and manganese in the Pacific Ocean. Geochim. Cosmochim. Acta **51:** 29-43.

Long, R.A., and F. Azam. 2001. Antagonistic interactions among marine pelagic bacteria. Appl. Envrion. Microbiol. **67:** 4975-4983.

Martin, J.H., and R.M. Gordon, and S.E. Fitzwater. 1990. Iron in Antarctic waters. Nature **345:** 156-158.

Measures, C.I., and S. Vink.1999. Seasonal variations in the distribution of Fe and Al in the surface waters of the Arabian Sea. Deep-Sea Res. II **46:** 1597-1622.

Millero, F.J., and S. Sotolongo. 1989. The oxidation of Fe(II) with H_2O_2 in seawater. Geochim. Cosmochim. Acta **53:** 1867-1873.

Millero, F.J., S. Sotolongo, and M. Izaguirre. 1987. The oxidation kinetics of Fe(II) in seawater. Geochim. Cosmochim. Acta **51:** 793-801.

Mills, M.M., and C. Ridame, M. Davey, J. La Roche, and R.J. Geider. 2004. Iron and phosphorus co-limit nitrogen fixation in the eastern tropical North Atlantic. Nature **429:** 292-294.

Moffett, J.W., and L.E. Brand. 1996. Production of strong, extracellular Cu chelators by marine cyanobacteria in response to Cu stress. Limnol. Oceanogr. **41:** 381-395.

Moffett, J.W., and J. Ho. 1996. Oxidation of cobalt and manganese in seawater via a common microbially catalyzed pathway. Geochim. Cosmochim. Acta **60:** 3415-3424.

Morrison, J.M., L.A. Codispoti, S.L. Smith, K. Wishner, C. Flagg, W.D. Gardner, S. Gaurin, S.W.A. Naqvi, V. Manghnani, L. Prosperie, and J.S. Gundersen. 1999. The oxygen minimum zone in the Arabian Sea during 1995. Deep-Sea Res. II **46:** 1903-1931.

Murray, J.W., B. Spell, and B. Paul. 1981. The contrasting geochemistry of manganese and chromium in the eastern tropical North Pacific. In: Wong, C.S., Boyle, E., Bruland, K.W., Burton, J.D., Goldberg, E.D. (Ed.), Trace metals in seawater, NATO Conference Series IV: Marine Sciences, Volume 9, Plenum Press, New York, pp. 643-669.

Nameroff, T.J., L.S. Balistrieri, and J.W. Murray. 2002. Suboxic trace metal geochemistry in the eastern tropical North Pacific. Geochim. Cosmochim. Acta **66:** 1139-1158.

Nozaki, Y., 2001. Elemental distribution/overview. In: Steele, J.H., Thorpe, S.A., Turekian, K.K. (Ed.), Encyclopedia of Ocean Sciences, Academic Press, San Diego, pp 840-846.

Okubo, A., 1971. Oceanic diffusion diagrams. Deep-Sea Res. **18:** 789-802.

O'Sullivan, D.W., A.K. Hanson, and D.R. Kester. 1995. Stopped flow luminol chemiluminescence determination of Fe(II) and reducible iron in seawater at subnanomolar levels. Mar. Chem. **49:** 65-77.

Pilipenko, A.T., E. Mitropolitska, and N.M. Lukovskaya. 1975. Chemiluminescent reaction of luminol oxidation with oxygen and hydrogen-peroxide in aqueous-solutions with presence of vanadium(IV). Ukr. Khim. Zh. **41:** 525-529.

Rose, A.L., and T.D. Waite. 2001. Chemiluminescence of luminol in the presence of iron(II) and oxygen: oxidation mechanism and implications for its analytical use. Anal. Chem. **73:** 5909-5920.

Rose, A.L., and T.D. Waite. 2002. Kinetic model for Fe(II) oxidation in seawater in the absence and presence of natural organic ligands. Environ. Sci. Technol. **36:** 433-444.

Rue, E.L., and K.W. Bruland. 1995. Complexation of iron(III) by natural organic ligands in the Central North Pacific as determined by a new competitive ligand equilibrium/adsorptive cathodic stripping voltammetric method. Mar. Chem. **50:** 117-138.

Rue, E.L., and K.W. Bruland. 1997. The role of organic complexation on ambient iron chemistry in the equatorial Pacific Ocean and the response of a mesoscale iron addition experiment. Limnol. Oceanogr. **42:** 901-910.

Rue, E.L., and G.J. Smith, G.A. Cutter, and K.W. Bruland. 1997. The response of trace element redox couples to suboxic conditions in the water column. Deep-Sea Res. **44:** 113-134.

Ruzic, I., 1982. Theoretical aspects of the direct titration of natural waters and its information yield for trace element speciation. Anal. Chim. Acta **140:** 99-113.

Saito, M.A., and J.W. Moffett, and G.R. DiTullio. 2004. Cobalt and nickel in the Peru upwelling region: a major flux of labile cobalt utilized as a micronutrient. Glob. Biogeochem. Cycles **18**: GB4030, doi:10.1029/2003GB002216.

Seitz, W.R., and D.M. Hercules. 1972. Determination of trace amounts of iron(II) using chemiluminescence analysis. Anal. Chem. **44:** 2143-2149.

Sunda, W.G., 2001. Bioavailability and bioaccumulation of iron in the sea. In: Turner, D.R., Hunter, K.A., (Ed.) The biogeochemistry of iron in seawater, Wiley, New York, pp 41-84.

Sunda, W.G, and S.A. Huntsman. 1997. Interrelated influence of iron, light, and cell size on marine phytoplankton growth. Nature **390:** 389-392.

Therberge, S.M., G.W. Luther, and A.M. Farrenkopf. 1997. On the existence of free and metal complexed sulfide in the Arabian Sea and its oxygen minimum zone. Deep-Sea Res. II **44:** 1381-1390.

Town, R.A., and H.P. van Leeuwen. 2005. Measuring marine iron(III) complexes by CLE-AdSV. Environ. Chem. **2:** 80-84.

Turner, D.R., M. Whitfield, A.G. Dickson. 1981. The equilibrium speciation of dissolved components in freshwater and seawater at $25^{o}C$ and 1 atm pressure. Geochim. Cosmochim. Acta **45:** 855-882.

Turoczy, N.J., and J.E. Sherwood. 1997. Modification of the van den Berg/Ruzic method for the investigation of complexation parameters of natural waters. Anal. Chim. Acta **354:** 15-21.

Ussher, S.J., M. Yaqoob, E.P. Achtenberg, A. Nabi, and P.J. Worsfold. 2005. Effect of model ligands on iron redox speciation in natural waters using flow injection with luminol chemiluminescence detection. Anal. Chem. **77:** 1971-1978.

van den Berg, C.M.G. 1982. Determination of copper complexation with natural organic ligands in seawater by equilibration with MnO_2: Theory. Mar. Chem. **11:** 307-322.

van den Berg, C.M.G., 1995. Evidence for organic complexation of iron in seawater. Mar. Chem. **50:** 139-157.

van den Berg, C.M.G., 2005. Organic iron complexation is real, the theory is used incorrectly. comment on 'Measuring marine iron(III) complexes by CLE-AdSV'. Environ. Chem. **2:** 88-89.

Vanysek, P., 2004. Electrochemical series. In: Lide, D.R. (Ed.) CRC Handbook of Chemistry and Physics, 85th edition, CRC Press, Boca Raton, FL. pp. 8-23 – 8-33.

Wanty, R.B., and M.B. Goldhaber. 1992. Thermodynamics and kinetics of reactions involving vanadium in natural systems: accumulation of vanadium in sedimentary rocks. Geochim. Cosmochim. Acta **56:** 1471-1483.

Wehrli, B., and W. Stumm. 1989. Vanadyl in natural waters: adsorption and hydrolysis promote oxygenation. Geochim. Cosmochim. Acta **53:** 69-77.

Witter, A.E., B.L. Lewis, and G.W. Luther. 2000. Iron speciation in the Arabian Sea. Deep-Sea Res. II **47:** 1517-1539.

Wu, J., E. Boyle, W. Sunda, and L.S. Wen. 2001. Soluble and colloidal iron in the oligotrophic North Atlantic and North Pacific. Science **293:** 847-849.

Wyrtki, K. 1962. The oxygen minima in relation to ocean circulation. Deep-Sea Res. **9:** 11-23.

Wyrtki, K. 1967. Circulation and water masses in the eastern tropical Pacific Ocean. Int. J. Oceanol. Limnol. **1:** 117-147.

Yuan, J., and A.M. Shiller. 2004. Hydrogen peroxide in deep waters of the North Pacific Ocean. Geophys. Res. Lett. **31:** L01310, doi: 10.1029/2003GL0184329.

V

Heme uptake by *Microscilla marina* and genomic evidence

for heme uptake systems in diverse marine bacteria

Abstract

The ability to acquire diverse and abundant forms of iron would be expected to confer a survival advantage in the marine environment where iron is scarce. Marine bacteria are known to use siderophores and inorganic iron, but their ability to use heme, an abundant intracellular iron form, has only been examined preliminarily. Suspecting a hydrophobic compound such as heme would largely be present on particles, *Microscilla marina*, a cultured relative of a bacterial group frequently found on marine particulates, served as a model organism to examine heme uptake. Searches of the genome revealed analogs to known heme transport proteins, and RT-Q-PCR analysis of these genes showed that they were expressed and upregulated under iron stress and during growth on heme. *M. marina* was found to take up heme bound iron and could grow on heme as a sole iron source, supporting the genetic evidence for heme transport. Similar putative heme transport components were identified in the genomes of diverse marine bacteria. These systems were found in the genomes of many bacteria thought to be particle associated, but were lacking in known free living organisms (e.g. *Pelagibacter ubique* and marine cyanobacteria). This distribution of transporters is consistent with the hydrophobic, light-sensitive nature of heme, suggesting it is primarily available on phytoplankton, detritus, or in rich environments.

Introduction

Acquisition of adequate iron for bacterial growth is difficult in many environments as a result of the low solubility of Fe(III) and consequent scarcity of the

element, or the limited bioavailability of potential iron sources. Ingenious mechanisms to access iron have been developed by bacteria, the most well known of which is the use of siderophores, small iron binding organic compounds, excreted to scavenge iron (Neilands 1995). Capable of binding various forms of iron, siderophores serve as a general iron acquisition pathway, and are employed by bacteria from the human body, where free iron is limited to impede microbial growth, to soils, where iron is abundant but present in inert mineral phases of limited bioavailability (Eaton et al. 1982; Hersman et al. 1995). However, bacteria also have the ability to directly internalize forms of iron which are abundant in their environment, most notably heme which is a large pool of iron in organisms and represents a major source of iron for mammalian pathogens (Stojiljkovic and Hantke 1992; Genco and Dixon 2001) and may also be important for some symbiotic bacteria (Nienaber et al. 2001). Targeted uptake of abundant iron forms reduces the energy and material costs associated with the production, excretion, and uptake of siderophores.

Bacterial heme uptake is accomplished using mechanisms similar to siderophore and B12 uptake pathways (Stojiljkovic and Hantke 1992). From the extracellular environment, a TonB dependent outer membrane receptor selectively transports heme into the periplasmic space. In the periplasm, an ABC transport system consisting of a periplasmic binding protein, membrane permease, and an ATPase is employed to transport heme into the cytoplasm (Koster 2001). Once the heme has been internalized, it may be directly incorporated into heme containing proteins or broken down with a heme oxygenase for storage or use in other forms (Suits et al. 2005).

In oxic marine environments minimal inputs of iron combined with Fe(III)'s low solubility lead to subnanomolar concentrations of iron which limit autotrophic and heterotrophic productivity in portions of the ocean (Martin et al. 1990; Coale et al. 1996; Church et al. 2000). Competition for iron among organisms is consequently expected to be intense and the ability to access a wide range of iron compounds would be advantageous. Various marine bacteria have been shown to use inorganic iron, produce their own siderophores, and use exogenous siderophores produced by other organisms (Granger and Price, 1999; Martinez et al. 2000; Weaver et al. 2003).

Thus far, however, heme-specific transport by environmentally important marine bacteria has not been considered. Some experiments indicate marine bacteria are able to acquire iron from heme and other porphyrin complexes (Weaver et al. 2003). However, the mechanisms behind heme iron uptake, and the generality of its bioavailbility to marine bacteria has not been studied in detail despite heme's abundance in biological systems. Additionally heme transport has been studied extensively in pathogenic marine *Vibrios* including *Vibrio cholerae*, *V.vulnificus*, and *V. anguillarum* (Henderson and Payne 1993; Litwin and Byrne 1998; Mourino et al. 2004). The heme uptake systems in these organisms are homologous to those studied in a range of bacteria suggesting similar systems could occur in other marine bacteria. However, the relevance of these systems to life in the marine environment is unclear, since heme uptake capabilites may be present in these organisms solely for use during infection. The ability to use heme iron may be beneficial in the oceans since phytoplankton iron is localized in heme-rich photosystems. Heme could represent as much as 45% of iron in phytoplankton, achieving micromolar intracellular concentrations, and form a substantial portion of particulate iron in oceanic

systems (Strzepek and Harrison 2004; Gledhill 2007). Bacteria living in association with phytoplankton or those involved in the recycling of particulate organic matter are especially likely to benefit from the ability to access heme iron.

We used the genome-sequenced bacterium *Microscilla marina* of the Flexibacteraceae family as a model organism to study heme uptake. As a cultured bacterium with 16s similarity to sequences associated with the cyanobacterium *Trichodesium* (Janson et al. 1999; Mann personal comm.) and member of the phylum Bacteroidetes which are abundant on marine particles (Delong et al. 1993; Crump et al. 1999; Pinhassi et al. 2004), *M. marina* was considered a good representative of the bacteria involved in organic matter remineralization on particles where heme may be a significant source of iron. In addition, we searched the genomes of numerous marine bacteria for heme transport systems in order to assess their distribution providing insight into the bioavailability and cycling of heme in the marine environment.

Materials and Methods

Cell culturing

M. marina was isolated from an aquarium outflow in La Jolla, CA and is available from the ATCC (ATCC# 23134). Stock cultures of *M. marina* were maintained in 2216 marine media (Difco). For experimentation, *M. marina* was grown in a modified version of the Aquil media supplemented with peptone and casein, herein referred to as PC media (Granger and Price 1999). 0.2 μm filtered coastal seawater was supplemented with 1 g/L bacteriological peptone, 1 g/L casein hydrolysate, and 400 μM ammonium chloride. Several drops of 50% NaOH were added to adjust the pH to 7.6 and the mixture was then

run through a Chelex column to remove trace metals. The mixture was microwave sterilized and allowed to cool overnight. After cooling, K_2HPO_4 (100 µM), trace metals (50 µM EDTA, 3.9×10^{-8} M Zn^{2+}, 2.3×10^{-7} M Mn^{2+}, 2.5×10^{-8} M Co, 9.8×10^{-9} M Cu), and appropriate iron sources were added from filter sterilized stocks. $FeCl_3$ stocks (5 mM or 30 µM) were in 1% HCl and filter sterilized. Heme stocks (1.5 mM or 5 mM) were made up in 20 mM NaOH, chelexed to remove potential contaminating iron, and filter sterilized. The cultures were axenic and their purity was tested by plating on 2216 agar plates and examination under the microscope. *M. marina* cells are long filaments, up to 100 µm, and readily distinguished from most contaminants. Growth was monitored by measuring optical density through a 1 cm quartz cell at 600 nm on a spectrophotometer.

Heme Uptake

To synthesize [^{55}Fe] heme, $^{55}FeCl_3$ (25 µM) was refluxed with equimolar protoporphyrin IX in glacial acetic acid containing 0.1 M sodium acetate for 2 hours to insert iron into the porphyrin ring forming heme (Buchler 1975). The glacial acetic acid solution was diluted to 50% strength with water and the mixture was then passed through a column of Diaion HP20S resin. Heme was retained on the column, washed with water, and eluted in acetone. The concentration and purity of the [^{55}Fe]heme were determined using UV-Vis spectroscopy by comparison with purchased heme standards (Sigma).

M. marina cultures for uptake experiments were grown in 30 nM Fe PC media to obtain iron deficient cells and in 5 µM Fe PC media to obtain iron replete cells. Cultures were harvested by centrifugation during exponential growth. Harvested cells were twice rinsed, resuspended in sterile seawater, and again pelleted by centrifugation to ensure all culture media was removed. Finally, cells were resuspended in filtered seawater. 5 nM

[^{55}Fe]heme was added to triplicate bottles containing the resuspened *M. marina* and a single glutaraldhyde (0.01%) killed control. To monitor uptake of [^{55}Fe]heme, 2 mL samples were taken from each bottle at regular intervals and filtered onto a 0.45 μm Durapore filter (Millipore). The filters were washed with Ti-EDTA-Citrate wash (Hudson and Morel 1989) and water, and retained ^{55}Fe was quantified by liquid scintillation counting.

Gene Expression

M. marina growing on different iron sources or at differing iron concentrations was harvested in mid-log phase for analysis of gene expression. Iron replete cultures in 2216 media were inoculated in 30 nM Fe PC media and allowed to grow for 24 hrs resulting in mild iron stress (data not shown). 1 mL of the mildly stressed culture was then inoculated into 20 mL PC media containing either 30 nM Fe, 5 μM Fe, or 1.5 μM heme. After 24 hours of growth, cells were harvested by centrifugation and RNA was isolated using TRIzol reagent (Invitrogen) following the manufacturer's instructions with the exception that cells were initially incubated with TRIzol at 50 ºC for 30 min to lyse cells. The isolated RNA was then treated with amplification grade DNase I (Invitrogen), recovered using an RNeasy purification kit (Qiagen), and quantified using 260 nm and 280 nm absorbances measured on a spectrophotometer. 200 ng total RNA was reverse transcribed with random hexamer primers to produce cDNA using SuperScript II Reverse Transcriptase and supplied buffers following the manufacturer's instructions (Invitrogen). Parallel reactions were run without reverse transcriptase to ensure there was no significant contaminating DNA.

Real time quantitative PCR (RT-Q-PCR) was performed on the cDNA to quantify relative transcript amounts on a Stragene Mx3000P using the Brilliant SYBR Green Q-PCR master mix (Stragene) and gene-specific primers (0.42 μM , Table 1) designed using the draft genome of *M. marina*. Temperature profiles for the PCR consisted of an initial 10 min at 95 ºC, followed by 40 cycles of 95 ºC for 1min, 30 s at an annealing temperature several degrees below the melting temperature of the primers (52 - 55 ºC) , and 30 s at 72 ºC. 5 dilutions of genomic DNA were analyzed for each gene to produce a standard curve for quantification of samples based on the crossing of a threshold fluorescence level chosen within the early range of exponential PCR amplification. The genomic DNA was isolated from *M. marina* cells grown on 2216 media using a DNeasy kit (Qiagen), and quantified on a spectrophotometer. RNA samples processed without reverse transcriptase had no products or amplified much later within the run than experimental samples. Melting curve analysis following the PCR, and selected analysis of products by gel electrophoresis (2.2 % agarose) verified that a single product of the expected length was amplified by each primer set.

<u>Genomic analyses</u>

Hidden markov models (HMMs) of heme uptake protein families were used to search the genomes of *M. marina* and 62 additional marine bacteria to identify candidate heme uptake proteins. An HMM for TonB dependent outer membrane receptors involved in heme transport was built with HMMER (Eddy 1998) using a training set of functionally characterized heme transporters from diverse bacterial lineages including gammaproteobacteria (19), betaproteobacteria (3), alphaproteobacteria (2), and Bacteroidetes (2) which were aligned using ClustalX (Table 5.2). To identify the heme

transport associated heme oxygenase the Pfam HMM HemS (PF05171) was used. For ABC transport components, not enough well characterized heme transporters are available to construct HMMs, and so BLAST searches against the curated Swissprot database were used to identify possible heme transport sequences.

Phylogenetic trees were constructed with the putative heme outer membrane receptors and HemS-type heme oxygenases identified from HMM searches of marine bacterial genomes. Marine bacterial sequences and reference genes were aligned using ClustalX and neighbor-joining or Fitch-Margoliash trees based on protein distances were built using Phylip 3.6. 16s rRNA gene trees were constructed in a similar manner.

Results

Growth experiments

The growth of *M. marina* was strongly limited by iron at added inorganic iron concentrations of 30 nM (Fig. 5.1). Addition of 5 µM heme allowed growth at rates approaching those in media containing 5 µM inorganic iron. Growth on heme as a sole iron source demonstrates *M. marina* is capable of accessing heme iron, but multiple mechanisms are possible including direct uptake of heme, capture of iron through siderophores, or external degradation of heme to release inorganic iron.

Heme uptake

Iron limited *M. marina* internalized ^{55}Fe from the [^{55}Fe] heme compound, taking up approximately 10% of the 5 nM ^{55}Fe added over the 4 hour time span of the experiment (Fig. 5.2). In contrast, no active uptake of [^{55}Fe] heme by iron replete *M.*

marina was observed, though there was significant non-specific heme binding similar in magnitude to heme binding to glutaraldhye killed cells (data not shown).

Putative heme uptake gene cluster

Using HMM and BLAST searches a cluster of genes was identified in the draft genome of *M. marina* with similarity to heme uptake genes of other bacteria (Fig. 5.3; Table 5.3). An HMM search for heme outer membrane receptors identified a sequence (EAY28123) as the best candidate for a heme receptor, though its best BLAST hit in the Swissprot database was a B12 receptor. Lack of conservation in TonB dependent receptors makes identification of substrate specificity difficult, but an adjacent downstream gene (EAY29122) had similarity to the HmuY heme transport protein of *P. gingivalis*, and no significant similarity to other proteins in the *P. gingivalis* genome nor in the Swissprot database (Table 5.3). In *P. gingivalis*, *hmuY* is part of the heme uptake operon though its precise function is unknown (Lewis et al. 2006). On the other strand, an ABC transport system, consisting of a periplasmic binding protein (*hmuT*), an inner membrane permease (*hmuU*), and an ATPase (*hmuV*) which powers substrate transport, is present with best BLAST hits in the Swissprot database to heme transport components of *Yersinia pestis* (Thompson et al. 1999). Downstream of this ABC transport system is a gene which BLAST and HMM searches indicate is very similar to the HemS family of proteins often found in heme transport operons, and thought to be a heme oxygenase used to free iron from transported heme (Suits et al. 2005). The co-location of these genes in an operon like structure provides additional evidence that the genes are involved in heme transport and possibly co-regulated.

Expression of putative heme uptake genes

Expression of the putative heme transport genes identified with bioinformatic analyses was examined under differing conditions of iron availability using RT-Q-PCR. Compared to growth under iron sufficient conditions (5µM Fe) all putative heme transport genes were upregulated 30-700 fold under iron stress (30 nM Fe; Fig. 5.4). *hmuY* was the most strongly upregulated gene, consistent with analyses of protein expression in *P. gingivalis* showing *hmuY* is the major protein upregulated under iron stress (Lewis et al. 2006). *hemS* transcripts were the most abundant of the putative heme transport genes examined under iron replete conditions (data not shown) and the least dramatically upregulated under iron stress (28 fold). Differential expression was observed within operon-like regions of the *M. marina* putative heme uptake cluster, but similar results have been seen in other heme transport gene clusters (Lewis et al. 2006). The putative heme transport genes were upregulated to similar extents when growing on 1.5 µM heme (Fig. 5.4) and transcript levels were also similar (data not shown).

The expression of two putative siderophore biosynthetic genes was also examined for comparison with heme uptake components (Fig. 5.4; Table 5.1). *M. marina* has a complement of siderophore synthesis genes (EAY27067-EAY27071) which appears to allow for production of a rhizobactin 1021-like siderophore, and the genes are named in accordance with their homologs in the rhizobactin 1021 biosynthesis pathway (Lynch et al. 2001). *rhbB* in *M. marina* has strong similarity to the *rhbB* gene product (GenBank Accession# AAK65917) of *Sinorhizobium meliloti* (36% identity/55% similarity) which decarboxylates a siderophore precursor (Lynch et al. 2001). *M. marina* also contains a gene with two domains, one of which has strong similarity to *rhbF*, a siderophore synthase of *Sinorhizobium meliloti* (AAK65921; 30% identity/50% similarity). The

second domain of the *M. marina* protein is similar to an acyl co-A transferase involved in rhizobactin 1021 synthesis (*rhbD*, AAK65919; 25% identity/46% similarity), suggesting these genes have been fused in *M. marina* (Lynch et al. 2001; Challis et al. 2005). Both of these genes are upregulated in *M. marina* under iron stress and when growing on heme (Fig. 5.4).

Transcript quantities were normalized to total RNA which is predominately ribosomal RNA. The essentially constant expression levels of two genes involved in DNA and RNA polymerization and commonly used as standards, *rpoD* and *gyrA* (Desroche et al. 2005), confirms that the observed upregulation of putative heme transport genes is not due to changes in the proportion of ribosomal RNA relative to messenger RNA under differing growth conditions (Fig. 5.4).

<u>Heme uptake genes in marine bacteria</u>

As with *M. marina,* the genomes of 62 marine bacteria were searched for heme transport components. Searches with the heme outer membrane receptor HMM yielded some high scoring sequences in the gamma- and alpha- proteobacteria, and additional sequences with intermediate scores which may also be heme transporters were identified (Table 5.4). The top hits to this HMM from each genome were tested with the PFAM PF00593 model for TonB dependent outer membrane receptors (Table 5.4). Those which scored above the trusted cutoff threshold on this model, and thus appeared to be TonB dependent receptors, were used to construct a phylogeny to determine where they clustered in relation to known heme receptors. High scoring receptors from gamma- (e.g. *P. haloplanktonis*, *P. profundum* 3TCK) and alpha- proteobacteria (e.g. *P. bermudensis*, *O. alexendrii*) were closely associated with characterized heme outer membrane receptors

with high bootstrap support. These sequences formed a distinct clade from siderophore and B12 outer membrane receptors, strongly suggesting the genes also code for heme receptors (Figs. 5.5, 5.6). In the alphaproteobacteria an additional group composed predominately of Roseobacter sequences (e.g. *Sulfitobacter sp.* NAS14.1, *R. nubinhibens, etc.*) with intermediate heme outer membrane receptor HMM scores was formed, which was more closely associated with a sister group containing known heme receptors than with siderophore or B12 receptors (Fig. 5.6). These proteins are likely to be heme transporters given their proximity to HemS proteins in the genomes of these Roseobacters (see below). Because of the dominance of proteobacterial sequences used to construct the heme outer membrane receptor HMM and the variability in these sequences, identification of heme outer membrane receptors as distinct from other TonB dependent receptors was difficult in the Bacteroidetes, and phylogentic analyses of the sequences proved unhelpful.

Sequences with high similarity to the HemS family of heme transport proteins were identified using an HMM model in gamma- and alpha-proteobacteria, in addition to the sequence found in the Bacteroidetes *M. marina* (Table 5.4). The greater conservation of HemS and lack of affiliated protein families (Suits et al. 2005) led to clear positive or negative results for HemS HMM searches in each genome. Whenever a putative *hemS* gene was identified in a genome it was always located adjacent to, or within several genes of, the top hit to the heme outer membrane HMM (with the exception of *Marinomonas sp. MED121*), providing further evidence that the identified sequences encode proteins involved in a coordinated process: heme transport. In particular this finding suggests that the Roseobacter sequences with intermediate scores to the heme

outer membrane receptor HMM and adjacent *hemS* genes are involved in heme transport. In many cases, ABC transport systems were also present in the genome neighborhood, but as it is difficult to attribute substrate specificity to these transporters they were not examined in more detail.

Discussion

Defining the dominant routes of iron cycling in oceanic ecosystems will allow a better understanding of how this limiting micronutrient controls productivity and ecosystem structure in significant portions of the ocean. One current theory, based on iron uptake studies, is that siderophore bound iron may be more accessible to marine bacteria, while heme sources might be taken up predominately by eukaryotes, leading to the possibility that the availability of these different forms of iron could modify community structure (Hutchins et al. 1999). However, it is well established that many bacteria are capable of using heme, although presence of heme uptake pathways in marine bacteria have not been well investigated. In this study the ability of a particle associated marine bacterium, *M. marina*, to use heme as an iron source is investigated using physiological and molecular techniques. Finding evidence that this bacterium can use heme iron, genomic searches of other marine bacteria were carried out to understand the prevalence and ecological role of the heme transport pathway.

A putative heme transport cluster in *M. marina*

In the draft genome of *M. marina* a cluster of putative heme transport genes was identified (Fig. 5.3; Table 5.3) and their regulation was monitored in response to changing iron availability (Fig. 5.4). Genes in the cluster are similar to known heme

transport systems in diverse bacteria which most frequently are composed of a specific

heme outer membrane receptor, dependent on TonB for energy transfer across the

periplasmic space, and a heme ABC transport system to guide heme through the

periplasm and transport it across the inner membrane (Stojilkovic and Hantke 1992).

These essential components of the bacterial heme transport system are related to other

iron and trace metal chelate transport systems, including siderophore and B12 transport

proteins (Stojilkovic and Hantke 1992). As such, it is relatively easy to identify

sequences involved in metal chelate transport in a genome, but more challenging to

define substrate specificity. In the putative heme uptake cluster of *M. marina*, the

presence of two additional genes, *hemS* and *hmuY*, with similarity to proteins involved

specifically in heme transport provide valuable additional information about the substrate

specificity of the cluster (Table 5.3). Proteins in the HemS family are an essential

component of heme uptake systems in many bacteria, and they are generally thought to

be heme oxygenases used to free heme bound iron for other cellular needs (Suits et al.

2005), though they may serve as heme carriers in some organsisms (Schneider et al.

2007). HmuY is an outer membrane heme binding protein found in certain Bacteroidetes

heme transport systems, and is highly expressed under iron limitation, though its specific

role in heme transport has not been defined (Simpson et al. 2000; Lewis et al. 2006).

Both *hemS* and *hmuY* are uniquely associated with heme transport in other organisms and

analogs of these genes in the *M. marina* gene cluster strongly suggest it is also involved

in heme uptake.

Analysis of gene expression showed the putative heme transporter genes are

expressed and upregulated under iron limiting conditions and when growing on heme as

an iron source (Fig. 5.4). The high upregulation and transcript level of the *hmuY* analog

relative to the outer membrane receptor has also been observed in other heme uptake

systems (Lewis et al. 2006). These results are consistent with the putative role of the

cluster in heme transport, but there is no evidence for selective upregulation of the cluster

when growing on heme. When *M. marina* is iron limited or growing on heme the

expression profile of putative heme transport and siderophore biosynthesis genes are

extremely similar, suggesting a similar physiological state (Fig. 5.4). Growth on heme

appears to induce iron stress and an activation of many iron acquisition mechansisms

including heme and siderophore uptake pathways, rather than specific upregulation of

heme uptake systems. General responses to iron availability are often regulated by Fur

proteins (Escolar et al. 1999), and putative *fur* genes (EAY31090, EAY24380) have been

identified in the *M. marina* draft genome providing a potential mechanism for the

observed response. In some cases, TonB dependent receptors participate in their own

regulation, acting as both transporters and sensors of their substrate. In these cases the

receptor protein contains an N terminal domain which interacts with an anti-sigma factor

in the cytoplasmic membrane (Kirby et al. 2001; Koebnik 2005). Substrate binding to the

TonB dependent receptor mediates release of an extracytoplasmic function (ECF) sigma

factor by the anti-sigma factor, which then induces transcription of the TonB dependent

receptor and associated components. The N terminal region of the putative heme receptor

(HmuR) in *M. marina* does not appear to have a signaling domain and no anti-sigma

factors or ECF sigma factors are located near the putative heme transport cluster (data not

shown). This suggests *M. marina* cannot sense external heme and must rely on a general

iron responsive element for regulation, consistent with the observed upregulation of multiple iron uptake pathways when growing on heme.

The genetic evidence that *M. marina* contains a heme transporter is also supported by physiological studies showing that *M. marina* is capable of taking up heme bound iron and can grow on heme as a sole iron source. Uptake of ^{55}Fe from [^{55}Fe]heme was observed under iron limited conditions, but suppressed when iron replete, showing uptake was mediated by an iron regulated pathway and consistent with gene expression patterns of the putative heme uptake cluster (Fig. 5.2). While internalization of ^{55}Fe from [^{55}Fe] heme does not conclusively demonstrate that the entire heme molecule was transported, the uptake was rapid and immediate, which might not be expected under some alternate explanations for ^{55}Fe uptake such as siderophore uptake. Siderophores would need to be excreted into the medium and extract iron from heme prior to initiation of uptake. *M. marina* has the ability to grow on heme as an iron source, and though this may be mediated by multiple iron uptake pathways it is consistent with the presence of a heme transport system. While genetic manipulations, including knockout experiments, could provide more definitive evidence that the putative heme transport cluster is responsible for heme uptake, such techniques are not currently available for *M. marina* nor have they been developed for other related marine bacteria. However, the strong sequence similarity of the cluster to known heme transport proteins and its regulatory behavior, in conjunction with physiological evidence demonstrating *M. marina*'s capability to access heme bound iron strongly suggest the cluster is involved in heme transport.

Distribution of putative heme transport genes in marine bacteria

Having carefully examined the putative heme transport system in *M. marina*, the genomes of numerous marine bacteria were searched for related transport systems to better understand the distribution of heme uptake capabilities and the role of heme in the marine iron cycle. The heme outer membrane receptor served as a starting point for searches as it is the most well studied protein in the pathway. A number of sequences in the alpha- and gamma- proteobacteria had high scores to a heme receptor HMM and were grouped in a phylogeny with known heme transporters strongly suggesting these sequences are also heme outer membrane receptors (Table 5.4; Figs. 5.5, 5.6). However, the low conservation of this gene complicates its identification in bacteria divergent from proteobacteria where most examples have been identified. In particular it is difficult to determine the substrate specificity of outer membrane receptors, as discussed above, making the co-location of homologs to genes specifically involved in heme transport (*hemS*, *hmuY*) with putative heme outer membrane receptors especially important for functional attribution. Putative heme transport systems were identified in representatives of the gamma- and alpha-proteobacteria, and the Bacteroidetes based on the identification of a putative heme receptor and in certain cases its proximity to a HemS-type heme oxygenase (Fig. 5.7). The most notable feature in the distribution is a lack of heme transporters in known free living bacteria including *Pelagibacter ubique*, *Silicibacter pomeroyi*, and all marine cyanobacteria (Giovannoni et al. 2005; Moran et al. 2007). In fact, these organisms do not appear to have any TonB dependent receptors, as no candidate sequences were identified using the Pfam PF00593 HMM for tonB dependent outer membrane receptors (Table 5.5). Although cyanobacteria are quite divergent from proteobacteria where these proteins have been best studied, abundant TonB dependent

receptors were identified in freshwater cyanobacteria using PF00593, indicating sequence divergence is not the only reason for our inability to identify TonB dependent receptors in marine cyanobacteria (Table 5.5). Putative heme transporters were generally found in bacteria from groups thought to live primarily on particles including detritus, phytoplankton, and zooplankton (Delong et al. 1993; Crump et al. 1999; Heidelberg et al. 2002; Pinhassi et al. 2004).

The Roseobacter clade, in which the habitats of sequenced representatives have been examined, provide a good example of this distribution of heme transporters (Fig. 5.7; Moran et al. 2007). *Silicibacter pomeroyi* which is thought to be mainly free living (Moran et al. 2004) lacks putative heme transporters along with other TonB dependent receptors. While Sulfitobacters and *Silicibacter* TM1040, which have been found associated with dinoflagellates (Alavi et al. 2001; Jasti et al. 2005), possess putative heme transporters (Table 5.4, Fig. 5.6). These putative heme receptors are one of the few TonB dependent receptors in the genomes, and in fact in *Silicibacter* TM1040 the putative heme receptor is the only TonB dependent receptor implying the ability to access heme is especially important for the survival of these bacteria.

Although major advances have been made in understanding the distribution of iron concentrations in the ocean (Moore et al. 2004), characterization of iron speciation at the molecular level and a mechanistic understanding of iron fluxes have been difficult as a result of the low concentration and complicated chemistry of iron. Organically complexed iron is known to dominate the dissolved iron pool, and microorganisms must access some component of this iron to maintain observed growth rates (Rue and Bruland 1995; Hutchins et al. 1999; Barbeau et al. 2001; Macrellis et al. 2001). The iron

acquisition strategies employed by marine microorganisms may provide greater insight

into the forms and cycling of oceanic iron as competition for iron would be expected to

result in selection of uptake mechanisms capable of accessing abundant iron species. The

presence of putative heme transporters in bacteria thought to thrive on particles and their

absence in free living bacteria indicates heme is primarily available in or near particles,

but is not present in seawater at significant concentrations in the dissolved form (Fig.

5.7). This distribution is consistent with the hydrophobic, light-sensitive nature of heme.

Heme is a major form of iron in organisms serving as a redox active cofactor particularly

in electron transport proteins. It may be especially abundant in phytoplankton where the

localization of iron in photosystems leads to a high proportion of heme iron (Strzepek and

Harrison 2004; Gledhill 2007), and the ability to acquire heme could be especially

advantageous for organisms living in association with or preying on phytoplankton, such

as *Silicibacter* TM1040 (Alavi et al. 2001). Cell death or lysis may also make heme

available for use by other organisms, but because heme is relatively hydrophobic it is

likely to remain with detrital material and if dissolved its photosensitivity would shorten

its lifetime in the dissolved phase.

Particle associated bacteria play an important role in the marine iron cycle directly

recycling cellular iron from phytoplankton or detritus which might otherwise be lost from

the ecosystem due to sinking fluxes. As an abundant intracellular iron pool, heme iron

may supply a significant portion of bacterial iron requirements which are quite substantial

in oligotrophic ecosystems, accounting for 20-45% of total iron uptake (Tortell et al.

1996). It appears that *M. marina* has a heme transport system similar to those described

in pathogenic and symbiotic bacteria based on bioinformatic analyses of the draft

genome, gene expression, and physiological studies. Analogous systems are present in the genomes of marine gamma- and alpha- proteobacteria, and Bacteroidetes who seem to primarily live on particles or in rich environments where heme is most likely to be available. Although the use of siderophores by marine bacteria is well known (Martinez et al. 2000; Barbeau et al. 2001), these organisms have diverse iron uptake capabilities valuable under differing environmental conditions. Further analysis of bacterial genomes and functional characterization of these genes will likely reveal additional capabilities and provide insight into the forms of iron available in the marine environment and their cycling.

Acknowlegements

This chapter is in preparation for submission as: Hopkinson, Brian M., Kelly Roe, and Katherine A. Barbeau. Heme uptake by *Microscilla marina* and genomic evidence for heme uptake systems in diverse marine bacteria.

Table 5.1. *M. marina* genes whose expression was assessed with RT-Q-PCR, and the primers used in the analysis.

Gene name	Putative function	Accession number	Left primer	Right primer
hmuR	TonB depenedent heme outer-membrane receptor	EAY29123	ACGAGCAAGACCAAAGTGTGT	AGCCTCTACCGACTCCAAGG
hmuY	Outer-membrane heme binding	EAY29122	CAGCAAGCGAGGAGTTTC	AATCAAGTGCGAAGGAGGT
hmuT	ABC periplasmic binding protein	EAY29124	TAATTCTCGCCTGGGTAGGG	TCGGTAATGGTTCCGTTTAGC
hmuU	ABC permease	EAY29125	CTATGATGTTGTTGGCAGGT	CTGTAGCAAGCCCAGTAGC
hmuV	ABC ATPase	EAY29126	TACGATTGGGAAGTGGTTC	ACAGTAGTTTGGAGGTGGTG
hemS	Heme oxygenase	EAY29127	ATG GCGAGGCTATTCACAAA	CGTCTGGATGTTCTTCTACCG
rhbB	Decarboxylase	EAY27067	CGACTACTTGAACCCGATAG	CTCGTCTACCATACGCAAAG
rhbD/F	Siderophore synthase/Acyl CoA transferase	EAY27070	GTTTGCTTTGTTGTGGTTG	TTGATGCTCTATGGTTTGATT
gyrA	DNA gyrase subunit A	EAY25959	GGGTATGGTATGTGTGGCAAG	CCTCGGTTTGTAATGCGGTA
rpoD	RNA polymerase sigma 70	EAY27798	CTTTGGTCTGAACGGAGAGC	TCGGGAAGTATGTCGCAGTC

Table 5.2. Biochemically characterized heme outer membrane receptor proteins used to construct an HMM.

Organism	Group	Protein	Accession #
Yersinia enterocolitica	Gammaproteobacteria	HemR	CAA48250
Shigella dysenteriae	Gammaproteobacteria	ShuA	AAC27809
Escherichia coli	Gammaproteobacteria	ChuA	AAG44838
Enterobacter cloacae	Gammaproteobacteria	EhuA	CAD61862
Listonella anguillarum	Gammaproteobacteria	HuvA	CAD43038
Serratia marcescens	Gammaproteobacteria	HasR	CAE46936
Vibrio parahaemolyticus	Gammaproteobacteria	HutA	BAC62225
Pseudomonas fluorescens	Gammaproteobacteria	HasA	BAA88490
Vibrio cholerae	Gammaproteobacteria	HutA	AAA20675
Photobacterium damselae	Gammaproteobacteria	HutA	BAC79167
Pseudomonas fluorescens	Gammaproteobacteria	PfhR	AAD31012
Pseudomonas aeruginosa	Gammaproteobacteria	Phu	AAC13289
Vibrio mimicus	Gammaproteobacteria	PhuR	BAB33171
Pseudomonas aeruginosa	Gammaproteobacteria	HasR	AAD31013
Haemophilus ducreyi	Gammaproteobacteria	TdhA	AAC35765
Haemophilus influenzae	Gammaproteobacteria	HxuC	AAA87059
Plesiomonas shigelloides	Gammaproteobacteria	HugA	AAG23395
Vibrio vulnificus	Gammaproteobacteria	HupA	AAC27029
Yersinia pestis	Gammaproteobacteria	HmuR	AAC64866
Bordetella avium	Betaproteobacteria	BhuR	AAM28268
Neisseria meningitidis	Betaproteobacteria	HmbR	AAF19056
Neisseria meningitidis	Betaproteobacteria	HpuB	AAC44893
Bradyrhizobium japonicum	Alphaproteobacteria	HmuR	CAC38746
Sinorhizobium meliloti	Alphaproteobacteria	ShmR	CAC46612
Porphyromonas gingivalis	Bacteroidetes	Tlr	AAD37808
Porphyromonas gingivalis	Bacteroidetes	HmuR	AAB47566

Table 5.3. Top BLAST hits of putative heme transport proteins in *M. marina* to the Swissprot database, except HmuY which had no hits in the Swissprot database and instead was searched against the GenBank nr database. The best hit with functional annotation is reported for this gene.

Accession number	Protein	Highest Swissprot hit	% identity	% similarity
EAY29123	HmuY	*Porphyromonas gingivalis*, HmuY	24	37
EAY29122	HmuR	*Vibrio cholerae* BtuB, B12 Outer membrane transporter	22	38
EAY29124	HmuT	*Yersinia pestis* HmuT, heme binding periplasmic protein	31	53
EAY29125	HmuU	*Yersinia pestis* HmuU, heme transport permease protein	40	61
EAY29126	HmuV	*Yersinia pestis* HmuV, heme transport ATPase protein	33	51
EAY29127	HemS	*Yersinia enterocolitica* HemS, heme degradation protein	36	58

Table 5.4. Results of HMM searches of marine bacterial genomes. 63 marine bacterial genomes were searched with HMMs for a heme receptor and a HemS-type heme oxygenase. Genbank accession numbers, HMM scores, and the E-values corresponding to these scores are reported for the top hit to each HMM in the genome. The HMMs returned matches up to E-values of 10. If no matches with E-values <10 were found, the result of the search is reported to be 'no hits'. Additionally a PFAM HMM for tonB dependent receptors (PF00593) was run on the top hit to the heme receptor HMM from each genome to determine whether the hit appeared to be tonB-dependent receptor and therefore included in phylogenetic analyses of the putative heme receptor sequences.

Organism	Group	Heme outer membrane receptor top hit				HemS top hit		
		Accession #	HMM Score	E-value	PF00593 Score	Accession #	HMM Score	E-value
Alteromonas macleodii 'Deep ecotype'	Gamma	EAR04019	-23	3E-09	100.7	EAR04385	-215	3.6
Blastopirellula marina DSM 3645	Planctomycete	EAQ78408	50	4.8E-12	72.6	EAQ78211	-214	4.6
Colwellia psychrerythraea 34H	Gamma	AAZ27419	157	1.5E-44	91.9	AAZ27330	-203	1
Congregibacter litoralis KT71	Gamma	EAQ98888	389	2.4E-114	95.8	EAQ96001	-214	3.1
Croceibacter atlanticus HTCC2559	Bacteroidetes	EAP87588	4	9.5E-10	94.7	no hits	<-225	>10
Dokdonia donghaensis MED134	Bacteroidetes	EAQ40450	16	5E-10	87.2	EAQ40036	-214	2.3
Erythrobacter litoralis HTCC2594	Alpha	ABC64253	-26	2.5E-09	94.5	ABC63893	-211	1.6
Erythrobacter sp. NAP1	Alpha	no hits	<-400	>10	NA	EAQ30468	-212	2
Flavobacteria bacterium BBFL7	Bacteroidetes	EAS20902	67	1.7E-17	98.8	EAS18946	-223	6.3
Flavobacteriales bacterium HTCC2170	Bacteroidetes	EAR01835	-2	1.9E-09	70.7	no hits	<-225	>10
Leeuwenhoekiella blandensis MED217	Bacteroidetes	EAQ48229	79	5.2E-21	94.5	EAQ50603	-212	2.4
Idiomarina baltica OS145	Gamma	EAQ31719	245	3.4E-71	101.2	EAQ32478	-212	1.7
Idiomarina loihiensis L2TR	Gamma	AAV80955	231	1.3E-68	116.6	AAV81222	-204	0.62
Loktanella vestfoldensis SKA53	Alpha	EAQ05716	249	2.60E-72	89.3	EAQ05717	388	2.90E-114
Marinomonas sp. MED121	Gamma	EAQ63912	-48	1.50E-08	81.9	EAQ63913	389	2.70E-114
Microscilla marina	Bacteroidetes	EAY29123	77	5.10E-20	96.0	EAY29127	394	1.30E-115
Nitrobacter sp. Nb-311A	Alpha	EAQ35397	-57	2.20E-08	90.5	EAQ36694	-217	5.0
Nitrococcus mobilis Nb-231	Gamma	EAR22851	-1	6.70E-10	83.4	EAR22000	-204	0.8
Nitrosococcus oceani ATCC 19707	Gamma	ABA57372	504	3.70E-149	98.9	ABA59377	166	2.00E-47
Oceanicaulis alexandrii HTCC2633	Alpha	EAP90190	367	5.50E-108	87.2	EAP88656	-206	0.9
Oceanicola batsensis HTCC2597	Alpha	EAQ04704	-31	4.90E-09	84.6	EAQ01284	-216	4.5
Oceanicola granulosus HTCC2516	Alpha	EAR52071	-355	7.30E-01	<-35	EAR49637	-213	2.8
Oceanospirillum sp. MED92	Gamma	EAR59591	184	8.30E-53	101.9	EAR59816	432	2.60E-127
Parvularcula bermudensis HTCC2503	Alpha	EAQ15110	393	7.80E-116	92.8	EAQ15547	-214	2.3
Pelagibacter ubique HTCC1062	Alpha	no hits	<-400	>10	NA	AAZ21334	-233	9.70E+00
Photobacterium profundum 3TCK	Gamma	EAS45043	868	5.30E-262	132.3	no hits	<-225	>10
Photobacterium profundum SS9	Gamma	CAG19946	870	1.10E-262	129.5	no hits	<-225	>10
Photobacterium sp. SKA34	Gamma	EAR56146	502	2.50E-148	120.8	EAR54582	-220	7.10E+00
Polaribacter dokdonensis MED152	Bacteroidetes	EAQ43149	72	3.10E-19	80.6	no hits	<-225	>10

Table 5.4, continued

Organism	Group	Heme outer membrane receptor top hit				HemS top hit		
		Accession #	HMM Score	E-value	PF00593 Score	Accession #	HMM Score	E-value
Polaribacter irgensii 23-P	CFB	EAR13839	51	6.60E-13	72.7	EAR12129	-224	6.8
Prochlorococcus marinus CCMP1375	Cyano	AAP99381	-377	8.70E+00	<-35	AAQ00480	-227	7.3
Prochlorococcus marinus CCMP1986	Cyano	CAE19599	-380	9.60E+00	<-35	CAE19135	-224	4.7
Prochlorococcus marinus MIT 9311	Cyano	no hits	<-400	>10	NA	EAQ08450	-222	4.3
Prochlorococcus marinus MIT 9312	Cyano	ABB49613	-379	9.20E+00	<-35	ABB50793	-230	9.8
Prochlorococcus marinus MIT 9313	Cyano	CAE20265	-352	2.30E+00	<-35	CAE22086	-213	1.7
Prochlorococcus marinus NATL2A	Cyano	AAZ58717	-374	7.30E+00	<-35	AAZ58680	-219	2.9
Pseudoalteromonas haloplanktis TAC125	Gamma	CAI89122	318	6.20E-95	78.4	CAI89123	190	1.40E-54
Pseudoalteromonas tunicata D2	Gamma	EAR26946	241	1.00E-69	87.7	EAR26947	285	4.60E-83
Psychromonas sp. CNPT3	Gamma	EAS39927	-38	4.80E-09	59.0	EAS38949	-215	2.6
Reinekea sp. MED297	Bacteroidetes	EAR09022	-26	3.70E-09	47.5	EAR10912	-213	3.1
Rhodobacterales bacterium HTCC2654	Alpha	EAQ14144	49	7.00E-12	66.4	EAQ14145	369	2.60E-108
Robiginitalea biformata HTCC2501	Bacteroidetes	EAR16092	82	3.90E-22	58.0	EAR16998	-214	2.6
Roseobacter sp. MED193	Alpha	EAQ47012	138	9.50E-39	81.7	EAQ47011	392	3.20E-115
Roseovarius nubinhibens ISM	Alpha	EAP77470	71	1.10E-18	70.0	EAP83651	445	3.20E-131
Roseovarius sp. 217	Alpha	EAQ25010	70	3.10E-18	71.9	EAQ25008	404	6.00E-119
Silicibacter pomeroyi DSS-3	Alpha	no hits	<-400	>10	NA	AAV94852	-213	3.0
Silicibacter sp. TM1040	Alpha	ABF63080	109	3.80E-30	57.2	EAN57367	364	8.60E-107
Sulfitobacter sp. EE-36	Alpha	EAP83652	106	2.70E-29	53.4	EAP83651	423	9.50E-125
Sulfitobacter sp. NAS-14.1	Alpha	EAP79822	113	2.10E-31	53.5	EAP79821	406	2.30E-119
Synechococcus sp. CC9605	Cyano	no hits	<-400	>10	NA	ABB33860	-221	5.0
Synechococcus sp. CC9902	Cyano	ABB27153	-348	1.80E+00	<-35	ABB25186	-222	4.6
Synechococcus sp. RS9917	Cyano	EAQ68974	-346	1.90E+00	<-35	EAQ68105	-222	5.6
Synechococcus sp. WH 5701	Cyano	no hits	<-400	>10	NA	EAQ75439	-222	6.9
Synechococcus sp. WH 7805	Cyano	EAR17375	-368	7.80E+00	<-35	EAR19514	-222	5.9
Synechococcus sp. WH 8102	Cyano	CAE08818	-354	2.90E+00	<-35	CAE06931	-213	1.7

Table 5.4, continued

Organism	Group	Heme outer membrane receptor top hit				HemS top hit		
		Accession #	HMM Score	E-value	PF00593 Score	Accession #	HMM Score	E-value
Trichodesmium erythraeum IMS101	Cyano	ABG49815	-346	3.00E+00	-24.4	ABG51813	-220	7.5
Vibrio cholerae O1 biovar eltor	Gamma	AAF96478	1019	4.40E-304	112.2	AAF95888	-211	2.1
Vibrio fischeri ES114	Gamma	AAW85729	785	1.60E-233	95.5	AAW86627	-220	6.1
Vibrio parahaemolyticus RIMD 2210633	Gamma	BAC62225	1032	0.00E+00	124.4	BAC60698	-219	6.8
Vibrio splendidus 12B01	Gamma	EAP93308	968	1.20E-288	119.2	EAP92052	-209	2.2
Vibrio sp. MED222	Gamma	EAQ52355	797	3.80E-237	114.6	EAQ51658	-215	4.0
Vibrio vulnificus CMCP6	Gamma	AAO07241	876	6.60E-261	122.7	AAO08378	-215	3.9
Vibrio vulnificus YJ016	Gamma	BAC96807	1042	0.00E+00	123.2	BAC93403	-215	4.5

Table 5.5. Marine bacteria in which no tonB dependent outer membrane receptors were found with the Pfam 00593 HMM, and freshwater cyanobacteria for reference. Included are taxonomic information on the organisms searched (alpha = alphaproteobacteria, cyano = cyanobacteria), a description of the top hit to the Pfam 00593 HMM, its GenBank accession number, score on the HMM, and the E-value associated with that score.

| Organism	Group	Top hit to PF00593	Accession #	Score	E-value
Pelagibacter ubique HTCC1062	alpha	outer membrane protein ompl	AAZ21726	-24.0	1.2
Silicibacter pomeroyi DSS-3	alpha	OMPP1/FadL/TodX family	AAV95382	-9.0	0.4
Prochlorococcus marinus CCMP1375	cyano	Adhesin-like protein	AAQ00335	-27.2	2.7
Prochlorococcus marinus CCMP1986	cyano	hypothetical protein	CAE19621	-27.3	2.5
Prochlorococcus marinus MIT 9211	cyano	hypothetical protein	EAQ08837	-14.4	0.4
Prochlorococcus marinus MIT 9312	cyano	porin precursor-like	ABB49781	-22.8	1.3
Prochlorococcus marinus MIT 9313	cyano	hypothetical protein	CAE21988	-14.5	0.4
Prochlorococcus marinus NATL2A	cyano	porin homolog	AAZ58268	-21.5	1.1
Synechococcus sp. CC9605	cyano	hypothetical protein	ABB34035	-26.4	3.4
Synechococcus sp. CC9902	cyano	hypothetical protein	ABB25916	-21.4	1.3
Synechococcus sp. RS9917	cyano	hemolysin activator protein	EAQ68972	-24.6	2.7
Synechococcus sp. WH 5701	cyano	alkaline phosphatase	EAQ75607	-22.3	2.3
Synechococcus sp. WH 7805	cyano	hypothetical protein	EAR18586	-20.4	1.4
Synechococcus sp. WH 8102	cyano	possible porin	CAE08643	-24.0	2.2
Anabaena variabilis ATCC 29413	cyano	siderophore receptor	ABA24929	107.7	2.10E-29
Nostoc punctiforme PCC 73102	cyano	Outer membrane receptor proteins	ZP_00110047	107.2	3.80E-29
Synechocystis sp. PCC 6803	cyano	ferrichrome-iron receptor	BAA16609	112.5	4.80E-31
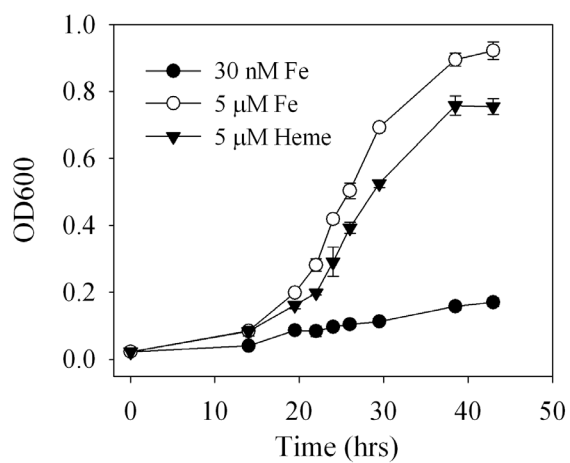
Figure 5.1. Growth of M. marina with 5 µM Fe (iron replete), 30 nM Fe (iron limited), and 5 µM heme.
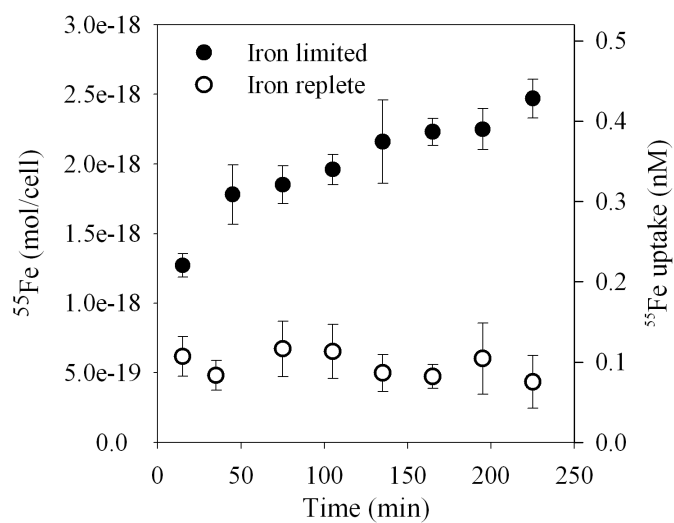
Figure 5.2. Uptake of [^{55}Fe] heme by iron limited (closed circles) or iron replete (open circles) *M. marina*.
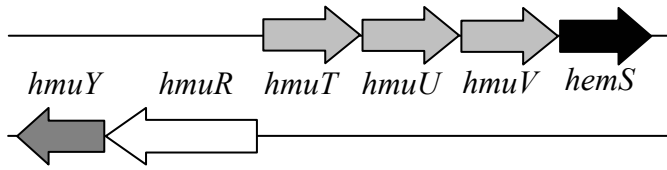
Figure 5.3. Organization of putative heme transport gene cluster in *M. marina*.
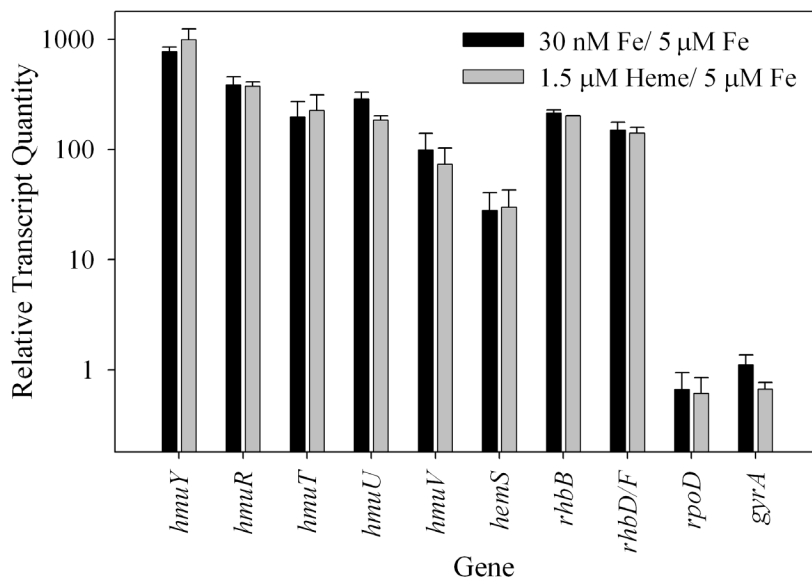
Figure 5.4. Expression of heme transport, siderophore biosynthesis, and housekeeping genes in *M. marina* under different growth conditions assessed with RT-Q-PCR. Quantity of transcripts when growing with 30 nM Fe (iron limited) or 5 µM heme were normalized to transcript quantities under iron replete conditions (5 µM Fe).
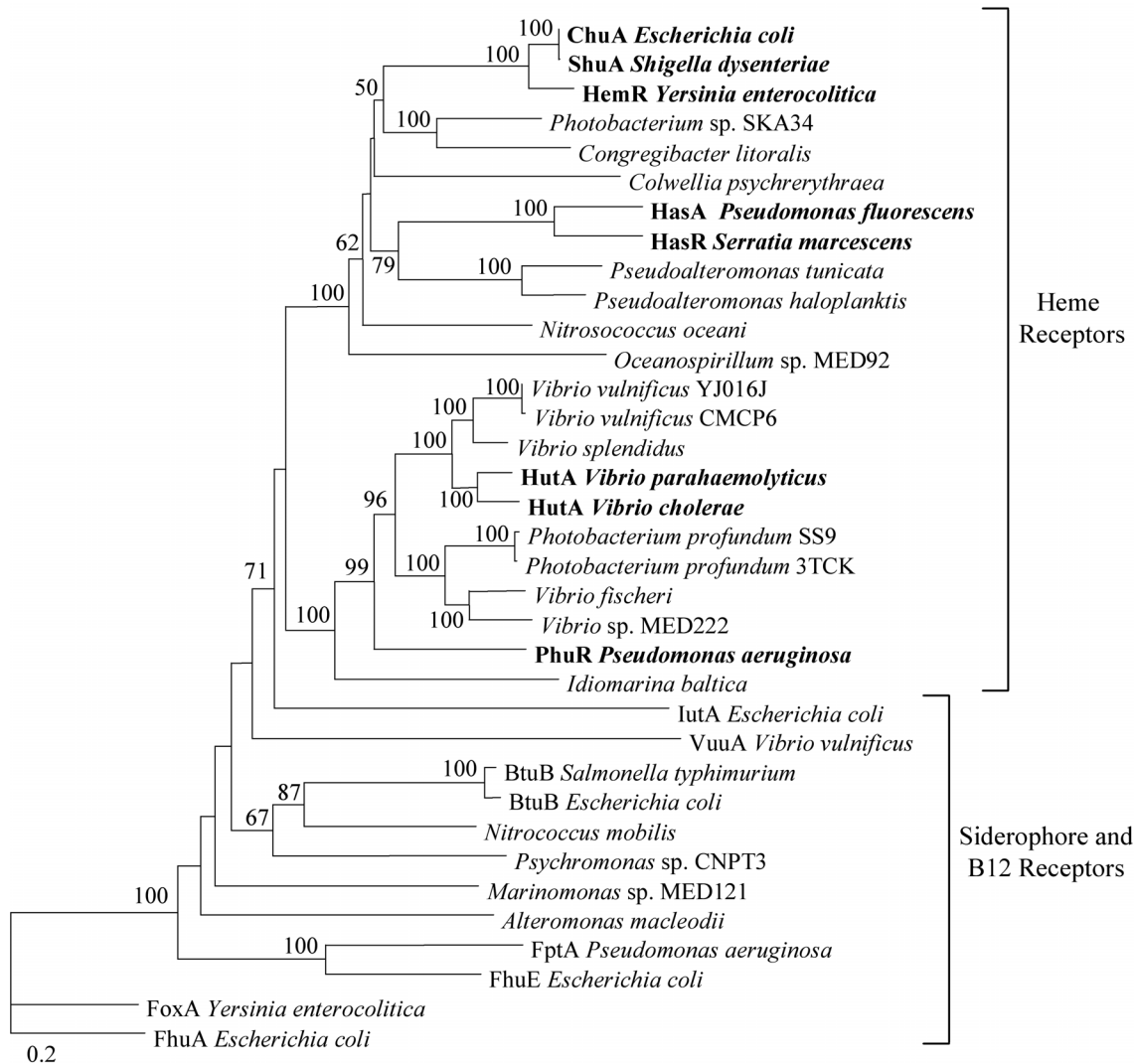
Figure 5.5. Phylogenentic tree of TonB dependent outer membrane receptor protein sequences from gammaproteobacteria. Top hits to the heme outer membrane receptor HMM in marine bacteria are included along with reference siderophore, B12, and heme(in bold) outer membrane receptors. Functional labels are placed on sequence groups based on substrate specificity of reference sequences within the group. The tree was constructed from phylogenetic distances using the Fitch-Margoliash method in phylip 3.6. Bootstrap values (from 100 resamplings) are indicated for nodes with values greater than 50. The scale bar indicates distances in substitutions per site. Reference heme receptors and their GenBank accession numbers: ChuA from *Escherichia coli* (AAG44838), ShuA *Shigella dysenteriae* (AAC27809), HemR *Yersinia enterocolitica* (CAA48250), HasR *Serratia marcescens* (CAE46936), HasA *Pseudomonas fluorescens* (BAA88490), HutA *Vibrio cholerae* (AAF96478), HutA *Vibrio parahaemolyticus* (BAC62225), PhuR *Pseudomonas aeruginosa* (AAC13289). Siderophore receptors: FhuA from *E. coli* (P06971), FhuE *E. coli* (P16869), IutA *E. coli* (P14542), FoxA *Y. enterocolitica* (Q01674), VuuA *Vibrio vulnificus* (AAF28471). B12 receptors: BtuB *Salmonella typhimurium* (P37409), BtuB *E. coli* (P06129).
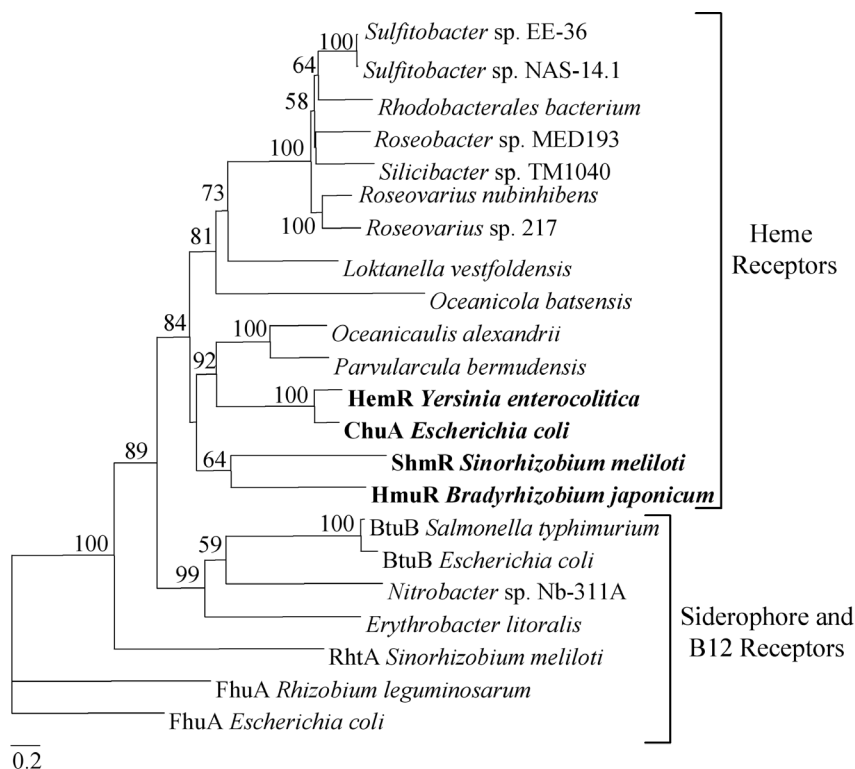
Figure 5.6. Phylogenetic tree of TonB dependent outer membrane receptor protein sequences from alphaproteobacteria. Top hits to the heme outer membrane receptor HMM in marine bacteria are included along with reference siderophore, B12, and heme(in bold) outer membrane receptors. Functional labels are placed on sequence groups based on substrate specificity of reference sequences within the group. The tree was constructed from phylogenetic distances using the Fitch-Margoliash method in phylip 3.6. The scale bar indicates distances in substitutions per site. Bootstrap values (from 100 resamplings) are indicated for nodes with values greater than 50. GenBank accession number for most references sequences are given in the caption to Fig. 5. Additional sequences in this tree are: Heme receptors: HmuR *Bradyrhizobium japonicum* (CAC38746), *Sinorhizobium meliloti* (CAC46612); Siderophore receptors: RhtA *S. meliloti* (Q9Z3Q5), FhuA *Rhizobium leguminosarum* (CAC48054).
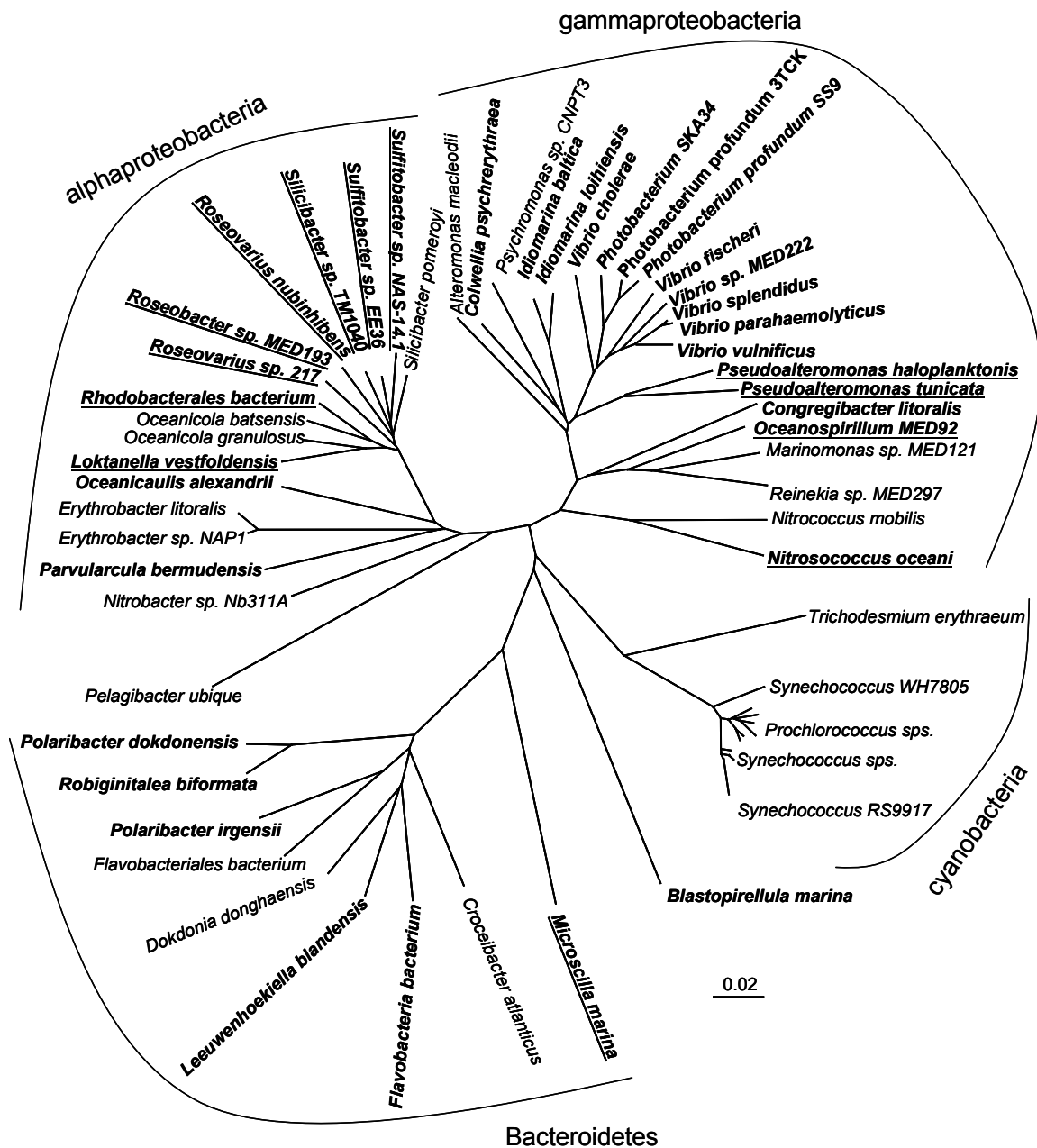
Figure 5.7. Distribution of putative heme transporters with respect to bacterial phylogeny. The tree is a 16s rRNA gene tree of marine bacteria whose genomes were searched for heme uptake components. Organisms which had a good hit to the heme receptor HMM (score >100 in gammaproteobacteria, >50 in alphaproteobacteria and Bacteroidetes) are indicated in bold, and those who had a HemS-type heme oxgenase in the same region of the genome are underlined.

References

Alavi, M., T. Miller, K. Erlandson, R. Schneide, and R. Belas. 2001. Bacterial community associated with *Pfisteria*-like dinoflagellate cultures. Environ. Microbiol. **3:** 380-396.

Barbeau, K., E.L. Rue, K.W. Bruland, and A. Butler. 2001. Photochemical cycling of iron in the surface ocean mediated by microbial iron(III)-binding ligands. Nature **413:** 409-413.

Buchler, J.W. 1975. Static coordination chemistry of metalloporphyrins. p 157-231. *In* K.M. Smith [ed.]. Porphyrins and metalloporphyrins. Elsevier.

Challis, G.L. 2005. A widely distributed bacterial pathway for siderophore biosynthesis independent of nonribosomal peptide synthetases. ChemBioChem **6:** 601-611.

Church, M.J., D.A. Hutchins, and H.W. Ducklow. 2000. Limitation of bacterial growth by dissolved organic matter and iron in the Southern Ocean. Appl. Environ. Microbiol. **66:** 455-466.

Coale, K.H., K.S. Johnson, S.E. Fitzwater, R.M. Gordon, S. Tanner, F.P. Chavez, L. Ferioli, C. Sakamoto, P. Rogers, F. Millero, P. Steinberg, P. Nightingale, D. Cooper, W.P. Cochlan, M.R. Landry, J. Constantinou, G. Rollwagen, A. Trasvina, and R. Kudela. 1996. A massive phytoplankton bloom induced by an ecosystem-scale iron fertilization experiment in the equatorial Pacific Ocean. Nature **383:** 495-501.

Crump, B.C., E.V. Armbrust, and J.A. Baross. 1999. Phylogenetic analysis of particle-attached and free-living bacterial communities in the Columbia river, its estuary, and the adjacent coastal ocean. Appl. Environ. Microbiol. **65:** 3192-3204.

Delong, E.F., D.G. Franks, and A.L. Alldredge. 1993. Phylogenetic diversity of aggregate-attached vs. free-living marine bacterial assemblages. Limnol. Oceangr. **38:** 924-934.

Desroche, N., C. Beltramo, and J. Guzzo. 2005. Determination of an internal control to apply reverse transcription quantitative PCR to study stress response in the lactic acid bacterium *Oenococcus oeni*. J. Microbiol. Methods **60:** 325-333.

Eaton, J.W., P. Brandt, and J.R. Mahoney. 1982. Haptoglobin: a natural bacteriostat. Science **215:** 691-693.

Eddy, S.R. 1998. Profile hidden Markov models. Bioinformatics **14:** 755-763.

Escolar, L., J. Perez-Martin, and V. deLorenzo. 1999. Opening the iron box: transcriptional metalloregullation by the Fur protein. J. Bacteriol. **181:** 6223-6229.

Genco, C.A., and D.W. Dixon. 2001. Emerging strategies in microbial heme capture. Mol. Microbiol. **39:** 1-11.

Gledhill, M. 2007. The determination of heme b in marine phyto- and bacterioplankton. Mar. Chem. **103:** 393-403.

Giovannoni, S.J., H.J. Tripp, S. Givan, M. Podar, K.L. Vergin, D. Baptista, L. Bibbs, J. Eads, T.H. Richardson, M. Noordewier, M.S. Rappe, J.M. Short, J.C. Carrington, and E.J. Mathur. 2005. Genome streamlining in a cosmopolitan oceanic bacterium. Science **309:** 1242-1245.

Granger, J., and N.M. Price. 1999. The importance of siderophores in iron nutrition of heterotrophic marine bacteria. Limnol. Oceanogr. **44:** 541-555.

Heidelberg, J.F., K.B. Heidelberg, and R.R. Colwell. 2002. Bacteria of the gamma subclass *Proteobacteria* associated with zooplankton in Chesapeake Bay. Appl. Envrion. Microbiol. **68:** 5498-5507.

Henderson, D.P. and S.M. Payne. 1993. Cloning and characterization of the *Vibrio cholerae* genes encoding the utilization of iron from hemin and hemoglobin. Mol. Microbiol. **7:** 461-469.

Hersman, L., T. Lloyd, and G. Sposito. 1995. Siderophore-promoted dissolution of hematite. Geochim. Cosmochim. Acta **59:** 3327-3330.

Hudson, R.J.M., and F.M.M. Morel. 1989. Distinguishing between extracellular and intracellular iron in marine-phytoplankton. Limnol. Oceanogr. **34:** 1113-1120.

Hutchins, D.A., A.E. Witter, A. Butler, and G.W. Luther III. 1999. Competition among marine phytoplankton for different chelated iron species. Nature **400:** 858-861.

Janson, S., B. Bergman, E.J. Carpenter, S.J. Giovannoni, and K. Vergin. 1999. Genetic analysis of natural populations of the marine diazotrophic cyanobacterium *Trichodesmium*. FEMS Microbiol. Ecol. **30:** 57-65.

Jasti, S., M.E. Sieracki, N.J. Poulton, M.W. Giewat, and J.N. Rooney-Varga. 2005. Phylogenetic diversity and specificity of bacteria closely associated with *Alexandrium* spp. and other phytoplankton. Appl. Environ. Microbiol. **71:** 3483-3494.

Kirby, A.E., D.J. Metzger, E.R. Murphy, and T.D. Connell. 2001. Heme utilization in *Bordetella avium* is regulated by RhuI, a heme-responsive extracytoplasmic function sigma factor. Infect. Immun. **69:** 6951-6961.

Koebnik, R. 2005. TonB-dependent trans-envelope signaling: the exception or the rule. Trends Microbiol. **13:** 343-347.

Koster, W. 2001. ABC transporter-mediated uptake of iron, siderophores, heme and vitamin B12. Res. Microbiol. **152:** 291-301.

Lewis, J.P., K. Plata, F. Yu, A. Rosato, and C. Anaya. 2006. Transcriptional organization, regulation and role of the *Porphyromonas gingivalis* W83 hmu haemin-uptake locus. Microbiol. **152:** 3367-3382.

Litwin, C. and B.L. Byrne. 1998. Cloning and characterization of an outer membrane protein of *Vibrio vulnificus* required for heme utilization: regulation of expression and determination of gene sequence. Infect. Immun. **66:** 3134-3141.

Lynch, D., J. O'Brien, T. Welch, P. Clarke, P. O Cuiv, J.H. Crosa, and M. O'Connell. 2001. Genetic organization of the region encoding regulation, biosynthesis, and transport of rhizobactin 1021, a siderophore produced by *Sinorhizobium meliloti*. J. Bacteriol. **183:** 2576-2585.

Macrellis, H.M., C.G. Trick, E.L. Rue, G. Smith, and K.W. Bruland. 2001. Collection and detection of natural iron-binding ligands from seawater. Mar. Chem. **76:** 175-187.

Martin, J.H., R.M. Gordon, and S.E. Fitzwater. 1990. Iron in Antarctic waters. Nature **345:** 156-158.

Martinez, J.S., G.P. Zhang, P.D. Holt, H.T. Jung, C.J. Carrano, M.G. Haygood, and A. Butler. 2000. Self-assembling amphiphilic siderophores from marine bacteria. Science **287:** 1245-1247.

Moore, J.K., S.C. Doney, and K. Lindsay. 2004. Upper ocean ecosystem dynamics and iron cycling in a global three-dimensional model. Global Biogeochem. Cycles **18:** GB4028 doi:10.1029/2004GB002220.

Moran, M.A., A. Buchan, J.M. Gonzalez, J.F. Heidelberg, W.B. Whitman, R.P. Kiene, J.R. Henricksen, G.M. King, R. Belas, C. Fuqua, L. Brinkac, M. Lewis, S. Johri, B. Weaver, G. Pai, J.A. Eisen, E. Rahe, W.M. Sheldon, W. Ye, T.R. Miller, J. Carlton, D.A. Rasko, I. T. Paulsen, Q. Ren, S.C. Daugherty, R.T. Deboy, R. J. Dodson, A.S. Durkin, R. Madupu, W.C. Nelson, S.A. Sullivan, M.J. Rosovitz, D. H. Haft, J. Selengut, and N. Ward. 2004. Genome sequence of *Silicibacter pomeroyi* reveals adaptations to the marine environment. Nature **432:** 910-913.

Moran, M.A., R. Belas, M.A. Schell, J.M. Gonzalez, F. Sun, S. Sun, B.J. Binder, J. Edmonds, W. Ye, B. Orcutt, E.C. Howard, C. Meile, W. Palefsky, A. Goesmann, Q. Ren, I. Paulsen, L.E. Ulrich, L.S. Thompson, E. Saunders, and A. Buchan. 2007. Ecological genomics of marine roseobacters. Appl. Environ. Microbiol. **73:** 4559-4569.

Mourino, S., C.R. Osorio, and M.L. Lemos. 2004. Characterization of heme uptake cluster genes in the fish pathogen *Vibrio anguillarum*. J. Bacteriol. **186:** 6159-6167.

Neilands, J.B. 1995. Siderophores: structure and function of microbial iron transport compounds. J. Biol. Chem. **45:** 26723-26726.

Nienaber, A., H. Hennecke, and H.M. Fischer. 2001. Discovery of a haem uptake system in the soil bacterium *Bradyrhizobium japonicum*. Mol. Microbiol. **41:** 787-800.

Pinhassi, J., M.M. Sala, H. Havskum, F. Peters, O. Guadayol, A. Malits, and C. Marrase. 2004. Changes in bacterioplankton composition under different phytoplankton regimens. Appl. Environ. Microbiol. **70:** 6753-6766.

Rue, E.L., and K.W. Bruland. 1995. Complexation of iron(III) by natural organic ligands in the Central North Pacific as determined by a new competitive ligand equilibration/adsoptive cathodic stripping voltammetric method. Mar. Chem. **50:** 117-138.

Schneider, S., K.H. Sharp, P.D. Barker, and M. Paoli. 2007. An induced fit conformational change underlies the binding mechanism of the heme transport proteobacteria-protein HemS. J. Biol. Chem. **281:** 32606-32610.

Simpson, W., T. Olczak, and C.A. Genco. 2000. Characterization and expression of HmuR, a TonB-dependent hemoglobin receptor of *Porphyromonas gingivalis*. J. Bacteriol. **182:** 5737-5748.

Stojiljkovic, I. and K. Hantke. 1992. Hemin uptake system of *Yersinia enterocolitica*: similarities with other TonB dependent systems in Gram-negative bacteria. EMBO J. **11:** 4359-4367.

Strzepek, R.F., and P.J. Harrison. 2004. Photosynthetic architecture differs in coastal and oceanic diatoms. Nature **431:** 689-692.

Suits, M.D.L., G.P. Pal, K. Nakatsu, A. Matte, M. Cygler, and Z. Jia. 2005. Identification of an *Escherichia coli* O157:H7 heme oxygenase with tandem functional repeats. Proc. Natl. Acad. Sci. USA **102:** 16955-16960.

Thompson, J.M., H.A. Jones, and R.D. Perry. 1999. Molecular characterization of the hemin uptake locus (*hmu*) from *Yersinia pestis* and analysis of *hmu* mutants for hemin and hemoprotein utilization. Infect. Immun. **67:** 3879-3892.

Tortell, P.D., M.T. Maldonado, and N.M. Price. 1996. The role of heterotrophic bacteria in iron-limited ocean ecosystems. Nature **383:** 330-332.

Weaver, R.S., D.L. Kirchman, and D.A. Hutchins. 2003. Utilization of iron/organic ligand complexes by marine bacterioplankton. Aquat. Microb. Ecol. **31:** 227-239.

VI

Conclusions and Future Directions

The relatively recent discovery that iron limits productivity and new production in large regions of the ocean has led to further research into its cycling and biological significance throughout the ocean. This thesis has contributed to the broader goals of understanding how iron is acquired by biota, when and where it is limiting, and how the element is supplied and transformed in the ocean. The research highlighted the importance of photosystem iron requirements for understanding iron limitation and iron cycling in the marine environment. Significant advances were made, but additional questions arose to be answered in future studies.

In Chapter 2 the discovery of iron-light co-limitation in subsurface chlorophyll maxima (SCMs) was reported. This finding contributes to the growing understanding that iron is scare throughout the ocean having impacts on phytoplankton community structure, nutrient dynamics, and nitrogen fixation outside of HNLC regions. Diatoms were found to be iron-light co-limited indicating their abundance at SCMs may be controlled by these factors which has consequences for phytoplankton community structure and nutrient cycling in SCMs as diatoms tend to promote carbon export. High iron requirements of the photosystem likely drove the responses to iron and light as suggested by the changes in PSII efficiency and C:Chl a ratios, but further investigations of photosynthetic physiology could help substantiate this claim. The concentration of iron containing photosynthetic reactions would be expected to increase when iron was added leading to an increase in photosynthetic rate per cell at low light. Because it is suspected that only a component of the phytoplankton community is co-limited by iron and light, it may be difficult to use traditional bulk measurements to test these hypotheses. Molecular techniques to measure gene and protein expression offer the advantage of using sequence

diversity to examine the responses of particular subsets of the community, but many photosynthetic genes are extremely well conserved. Analyses of single cells would be ideal, and flow cytometric and microscopic techniques are available to measure single cell photosynthetic fluorescence characteristics giving insight into iron stress (Olson et al. 2000). It may also be possible to using flow cytometry or microscopy in combination with molecular probes or antibodies to examine protein expression in single cells, and with the advent of single cell DNA analyses (Ottesen et al. 2006; Zhang et al. 2006), single cell RNA analysis of gene expression could follow. Regarding the ecological importance of iron-light co-limitation, investigation of the phenomenon at the base of the euphotic zone in oligotrophic gyres would be an important further step. In the gyres eddies are major mechanisms for nutrient input, and iron-light co-limitation may have an especially strong influence on eddy communities. Whether iron-light co-limitation occurs at SCMs in other ocean basins, notably the Atlantic, would also be of interest.

Work in the Southern Ocean, described in chapter 3, on natural iron fertilization provided information about mechanisms of iron supply and biological responses in this biogeochemically important region. By conducting a large set of incubation experiments across gradients in iron stress, the utility of photosynthetic parameters as indicators of iron stress was assessed, and several (F_v/F_m, σ_{PSII}) were found to correlate with the degree of iron stress. Although we conducted a large number of labor intensive experiments (9), it would be useful to conduct additional incubation experiments to substantiate these results, since the significance of some of the correlations were marginal. To better understand Southern Ocean iron supplies further studies of iron distributions and inputs further downstream in the Antarctic Circumpolar Current should

be pursued in conjunction with the satellite based observations of currents and phytoplankton biomass already being conducted (Kahru et al. 2007).

A thorough examination of iron speciation in an oceanic suboxic zone and overlying waters was conducted in the Eastern Tropical North Pacific (ETNP) to better understand the effect of suboxic conditions on iron cycling (Chapter 4). Suboxic conditions did not promote the accumulation of iron, but ~20% of dissolved iron was reduced to Fe(II). A better understanding of the origin and cycling of suboxic zone Fe(II) could be obtained by conducting an onshore-offshore transect in the ETNP, where strong gradients in important factors (suboxic zone depth, productivity, proximity to shelf sediments, etc) exist potentially allowing correlation of Fe(II) concentrations with changing conditions (Moffett et al. 2007). Measurements of Fe(II) decay rates under suboxic conditions would provide an important constraint on production rates and local sources of Fe(II). The suboxic zone Fe(II) may provide a labile source of iron for denitrifiers and the unique population of *Prochlorococcus* living within the suboxic zone. Further studies of the relevance of iron speciation to the suboxic *Prochlorococcus* are planned by the Barbeau group as part of a series of experiments to understand factors allowing this population of *Prochlorococcus* to exist despite the extremely low light levels occurring within the suboxic zone.

The high concentration of heme in photosynthetic proteins suggested that heme uptake may be an important capability for marine bacteria. As detailed in Chapter 5, the marine, particle-associated bacterium *Microscilla marina* is capable of taking up and growing on heme, and has a cluster of genes with similarity to heme transporters which are upregulated under iron stress and during growth on heme. Searching the many, newly

available, marine bacterial genomes revealed genes with strong similarity to heme transporters in the gamma- and alpha- proteobacteria. The genes were observed in bacteria thought to be living in association with phytoplankton, zooplankton, or other particles where the hydrophobic heme compound may be present in substantial quantities. These findings further our understanding of bacterial iron uptake mechanisms and the cycling of heme in the marine environment. While we were able to identify strong candidate sequences for heme transporters in a number of organisms and demonstrate uptake of heme bound iron and upregulation of putative heme transport genes, the techniques available to us did not allow us to conclusively demonstrate that the candidate genes are responsible for heme uptake. The ideal experiment to do so would be a gene knockout experiment, and the capabilities to transform some of the alpha-proteobacteria, which had candidate heme transporters, are being developed in other labs. While this study has been entirely lab based, future work on heme uptake capabilities in the field would be rewarding but challenging. Direct measurements of heme uptake could be attempted, but there is substantial non-specific binding of the compound to cellular material complicating these experiments. Alternative approaches could include microscopic autoradiography to assess uptake of individual cells rather than bulk material. Combined with molecular probes this could allow identification of bacterial taxa responsible for heme uptake. Although the genes involved in heme uptake are not strongly conserved, an attempt could be made to design primers for the most well conserved gene, HemS, allowing an assessment of the organisms responsible for heme uptake and their diversity.

This thesis has advanced our understanding of the role of iron in ocean ecosystems and its cycling in the marine environment. Investigation of the role of iron and other trace metals in oceanic ecosystems continues to yield exciting new findings. Connections between the biogeochemical cycling of certain metals and their use by marine microorganisms have become apparent as was long known for macronutrients, and further work to define these interactions will likely reveal complicated positive and negative feedbacks between the physical and biological components of the oceanic system.

References

Kahru, M., B.G. Mitchell, S.T. Gille, C.D. Hewes, and O. Holm-Hansen. 2007. Eddies enhance biological production in the Weddell-Scotia confluence of the Southern Ocean. Geophys. Res. Lett. **34**, L14603, doi:10.1029/2007GL030430.

Moffett, J.W., T.J. Goepfert, S.W.A. Naqvi. Reduced iron associated with secondary nitrite maxima in the Arabian Sea. Deep-Sea Res. I **54:** 1341-139.

Olson, R.J., H.M. Sosik, A.M. Chekalyuk, and A. Shalapyonok. 2000. Effects of iron enrichment on phytoplankton in the Southern Ocean during late summer: active fluorescence and flow cytometric analyses. Deep-Sea Res. II. **47:** 3181-3200.

Ottesen, E.A., J.W. Hong, S.R. Quake, and J.R. Leadbetter. 2006. Microfluidic digital PCR enables multigene analysis of individual environmental bacteria. Science **314:** 1464-1467.

Zhang, K., A.C. Martiny, N.B. Reppas, K.W. Barry, J. Malek, S.W. Chisholm, and G.M. Church. 2006. Sequencing genomes from single cells by polymerase cloning. Nature Biotech. **24:** 680-686.